

UNIVERSITY OF ILLINOIS, URBANA-CHAMPAIGN

ELECTRICAL AND COMPUTER ENGINEERING DEPARTMENT

THE DOCTORAL PRELIMINARY EXAMINATION DOCUMENT

---

**Analysis and measurement of  
anti-reciprocal systems**

---

*Author:*  
Noori KIM  
(UIN:677205530)

*Committee:*  
*Associate Professor* Jont B. ALLEN  
(Advisor, Chair)  
*Professor* Stephen BOPPART  
*Professor* Steven FRANKE  
*Associate Professor* Michael OELZE

October 12, 2014

## Abstract

Loudspeakers, mastoid bone-drivers, hearing-aid receivers, hybrid cars, and more - these “anti-reciprocal” systems are commonly found in our daily lives. However, the depth of understanding about the systems has not been well addressed since McMillan in 1946. The goal of this study is to guide an intuitive and clear understanding of the systems, beginning from modeling one of the most popular hearing-aid receivers, a balanced armature receiver (BAR).

Models for acoustic transducers are critical in many acoustic applications. This study analyzes a widely used commercial hearing-aid receiver ED series, manufactured by Knowles Electronics, Inc. Electromagnetic transducer modeling must consider two key elements: a *semi-inductor* and a *gyrator*. The semi-inductor accounts for electromagnetic eddy-currents, the “skin effect” of a conductor (Vanderkooy, 1989), while the gyrator (McMillan, 1946; Tellegen, 1948) accounts for the anti-reciprocity characteristic [Lenz’s law (Hunt, 1954, p. 113)]. Aside from Hunt (1954), to our knowledge, no publications have included the gyrator element in their electromagnetic transducer models. The most prevalent method of transducer modeling evokes the *mobility method*, an ideal transformer alternative to a gyrator followed by the dual of the mechanical circuit (Beranek, 1954). The mobility approach (Firestone, 1938) greatly complicates the analysis. The present study proposes a novel, simplified and rigorous receiver model. Hunt’s two-port parameters as well as the electrical impedance  $Z_e(s)$ , acoustic impedance  $Z_a(s)$  and electro-acoustic transduction coefficient  $T_a(s)$  are calculated using ABCD and impedance matrix methods (Van Valkenburg, 1964). The model has been verified with electrical input impedance, diaphragm velocity *in vacuo*, and output pressure measurements. This receiver model is suitable for designing most electromagnetic transducers, and it can ultimately improve the design of hearing-aid devices by providing a simplified yet accurate, physically motivated analysis.

As a utilization of this model, we study the motional impedance ( $Z_{mot}$ ) that was introduced by Kennelly and Pierce (1912) and highlighted by many researchers early in the 20th century (T.S.Littler, 1934; Fay and Hall, 1933; Hanna, 1925). Our goal for this part of the study is to search for the theoretical explanation of the negative real part (resistance) observed in  $Z_{mot}$  in an electro-mechanical system, as it breaks the positive-real (PR) property of Brune’s (1931) impedance, as well as the conservation of energy law. Specifically, we specify conditions that cause negative resistance in the motional impedance using simple electro-mechanical network models. Using Hunt’s two-port system parameters (a simplified version of an electro-acoustic system),  $Z_{mot}$  is defined as  $-\frac{T_{em}T_{me}}{Z_m}$ , where the subscript  $m$  stands for “mechanic,”  $T_{em}$  and  $T_{me}$  are transfer impedances, and  $Z_m$  is the mechanical impedance of the system Hunt (1954). Based on the simplified electro-mechanical model simulation, we demonstrate that  $Z_{mot}(s)$  is a minimum-phase function, but does not have to be a positive-real (PR) function. Any electro-mechanical network with shunt losses in the electrical side (including a semi-inductor and a resistor) sees a negative real part in  $Z_{mot}$  which may arise when there are frequency-dependent real parts. In conclusion,  $Z_{mot}$  is not a PR impedance because of the phase lag.

Several significant topics will be discussed in addition to these two larger issues (modeling the balanced armature receiver (BAR) and investigating  $Z_{mot}$ ). We generalize the gyrator with the non-ideal gyrator, analogous to the ideal *vs.* non-ideal transformer cases. This formula is reinterpreted via electromagnetic fundamentals. This work helps to transparently explain the anti-reciprocal property embedded in a gyrator. Explaining the “matrix composition method” is another contribution, which is characterized by the Möbius transformation. This is a significant generalization of the ABCD (transmission) matrix cascading method. Systems where the quasi-static approximation fails will also be considered (i.e., derivation of KCL, KVL from Maxwell’s equations). This leads us to the definition of “wave impedance” which is distinct from the traditional Brune impedance, discussed in modern network theory Vanderkooy (1989). The Brune impedance is defined by a reflectance that is minimum phase which is a significant limitation on this classical form of impedance (Brune, 1931). The typical example of a non-Brune impedance is a transmission line. This ‘non-Brune’ distinction is important and we believe it to be a novel topic of research

54 **Contents**

55	<b>I Introduction</b>	<b>4</b>
56	<b>1 Comparison of a telephone receiver and a moving-coil receiver</b>	<b>5</b>
57	<b>2 Goal of this study</b>	<b>9</b>
58	<b>3 Historical notes</b>	<b>11</b>
59	<b>II Theoretical Methods</b>	<b>13</b>
60	<b>1 Two-port anti-reciprocal network with Hunt parameters</b>	<b>13</b>
61	1.1 Calibration of Hunt parameters for an electro-acoustic transducer . . . . .	15
62	<b>2 Network postulates</b>	<b>15</b>
63	2.1 Additional postulates to include Brune’s impedance (Brune, 1931) . . . . .	17
64	<b>3 Generalization of the ABCD matrix using Möbius transformation</b>	<b>19</b>
65	<b>4 Motional Impedance (<math>Z_{mot}</math>)</b>	<b>22</b>
66	4.1 Definition of $Z_{mot}$ . . . . .	27
67	4.2 $Z_{mot}$ interpretation with Eq. 50 . . . . .	28
68	4.3 $Z_{mot}$ interpretation with Eq. 47 . . . . .	29
69	<b>5 Hidden, quasi-static assumptions in classic circuit theories</b>	<b>30</b>
70	5.1 Arguments about quasi-static approximation . . . . .	30
71	5.1.1 Quasi-static in electromagnetism . . . . .	31
72	5.1.2 Quasi-static descriptions . . . . .	32
73	5.1.3 Transmission line and delay . . . . .	32
74	5.2 Kirchhoff’s voltage and current laws (KVL, KCL) . . . . .	35
75	5.3 Gyrator . . . . .	37
76	5.4 Eddy currents and diffusion waves . . . . .	41
77	5.5 Reinterpretation of quasi-static . . . . .	44
78	<b>III Experimental Methods</b>	<b>46</b>
79	<b>1 Measurements for BAR modeling</b>	<b>46</b>
80	1.1 Electrical input impedance measurements for the Hunt parameter calculation . . . .	46
81	1.2 Laser vacuum measurements . . . . .	48
82	1.3 Pressure measurements . . . . .	49
83	<b>2 Technical analysis of an OAE hearing measurement probe</b>	<b>49</b>
84	2.1 Physical structure of ER10C . . . . .	50
85	2.2 Crosstalk measurement . . . . .	52
86	2.3 Calibration issues . . . . .	53

87	<b>3 A new probe design</b>	<b>54</b>
88	3.1 Choice of transducers . . . . .	54
89	3.2 Sound delivery path for the microphone . . . . .	54
90	3.3 Sound delivery path for the receiver . . . . .	56
91	3.4 Probe evaluation . . . . .	56
92	<b>IV Results</b>	<b>59</b>
93	<b>1 Hunt parameter calibration</b>	<b>59</b>
94	<b>2 Receiver model</b>	<b>60</b>
95	2.1 Hunt parameters comparison . . . . .	61
96	2.2 Verification 1: Electrical impedance <i>in vacuo</i> . . . . .	62
97	2.3 Verification 2: Mechanical velocity measurement using Laser <i>in vacuo</i> . . . . .	63
98	2.4 Verification 3: Thevenin pressure comparison . . . . .	64
99	<b>3 <math>Z_{mot}</math> simulation of simplified electro-mechanic systems</b>	<b>64</b>
100	<b>4 Calibration results from both the modified and the manufactured probes</b>	<b>66</b>
101	4.1 The modified ER10C . . . . .	69
102	4.2 Prototype probes: MA16 and MA17 . . . . .	70
103	<b>V Conclusions and Contributions</b>	<b>73</b>
104	<b>VI Appendix</b>	<b>74</b>
105	<b>A Definition of Energy Conservation, Starting from Modality</b>	<b>74</b>
106	<b>B Tellegren's Theorem &amp; KCL/KVL</b>	<b>76</b>
107	<b>C Sensitivity Analysis of ED Series SPICE Model</b>	<b>79</b>
108	<b>D <math>Z_{mot}</math>: Spatial Relationships Between <math>\Phi</math>, I, B, F, and I</b>	<b>81</b>
109	<b>E Calculation of Hunt Parameters</b>	<b>84</b>
110	<b>F Hysteresis Loop for a Ferromagnetic Material: B vs. H</b>	<b>85</b>

## Part I

# Introduction

A typical hearing-aid consists of three parts: a microphone (picks up sound), an amplifier (transforms sound into different frequencies, filters noise, and selectively amplifies each frequency region based on the difference in individual hearing loss<sup>1</sup> via multi-band compression), and a receiver (sends the processed signal from the amplifier into the ear). A proper understanding of each component in the hearing-aid can facilitate better and clearer sound quality

The current study starts by modeling one of the most important and complex hearing-aid components, the balanced armature receiver (BAR). The BAR is an electromagnetic loudspeaker that converts an electrical signal (current) into acoustical pressure (or force, in the case of an electro-mechanical system). It is referred to as an electromagnetic transducer because small magnets are involved. These miniature loudspeakers are widely used and remain one of the most expensive components of modern hearing-aids; they are also the most poorly understood. Therefore, a detailed understanding of these transducers is critical to optimize their design.

In the electromagnetic transducer models of both Weece and Allen (2010) and Thorborg et al. (2007), an ideal transformer was used to convert electrical current into mechanical force (or acoustical pressure) in the transducer. As described in Beranek (1954), the mobility analogy (Firestone, 1938), along with an ideal transformer, is a valid way to represent electrical-to-mechanical transduction when modeling anti-reciprocal electromagnetic transducers. The mobility method, which requires using the dual network (swapping current and voltage), fails to provide an intuitive explanation of the anti-reciprocity characteristic of the electromagnetic transducer, which follows from Maxwell-Faraday’s (1831) law and Lenz’s (1834) law. The impedance and mobility methods are mathematically equivalent, meaning one can use either method to describe the system. However, including the gyrator in transducer models allows for a logical, intuitive, and accurate interpretation of the physical properties. For example, when using a gyrator to represent the mechanical and electrical transformation, stiffness can be represented as a capacitor and mass as an inductor in the series combination. Given the mobility (dual) network, it is necessary to swap the inductor and capacitor, placing them in parallel combination. Thus, we feel that the dual network combined with the mobility method is less intuitive and more difficult to quantify when describing the system.

Kim and Allen (2013) suggested a two-port network model of the BAR (Fig. 1) having a *semi-inductor*, a *gyrator* (two poorly understood elements of special interest in the electromagnetic transducer), and a *delay*. Our network has two wave speeds, the speed of light ( $3 \times 10^8$  [m/s]) and the speed of sound (345 [m/s]). Both speeds are important for proper modeling. The acoustic delay becomes significant due to the relatively slow speed of sound. This delay is represented using a transmission line in the model. With a quasi-static (QS) assumption, there is no delay in the system.

The semi-inductor component is necessary to account for eddy-current diffusion (the “skin effect”). In 1989, Vanderkooy demonstrated that, at high frequencies, the behavior of the impedance of a loudspeaker changes from the behavior of a normal inductor to that of a semi-inductor because of the eddy-current diffusing into the iron pole structure of the loudspeaker (i.e., the skin effect). Using a Bessel function ratio, Warren and LoPresti (2006) represented Vanderkooy’s semi-inductor

---

<sup>1</sup>The percentage of people in the United States who are suffering from Hearing Loss 12.7% in their age of 12 years and older Lin et al. (2011). Also two-thirds of Americans older than 70 years have experienced mild to severe HL. The importance of designing Hearing-aid properly, therefore, is come to the fore in contemporary society along with the Population ageing Population ageing is a shift in the distribution of a country’s population towards older ages ([http://en.wikipedia.org/wiki/Population\\_ageing](http://en.wikipedia.org/wiki/Population_ageing))

152 model as a “diffusion ladder network,” a continued fraction expansion or a combination of resistors  
 153 and inductors. In 2010, Weece and Allen used this representation in a bone-driver model. After  
 154 demagnetizing the bone-driver, they established the  $\sqrt{s}$  behavior and determined the ladder network  
 155 elements from the measured electrical impedance of the transducer. Thorborg et al. (2007) also  
 156 introduced a loudspeaker model with lumped circuit elements, including a semi-inductor.

157 In 1946, McMillan introduced the anti-reciprocal component as a network element. Two years  
 158 later, Tellegen (1948) coined the term gyrator and categorized it as a fifth network element, along  
 159 with the capacitor, resistor, inductor, and ideal transformer. Other than Hunt’s 1954 publication,  
 160 we remain unaware of any publication which implements anti-reciprocity in its electromagnetic  
 161 transducer model using a gyrator.

162 Leading to their new circuit model of the BAR (Fig. 1), Kim and Allen (2013) measured the  
 163 electrical input impedance, solving for the Hunt parameters (1954) of the receiver. An intuitive  
 164 design of an electromagnetic transducer was developed by using the gyrator and the asymptotic  
 165 property as  $\omega \rightarrow \infty$  was properly described by using a parallel relationship between a semi-inductor  
 166 and a normal inductor (electrical part in Fig. 1). Approximations for two extreme frequency limits  
 167 of the input impedance ( $Z_{in} = \sqrt{s}||s$ ) are defined as follows:

$$Z_{in}(s) = \frac{1}{\frac{1}{\sqrt{s}} + \frac{1}{s}} \approx \begin{cases} \frac{1}{\frac{1}{\sqrt{s}} + \frac{1}{s}} \underset{0}{=} \sqrt{s}, & s \rightarrow \infty \\ \frac{1}{\frac{1}{\sqrt{s}} + \frac{1}{s}} \underset{0}{=} s, & s \rightarrow 0 \end{cases} \quad (1)$$

168 where  $s$  is the Laplace frequency ( $j\omega$ ).

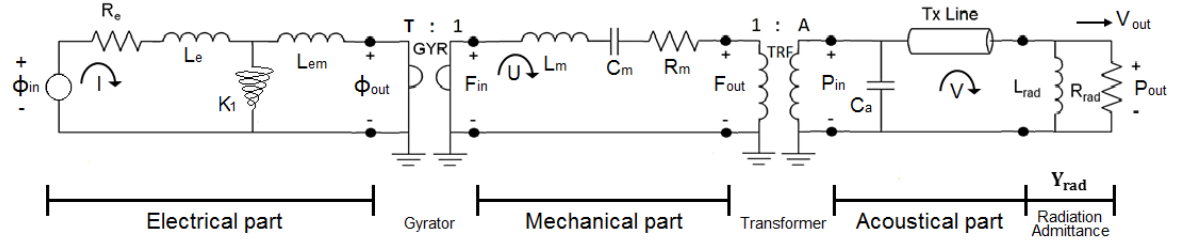
169 We believe that this is the only published model to describe the BAR’s behavior using these two  
 170 essential components. This model is presented in Fig. 1, and the modeled BAR<sup>2</sup> and its internal  
 171 structure are shown in Fig. 2.

## 172 1 Comparison of a telephone receiver and a moving-coil receiver

173 The oldest telephone receiver is the BAR type, and it is still in use. The original technology goes  
 174 back to the invention of the electric loudspeaker by A. G. Bell in 1876. Attraction and release of  
 175 the armature are under the control of the current in the windings of an electromagnet (Hunt (1954)  
 176 chapter 7, and Beranek and Mellow (2014)). As the electrical current goes into the electric terminal  
 177 of the receiver, it generates an alternating current (AC) magnetic field surrounded by a coil. Due to  
 178 the polarity between the permanent magnet and the generated magnetic field, an armature, which  
 179 sits within the core of the coil and the magnet, feels a force. The very basic principles for explaining

---

<sup>2</sup>ED7045 Knowles Electronics, Itasca, IL (<http://www.knowles.com>)



$$\begin{bmatrix} \Phi_{in} \\ I \end{bmatrix} = \begin{bmatrix} 1 & R_e \\ 0 & 1 \end{bmatrix} \begin{bmatrix} 1 & sL_e \\ 0 & 1 \end{bmatrix} \begin{bmatrix} 1 & 0 \\ 1/K_1\sqrt{s} & 1 \end{bmatrix} \begin{bmatrix} 1 & sL_{em} \\ 0 & 1 \end{bmatrix} \begin{bmatrix} 0 & T \\ 1/T & 0 \end{bmatrix} \begin{bmatrix} 1 & sL_m \\ 0 & 1 \end{bmatrix} \begin{bmatrix} 1 & 1/sC_m \\ 0 & 1 \end{bmatrix} \begin{bmatrix} 1 & R_m \\ 0 & 1 \end{bmatrix} \begin{bmatrix} 1/A & 0 \\ 0 & A \end{bmatrix} \begin{bmatrix} 1 & 0 \\ sC_a & 1 \end{bmatrix} \begin{bmatrix} \cosh(\frac{S\ell}{c}) & z_0 \sinh(\frac{S\ell}{c}) \\ \sinh(\frac{S\ell}{c})/z_0 & \cosh(\frac{S\ell}{c}) \end{bmatrix} \begin{bmatrix} 1 & 0 \\ Y_{rad} & 1 \end{bmatrix} \begin{bmatrix} P_{out} \\ V_{out} \end{bmatrix}$$

Figure 1: The Balanced Armature Receiver (BAR) circuit as a model (Kim and Allen, 2013) as defined by a transmission (ABCD) matrix representation. The chained properties of an ABCD matrix are followed by the Möbius transformation. This factored nature of the ABCD matrix is discussed in detail in section 3. The electrical and mechanical circuits are coupled by a gyrator (GYR, realizing an anti-reciprocal network), while a transformer (TRF) is used for the coupling of the mechanical and acoustical circuits. The  $K1$  is a semi-inductor representing electromagnetic diffusion due to the skin effect. The  $TxLine$  stands for a transmission line to involve a delay in the system, violating a quasi-static assumption in this electro-acoustic system. Using this non-quasi-static element is the proper way to model this system. By computing the defined ABCD matrix and converting the result to the impedance matrix, Hunt parameters for the transducer model can be calculated (Eq. 13). The impedance matrix is useful when making measurements, while the ABCD matrix representation is useful for network modeling but then may be transformed into an impedance matrix for experimental verification. In this model, the input and output potentials for each section are specified as voltage ( $\Phi$ ), force ( $F$ ), and pressure ( $P$ ). Current ( $I$ ), particle velocity ( $U$ ), and volume velocity ( $V$ ) represent the flow for each of the three physical sections.

180 this movement are Hooke's law ( $F_{hook}$ ) and the magnetic force due to a current  $\mathbf{I}$  ( $\mathbf{F}_{mag}$ )<sup>3</sup>

$$F_{hook} = k\xi, \quad (3)$$

181 where  $\xi$  is the displacement, and  $k$  is a constant characterizing stiffness of spring (or armature in  
182 our case), and

$$\mathbf{F}_{mag} = \mathbf{I} \times \mathbf{B}_0, \quad (4)$$

183 where  $\mathbf{I}$  is the current and  $\mathbf{B}_0$  is the static magnetic field.

184 As shown in Fig. 2, since a diaphragm is connected to the end of the armature, when the  
185 armature moves, so does the diaphragm. The sound wave is propagated out of the sound delivery  
186 port. A large number of coil turns is required since the generated magnetic field (from the coil,  
187 time-varying magnetic field) should be compatible with the static direct current (DC) magnetic  
188 field (permanent magnet) to balance the mutual magnetic force. The size, weight, and sensitivity  
189 of this type can be greatly improved by using a light (low-mass) pole piece (i.e., armature) with  
190 small permanent magnets. This is the main reason for using this type of transducer in hearing-aid  
191 products.

<sup>3</sup>A new theory about operation of the BAR was introduced by Jensen et al. (2011). This paper derives a non-linear time-domain force for the BAR-type receiver. Based on their theory, the input force of the moving-armature transducer system employs "the tractive force," which attempts to minimize the air gap between the armature and the magnet. According to this theory

$$F_{bar} = \frac{\mathbf{S}_a \mathbf{B}^2}{2\mu_0} = \frac{\Psi_0^2}{2\mu_0 \mathbf{S}_a}, \quad (2)$$

where  $\mathbf{B}$ [Wb/m<sup>2</sup>] is the magnetic field across the air gap,  $S_a$ [m<sup>2</sup>] is the transverse area of the armature with the permanent magnet,  $\mu_0$  is the permeability in free space ( $4\pi \cdot 10^{-7}$ [H/m]), and  $\Psi_0 (= \mathbf{B}_0 S_a)$ [Wb] is the total magnetic flux in the air gap. To justify this theory, one must construct a relationship between  $F_{bar}$  in Eq. 2 and current similar to the relationship shown in Eq. 4 due to the gyrator nature in electro-magnetic system.

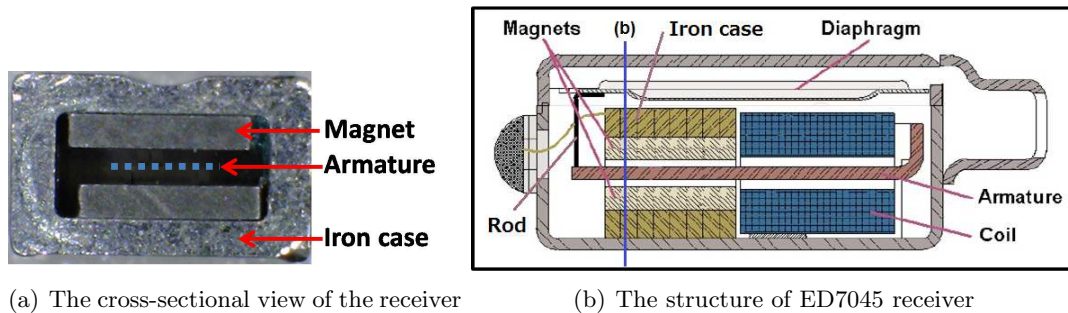


Figure 2: (a): The picture of the BAR at the “Cut Z” line in panel (b). There is space for the armature to vibrate vertically between the magnets. Magnets are sandwiching the armature (the blue, dotted line). A laminated iron case surrounds the magnets and the armature. (b): A schematic of a BAR. An electrical current in the coil comes from the transducer’s electrical input terminals; the current induces a Lorentz force on the armature via the induced magnetic field (modified from Knowles documentation of the ED receiver series). Note that the port location of the ED7045 receiver is rotated  $90^\circ$  to the longer side.

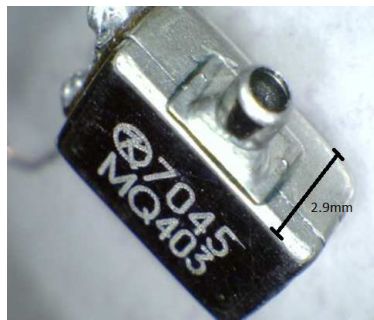


Figure 3: A picture of the ED7045, a BAR used in this study. The black line shows the depth of the transducer, 2.9 [mm].

192 Knowles Electronics<sup>4</sup> ED series receivers shown in Fig. 2(a) and Fig. 3, including the ED7045  
 193 and ED1913, are BARs, used in all hearing-aids. The ED receiver is 6.32 x 4.31 x 2.9[mm] in  
 194 size. These receivers consist of a coil, an armature, two magnets, and a diaphragm. Unlike the  
 195 alternative moving-coil drivers, the coil of the BAR has a fixed position, (Jensen et al., 2011),  
 196 thereby reducing the internal mass and providing more space for a much longer coil. As a result  
 197 of the lower mass, the BAR frequency response is higher, and due to the greater coil length, the  
 198 sensitivity is greater.

199 The armature used for the ED7045 is an E-shaped metal reed (Bauer, 1953), whereas a U-  
 200 shaped armature was widely used for early telephone instruments (Mott and Miner, 1951). Both  
 201 shapes have advantages and disadvantages. For example, the U-shaped armature has better acoustic  
 202 performance (i.e., wide-band frequency response) while the E-shaped armature lowers the vibration  
 203 of the body more effectively. The armature is placed through the center of the coil and in between  
 204 two magnets, without touching them. The movement of the armature is directly connected to the  
 205 diaphragm through a thin rod (Fig. 2 (B)). Figure 4 shows the types of ring armature receivers  
 206 adapted from Mott and Miner (1951).

207 The other popular type of speaker is the moving-coil, or dynamic, speaker proposed by Oliver  
 208 Lodge in 1898 (Hunt, 1954) (Fig.5). In this type of speaker, a voice coil surrounds a magnet and  
 209 the coil is attached to a diaphragm (or sound cone). When there is input through the coil, the coil

<sup>4</sup>Knowles Electronics, Itasca, IL (<http://www.knowles.com>)

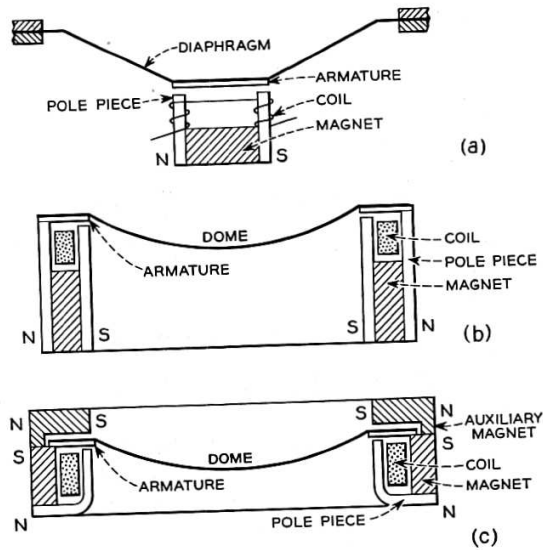


Fig. 2—(a) Early composite diaphragm receiver.  
 (b) Simple ring armature receiver.  
 (c) Ring armature receiver with auxiliary magnet.

Figure 4: Sectional view of ring armature receivers (three types) adapted from Mott and Miner (1951), Fig. 2 in the original manuscript.

210 is forced to move (up and down), as described by Faraday’s law. The coil drives the cone, which  
 211 radiates the sound. As a result, the air particles around the sound cone vibrate; therefore, sound  
 212 waves are created.

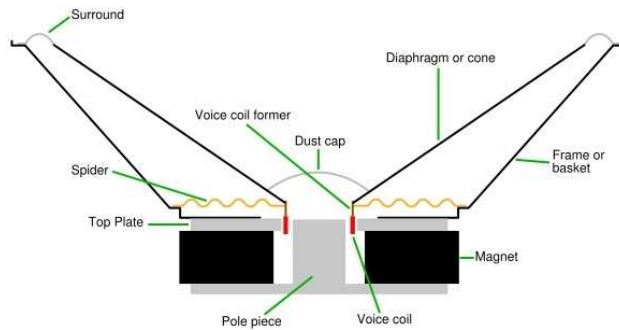


Figure 5: The cross-section view of the moving-coil loudspeaker. Up-and-down motion of the voice coil around a permanent magnet creates a time-varying magnetic field. As a voice coil moves around the pole piece, it becomes an “electro-magnet.” The image is from <http://il-news.softpedia-static.com>.

213 To limit the mass of the coil in the dynamic speaker, the number of coil turns must be greatly  
 214 reduced (e.g., 100 times less than in the BAR case). Rather, the dynamic speaker needs a strong  
 215 core magnet to float the cone (with the coil), which leads to a size generally larger than the BAR.  
 216 This acoustic characteristic of the dynamic speaker is easier to understand after controlling the  
 217 speaker mass and the stiffness of the diaphragm.

## 218 2 Goal of this study

219 The goal of this study is to provide clear insight into anti-reciprocal (or broadly non-reciprocal)  
 220 system. We are exposed to anti-reciprocal systems in our daily lives; however, the depth of our  
 221 understanding of them has not been well addressed since McMillan in 1946. The keyword is “anti-  
 222 reciprocity.”

223 As discussed in the appendix C, the motivation for this study began with a PSPICE simulation  
 224 using the BAR-type ED series receiver model from Knowles Electronics (Kim and Allen (2013),  
 225 Fig. 54). We then proceeded to redefine a new circuit model to characterize a BAR-type receiver, the  
 226 Knowles ED7045 (Kim and Allen, 2013), and then developed theoretical insights and observations  
 critical to understanding the BAR.

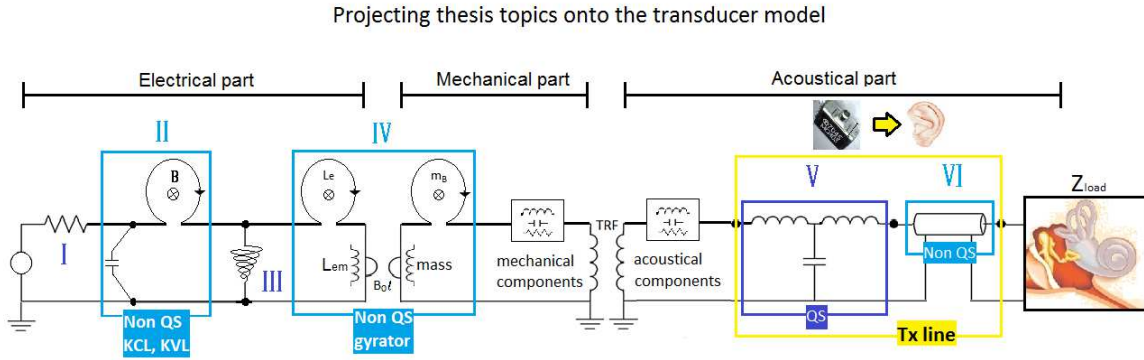


Figure 6: Overview of this study via the BAR model. All concepts discussed in this thesis can be tied together to understand the BAR transducer. The important concepts are highlighted using Roman characters. Note that QS components are marked as dark blue and non-QS components are in light blue.

227

228 The specific concepts covered in this study follow from a conceptual version of the BAR model  
 229 shown in Fig. 6. There are six highlighted parts in this figure labeled with capital Roman numerals.  
 230 Dark blue represent QS elements, while light blue shows non-QS elements. The left-most resistor  
 231 (part I) on the electrical side stands for the DC resistance of wire. It depends on the real part  
 232 of the wire resistance, with the internal noise attributed to the Brownian (thermal) motion of the  
 233 electrons in the resistor. The second part (II) defines two missing parameters (Lewin, 2002a,b) in  
 234 classic circuit theory, KVL and KCL, lead inductance due to the emf created by the magnetic field  
 235 ( $\dot{\mathbf{B}}$ ), and stray capacitance due to displacement current ( $\dot{\mathbf{D}}$ ), respectively. These components are  
 236 frequency-dependent terms embedded in Faraday’s law and Ampere’s law. According to Woodson  
 237 and Melcher (1968) either the lead inductance or the stray capacitance must be zero when defining  
 238 QS circuits. They define two cases: the stray capacitance ( $\dot{\mathbf{D}}$ ) is zero for electrostatic and the lead  
 239 inductance ( $\dot{\mathbf{B}}$ ) is zero for magnetostatic.

240 There are two types of leakage inductances. One is due to the air side of the coil ( $L_e$  in part IV)  
 241 and the other is from the semi-inductor leakage (part III) due to the magnetic field diffusion which  
 242 leads to the eddy-current in the iron core (Vanderkooy, 1989). This diffusive current is described  
 243 by the skin depth of the ferromagnetic material ( $\sqrt{\frac{2}{\mu\sigma\omega}}$ ), where  $\mu$ ,  $\sigma$  are the permeability and  
 244 conductivity of the material and  $\omega$  is the angular frequency.

245 Part IV characterizes the behavior of a non-ideal gyrotator. Two loop inductors ( $L_e$ ,  $m_B$ ) due  
 246 to the induced magnetic fields are associated with the self-inductor (mass in the mechanical side).  
 247 The ideal gyrotator, introduced by Tellegen (1948) does not employ these non-ideal loop inductors,

248 considering only the DC magnetic field of permanent magnets and the wire’s self-inductances (i.e.,  
 249 ‘ $F = B_0 l I$ ’ relationship from an ideal gyrator, where  $B_0$  is static magnetic field density due to the  
 250 permanent magnet and  $l$  is the length of the wire). Note that the non-ideal coupling coefficients  
 251 (or transfer impedances) are analogues to mutual inductance of a non-ideal transformer. Both the  
 252 ideal and non-ideal gyrators assume the QS approximation. This gyrator describes the transfer  
 253 impedances of electro-mechanical (or electro-acoustic) systems, namely  $T_{em}$ ,  $T_{me}$ , which have anti-  
 254 reciprocal characteristics due to Lenz’s law (1833).

255 Parts V and VI represent transmission lines, with (V) and without (VI), the QS approximation.  
 256 The behavior of this line in the low-frequency region can be estimated by lumped circuit elements, as  
 257 shown in part V. However, any delay, identified by the non-QS transmission line, cannot be modeled  
 258 via the QS approximation. Infinite numbers of resonance and anti-resonance (poles and zeros) are  
 259 observed in the magnitude of the impedance of the non-QS transmission line (VI). Therefore, it  
 260 is critical to clearly understand the transmission line, whether it is QS or non-QS, to describe the  
 261 system correctly. A typical and important application of this kind of transducer is the human  
 262 ear, as depicted in Fig. 6 as the terminating impedance,  $Z_{load}$ . The outer ear (i.e, ear canal) and  
 263 tympanic membrane (TM) can be modeled as a lossless transmission line (Puria and Allen, 1998;  
 264 Robinson and Allen, 2013; Parent and Allen, 2010), then the specific load is the middle ear.

265 Along with these concepts (parts I - VI), we also study the *motional impedance*  $Z_{mot}$ , a unique  
 266 characteristic of anti-reciprocal systems invented early in the 20th century. It was first introduced  
 267 experimentally (Kennelly and Pierce, 1912; Kennelly and Affel, 1915; Kennelly and Nukiyama, 1919;  
 268 Kennelly and Kurokawa, 1921; Kennelly, 1925); however, it has rarely been explained theoretically  
 269 (Mott and Miner, 1951). Along with the modeling work, we investigate  $Z_{mot}$ , based on an in-depth  
 270 analysis of the anti-reciprocal system. For this, we reduce the complexity of the proposed BAR  
 271 model, leaving only the essential elements, to represent a simpler electro-magnetic motor network.

272 We also reconsider the  $Z_{mot}$  formula based on each parameter’s spatial relationship. When  
 273 Maxwell formulated his equations, he used quaternions working in 4D space ( $x, y, z$  in the spatial  
 274 domain plus time  $t$ ). This work is critical because when we perform circuit simulation we usually do  
 275 not consider the spatial variation of each variable. Using quaternions to reformulate the definitions  
 276 of the Hunt parameters and  $Z_{mot}$  does not change the original formulas, discussed in previous  
 277 section (appendix D).

## 278 **A note about the ECE curriculum**

279 When modeling transducers, frequency domain tools are critical for both analysis and understand-  
 280 ing. These include 1-port and 2-port Network Theory (Van Valkenburg, 1964, 1960). This tools  
 281 naturally include the Fourier and Laplace Transforms, Power, Impedance, and various generaliza-  
 282 tions of these tools including the Impedance and transmission (ABCD) matrix, scattering matrices,  
 283 reflectance (Smith Chart). Also important are time domain tools, especially for nonlinear systems.  
 284 Popular tools include Matlab (ECE310/311) and Spice (ECE-342/343). At the heart of such anal-  
 285 ysis is the quasi-static (QS) approximation, which is typically defined in terms of the ratio of the  
 286 wavelength over the dimensions of the physical structure being analyzed. This ratio is typically  
 287 quoted as  $ka \ll 1$  where  $k = 2\pi/\lambda$  and  $a$  is the radius of the system or object being modeled.

288 Digital signal processing (DSP) is based on time domain processing but also uses the frequency  
 289 domain in the form of the DFT and Z-transform. The quasi-static approximation is not typically  
 290 assumed in DSP processing, since there is explicit delay built into the analysis in terms of the  
 291 sampling period, based on an estimate of the highest frequency being analyzed. Thus again an  
 292 upper bound on frequency is assumed, but not in terms of QS. This is a different model that  
 293 includes explicit delay.

294 Once the student is introduced to Maxwell's equations (ME), all these superficial distinctions  
295 are replaced by vector calculus, the wave equation, Gauss's Law, and Poynting's Power theorem  
296 ( $\mathbf{E} \times \mathbf{H}$ ) (1884).

297 In this thesis all of these ideas necessarily come into play at the same time. This is in part due  
298 to the merging of acoustics, with its slow wave speed, thus short wavelengths relative to the EM  
299 wavelengths (i.e., speed of sound and speed of light). While we use the QS approximation and its  
300 associated Brune impedance relationships, we must also generalize impedance to include the *wave*  
301 *impedance* seen in EM and acoustics. These two types of impedance complement each other. Wave  
302 impedance requires delay, as we have learned from DSP, whereas the Brune impedance obeys the  
303 QS approximation.

### 304 3 Historical notes

305 Two honored people inspired this study.

- 306 1. Arthur Edwin Kennelly (Dec. 17, 1861, Colaba, India - Jun. 18, 1939, Boston, U.S.A.) for  
307 the  $Z_{mot}$  study, and
- 308 2. Frederick Vinton Hunt (Feb. 15, 1905, Barnesville, OH - Apr. 21, 1972, Buffalo, New York)  
309 for the modeling BAR.

310 The first is Arthur Edwin Kennelly (Fig. 7 (a)), who was born in 1861 in India. Kennelly was 15  
311 years old when Bell submitted the telephone patent and 16 years old when Edison invented the  
312 carbon microphone. He is famous for working with Edison starting in 1887 in support of Edison's  
313 weaknesses (i.e., math, AC, and electro-magnetic studies); he was 26 years old when he joined  
314 Edison's group. He was a professor of electrical engineering at Harvard University from 1902-1930.  
315 He wrote his first paper on a loudspeaker in 1912 and worked at the Massachusetts Institute of  
316 Technology (MIT) from 1913-1924. Also, he was the first person to use the term impedance for AC  
317 circuits (A. E. Kennelly, "Impedance" American Institute of Electrical Engineers (AIEE), 1893).  
318 In this paper, he discussed the first use of complex numbers as applied to Ohm's law (1827) in  
319 alternating current circuit theory.

320 Along with these academic achievements in electro-engineering, the first analysis of the mag-  
321 netically driven moving-coil speaker's behavior, seen from the electrical side, was highlighted by  
322 Kennelly and Pierce (1912) and he, the creator of *impedance* analogy in AC circuits, called it mo-  
323 tional *impedance* ( $Z_{mot}$ ). This concept was intensively studied early in the 20th century based on  
324 experimental facts, without theoretical criticism. Kennelly actively published many investigations  
325 on  $Z_{mot}$ , making him a pioneer in loudspeaker analysis. However, a significant problem regarding  
326  $Z_{mot}$  is its negative real part, which appears to be a violation of energy conservation (Eq. 140).  
327 Including Kennelly's papers, the negative real part in  $Z_{mot}$  has never been clarified with regard to  
328 its physical properties (T.S.Littler (1934); Fay and Hall (1933); Hanna (1925)).

329 The second person who inspired this study was Frederick Vinton Hunt (Fig. 7 (b)), who was  
330 born in 1905 in Barnesville, Ohio. He was a professor at Harvard University, working in acoustic  
331 engineering. He contributed to underwater acoustics during World War II by developing the first  
332 modern sonar system. Other inventions and studies, including room acoustics, regulated power  
333 supply, lightweight phonograph pickups, and electronic reproduction equipment, are also important  
334 contributions he made to the field of electrical engineering.

335 Hunt published *Electroacoustics* in 1954, which is the basis of the current thesis (Hunt, 1954).  
336 In that book, he analyzed and synthesized the electro-acoustic (or electro-mechanical) system by



(a) A. E. Kennelly

(b) F. V. Hunt

Figure 7: (a): A. E. Kennelly (1861, India - 1939, U.S.A.) (b): F. V. Hunt (1905 - 1972, U.S.A.)

337 modeling it as 2-by-2 matrix using scalar forms of Lorenz's force and Maxwell's equations (i.e.,  
338 Ampere's law and Faraday's law).<sup>5</sup>

339 The remainder of this study is structured as follows: Chapter 2 introduces the theoretical con-  
340 cepts specifically related to designing electro-magnetic transducer models. Chapter 3 presents the  
341 experimental methods used in the study of the BAR. Chapter 4 includes the results from both the  
342 theoretical and experimental methods. Finally, the conclusions and contributions of this study are  
343 summarized in Chapter 5.

---

<sup>5</sup>It was done by distinguishing two constants  $j = \sqrt{-1}$  for a 90° phase shift and  $k = \sqrt{-1}$  for a 90° spatial phase shift. Hunt (1954) Chapter 3 pp.114,  $F = BlkI$ ,  $\Phi = Blku$ , where  $F$ ,  $I$ ,  $\Phi$ ,  $u$ ,  $B$ ,  $l$  are force, current, voltage, velocity, magnetic intensity, and length of wire respectively.

344 **Part II**

345 **Theoretical Methods**

346 In this section, we research important theoretical concepts to appreciate anti-reciprocal network,  
 347 such as Hunt’s two port network, Möbius transformation, Carlin’s network postulate, a gyrator,  
 348 a semi-inductor, and the motional impedance.

349 It will be useful to discuss a proper way to choose frequency domains for signals (i.e.,  $\Phi$ ,  $I$ )  
 350 and systems (i.e., power and impedance) at this point. Laplace frequency  $s = \sigma + j\omega$  is used to  
 351 indicating a Positive-Real (PR) characteristic of a system. In Laplace frequency plane, the abscissa  
 352 (x-axis) is for a real part ( $\sigma$  referring to any loss in a system) while the ordinate (y-axis) is for  
 353 an imaginary part ( $j\omega$  where  $\omega$  is an angular frequency or a Fourier frequency). PR functions  
 354 are strictly non negative on the right half of the Laplace plane to assume they obey the passive  
 355 condition (see, C3 in section 2). However,  $\Phi$  and  $I$  are classified as signals (not systems). They  
 356 do not need to obey the PR property. Therefore the angular Fourier frequency  $\omega$  is used for  $\Phi(\omega)$   
 357 and  $I(\omega)$ . For example, one can use Fourier transform to convert a voltage in the time domain  
 358 to a voltage in the frequency domain. But to convert power from one domain to the other, the  
 359 Laplace transform must be applied. Since impedance is a necessary part of power, the concept of  
 360 impedance ( $\mathcal{Z}$ ) is also described as a system, especially in a frequency domain, therefore we use  
 361 the Laplace frequency ‘s’ for  $\mathcal{Z}(s)$ . It is true for one or two port systems.

362 **1 Two-port anti-reciprocal network with Hunt parameters**

363 Hunt (1954) modeled an electro-mechanic system into a simple  $2 \times 2$  impedance matrix relationship.  
 364 There are four Hunt’s two-port network parameters, following Wegel (1921),  $Z_e(s)$ ,  $Z_m(s)$ ,  $T_{em}(s)$ ,  
 365 and  $T_{me}(s)$  where ‘ $s = \sigma + j\omega$ ’ is the Laplace frequency.

366 To explain each parameter, we convert a two-port ABCD matrix to the Hunt impedance matrix.  
 367 A schematic representation of this network is shown in Fig. 8 as depicted by Kim and Allen (2013).  
 368 As shown in Fig. 8, each network element may be represented with a 2 by 2 ABCD matrix, with the  
 369 velocity  $U$  defined as flowing out of the element (resulting in the ‘-’ sign). Thus multiple elements’  
 370 matrices can be ‘chained’ (i.e., factored) in accordance with different combinations of the elements  
 371 (i.e., series or shunt). This allows one to represent the network using matrix multiplication, which  
 372 enables convenient algebraic manipulation. Since the current (flow) is always defined into the port,  
 373 when we transform the ABCD matrix to an impedance matrix, it is necessary to force a negative  
 374 sign for the volume velocity to maintain tradition matrix requirements.

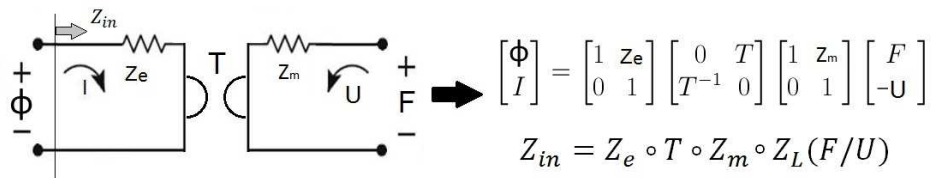


Figure 8: A schematic representation of an electro-mechanic system using Hunt parameters and Möbius composition of the ABCD matrix (Kim and Allen, 2013). Note how the ABCD matrix method “factors” the model into  $2 \times 2$  matrix. This allows one to separate the modeling from the algebra.

375 In practical electro-mechanical systems, all variables in the system ( $\Phi$ ,  $I$ ,  $\mathbf{F}$ ,  $\mathbf{U}$ ) are constrained  
 376 to a fixed direction of action (without considering spatial dependency), therefore relationships

377 between each quantity become scalar (Hunt, 1954). Especially when we analyze the system using  
 378 the ABCD matrix, we must treat all variables as the scalars.

379 The Hunt impedance matrix representation of the same system is

$$\begin{bmatrix} \Phi(\omega) \\ F(\omega) \end{bmatrix} = \begin{bmatrix} Z_e(s) & T_{em}(s) \\ T_{me}(s) & Z_m(s) \end{bmatrix} \begin{bmatrix} I(\omega) \\ U(\omega) \end{bmatrix}, \quad (5)$$

380 where  $s = \sigma + j\omega$ , and

$$Z_e(s) = \frac{\Phi(\omega)}{I(\omega)} \text{ when } U(\omega)=0, \quad (6)$$

381

$$T_{em}(s) = \frac{\Phi(\omega)}{U(\omega)} \text{ when } I(\omega)=0, \quad (7)$$

382

$$T_{me}(s) = \frac{F(\omega)}{I(\omega)} \text{ when } U(\omega)=0, \quad (8)$$

383

$$Z_m(s) = \frac{F(\omega)}{U(\omega)} \text{ when } I(\omega)=0. \quad (9)$$

384 For DC electromagnetic coupling,  $-T_{em} = T_{me} = T = B_0 l$ , where  $B_0$  and  $l$  are DC magnetic  
 385 field and length of wire, respectively. Along with Eq. 5, the two-port ‘electro-mechanic’ transducer  
 386 equation can alternatively be represented in ABCD (a.k.a. transmission matrix) form, as given by

$$\begin{bmatrix} \Phi(\omega) \\ I(\omega) \end{bmatrix} = \begin{bmatrix} A(s) & B(s) \\ C(s) & D(s) \end{bmatrix} \begin{bmatrix} F(\omega) \\ -U(\omega) \end{bmatrix}. \quad (10)$$

387 Here  $A$ ,  $B$ ,  $C$ ,  $D$  are functions of  $s$  to show they are causal (see, C4 in section 2) and complex  
 388 analytic ‘system’ variables. The signal variables  $\Phi$ ,  $I$ ,  $F$ ,  $U$  on the other hands are functions of  $\omega$ ,  
 389 to indicate they are neither causal, nor analytic.

390 The fundamental difference between the two matrix representations lies in the coupling of the  
 391 ‘electro-mechanic’ transducer, between the mechanical and the electric signals. Specifically, the  
 392 electrical input parameters  $\Phi$  and  $I$  on the left side of the network and Eq. 10 are expressed in  
 393 terms of the mechanical variables, the force  $F$  and the velocity  $U$ , on the right side of the network,  
 394 via the four frequency dependent parameters  $A$ ,  $B$ ,  $C$ , and  $D$ .

395 Conversion between Eq. 10 and Eq. 5 has the following relationships,

$$\mathcal{Z} = \begin{bmatrix} z_{11}(s) & z_{12}(s) \\ z_{21}(s) & z_{22}(s) \end{bmatrix} = \frac{1}{C} \begin{bmatrix} A(s) & \Delta_T(s) \\ 1 & D(s) \end{bmatrix}, \quad (11)$$

396

$$\mathcal{T} \begin{bmatrix} A(s) & B(s) \\ C(s) & D(s) \end{bmatrix} = \frac{1}{T_{me}(s)} \begin{bmatrix} Z_e(s) & \Delta_Z \\ 1 & Z_m(s) \end{bmatrix}. \quad (12)$$

397 where  $\Delta_Z = Z_e Z_m - T_{em} T_{me}$  and  $\Delta_T = AD - BC$ . Note that if  $C = 0$ ,  $Z$  does not exist. Eq. 12  
 398 represents Eq. 11’s inverse transformation, the conversion from impedance matrix to transmission  
 399 matrix.

400 Note that the impedance matrix is useful when making measurements. For instance, system’s  
 401 electrical input impedance and output acoustic impedance (or output mechanical impedance) can  
 402 be represented with the impedance matrix elements,  $z_{11}$  and  $z_{22}$ . The ABCD matrix representation  
 403 is useful for network modeling, but then may be transformed into an impedance matrix for exper-  
 404 imental verification. Symmetry relationships of the network (i.e., reversibility, reciprocity) based  
 405 on Eq. 11 are discussed in section 2.

## 406 1.1 Calibration of Hunt parameters for an electro-acoustic transducer

407 In this section, we employ Hunt parameters to electro-acoustic system,  $Z_e$ ,  $Z_a$  and  $T_a$ , where  
 408 subscript ‘a’ stands for ‘acoustic.’ the electro-acoustic Hunt parameters can be estimated from  $Z_{in}$   
 409 given three different acoustic load conditions. Similar to Eq. 5, the BAR can be represented by its  
 410 electro-acoustic impedance matrix as

$$\begin{bmatrix} \Phi(\omega) \\ P(\omega) \end{bmatrix} = \begin{bmatrix} Z_e(s) & -T_a(s) \\ T_a(s) & Z_a(s) \end{bmatrix} \begin{bmatrix} I(\omega) \\ V(\omega) \end{bmatrix}. \quad (13)$$

411 The acoustic load impedance  $Z_L$  is defined by Ohm’s law as ( $V$  is volume velocity defined as flowing  
 412 into the port)

$$Z_L \equiv \frac{P}{-V}. \quad (14)$$

413 Combining Eq. 13 and Eq. 14 and solving for  $V$  gives

$$V = \frac{-T_a I}{Z_L + Z_a}. \quad (15)$$

414 Replacing  $V$  in Eq. 13 gives an expression for the loaded electrical input impedance ( $V \neq 0$ )

$$Z_{in} \equiv \frac{\Phi}{I} = Z_e + \boxed{\frac{T_a^2}{\underbrace{Z_L + Z_a}_{Z_{mot}}}}, \quad (16)$$

415 where  $Z_{mot}$  is denoted the *motional impedance* due to the acoustic load shown in the electric  
 416 terminals (Hunt, 1954). Note that the sum of  $Z_a$  and  $Z_L$  in  $Z_{mot}$ ’s denominator is treated as  
 417 total acoustic impedance when it is looked at electrical side. Thus the  $Z_{in}$  obtained through  
 418 measurements depends on the acoustic load,  $Z_L$ . Varying the acoustic load, which can be done  
 419 by varying the length of the acoustic tube, results in different  $Z_{in}$  values (Fig. 25). The algebraic  
 420 details are provided in Appendix E.

## 421 2 Network postulates

422 An important terminology may be used to describe one-port and two-port networks, as defined  
 423 in this section. One can relate the limitations of the Brune’s impedance based on the one-port  
 424 network theory (Brune (1931); Serwy (2012)). To cross from one physical modality from the other  
 425 (Table 3), a two-port network must be used (Hunt, 1954; Carlin and Giordano, 1964).

426 Carlin and Giordano (1964) summarized two-port networks in terms of 6 postulates: C1-  
 427 Linearity, C2-time-invariance, C3-passivity, C4-causality, C5-real-time function, and C6-reciprocity.  
 428 Note that C6 only applies to two-port networks while others are for both one-port or two-port net-  
 429 works.

430 C1 Linearity (*vs.* Non-linearity): A system obeys superposition.

$$\alpha f(x_1) + \beta f(x_2) = f(\alpha x_1 + \beta x_2) \quad (17)$$

431 C2 Time-invariance (*vs.* time-variance): A system does not depend on the time of excitation,

$$f(t) = f(x(t)) \rightarrow f(t - t_1) = f(x(t - t_1)). \quad (18)$$

432 C3 Passivity (*vs.* Active): Conservation of energy law, Eq. 140. A system cannot provide more  
 433 power than supplied amount, where power is defined as

$$power(t) = \int^t i(t) \cdot v(t) dt. \quad (19)$$

434 C4 Causality (*vs.* Non-causality *vs.* Anti-causality): A response of a system cannot be affected  
 435 by a future response.

436 C5 Real-time function (*vs.* Complex-time function): The system's time response is real.

437 The systems' stability can be discussed via the impulse response, the transfer function, and the  
 438 poles and zeros of the system. An impedance can be interpreted as a transfer function for one-port  
 439 system, and through the inverse Laplace transform ( $\mathcal{L}^{-1}$ ), we can have its impulse response. In  
 440 terms of region of convergence (ROC) of the transfer function, the imaginary axis of the  $s$ -plane is  
 441 included in the ROC for a stable system. Specifically, for a system to be stable and bounded, all  
 442 poles are in the left half plane (LHP) in a causal system case, whereas all poles must be in the right  
 443 half plane (RHP) in an anti-causal bounded system case. A third category exists if the system  
 444 is causal and unbounded, when the poles are in the RHP. In this case, (there may be multiple  
 445 ROCs but usually) the ROC is the right sided plane from the most right pole.<sup>6</sup> Either BAR or  
 446 dynamic speaker, both types of transducers are categorized as two-port electro-acoustic systems,  
 447 converting electrical energy into acoustic pressure. Other examples of the two-port network can be  
 easily found in our daily lives. Table 1 shows some real life examples of the two-port networks.

Two-port network system	examples
Electro-mechanic	motors, bone vibrators
Electro-acoustic	loud speakers, ear-phones

Table 1: Example of two-port networks

448 All one-port postulates we discussed (C1-C5), can also be applied to two-port networks. One  
 449 strictly two-port postulate is Carlin's last postulate:  
 450

451 C6 Reciprocity (*vs.* Non-reciprocity *vs.* Anti-reciprocity): To be a reciprocal network, in terms  
 452 of conjugate variables described in Table 3, a generalized force is swapped to a flow across  
 453 one modality to the other (Eq. 20a). In other words, the two transfer impedances (the  
 454 two off-diagonal components) of the system's impedance matrix must be equal. The anti-  
 455 reciprocal network swaps the force and the flow, but one variable changes to the opposite  
 456 direction (Eq. 20b). A non-reciprocal network is a network which does not have reciprocal  
 457 characteristic. Note that the special case of a non-reciprocal network is the anti-reciprocal  
 458 networks (McMillan, 1946).

$$\begin{bmatrix} \Phi \\ F \end{bmatrix} = \begin{bmatrix} 0 & 1 \\ 1 & 0 \end{bmatrix} \begin{bmatrix} I \\ U \end{bmatrix} \quad (20a)$$

$$\begin{bmatrix} \Phi \\ F \end{bmatrix} = \begin{bmatrix} 0 & -1 \\ 1 & 0 \end{bmatrix} \begin{bmatrix} I \\ U \end{bmatrix} \quad (20b)$$

---

<sup>6</sup>If a pole ( $s_k$ ) is represented as  $s_k = \sigma_0 + j\omega_0$  where  $\sigma_0$  and  $\omega_0$  are the real and the imaginary parts of the pole. Then the 'right-most' pole of the system has the largest, the most positive  $\sigma_0$ .

460

$$\begin{bmatrix} \Phi \\ F \end{bmatrix} = \begin{bmatrix} 1 & 0 \\ 0 & 1 \end{bmatrix} \begin{bmatrix} I \\ U \end{bmatrix} \quad (20c)$$

461

462 There is another important property denoted ‘Reversibility’ (Van Valkenburg, 1964), where  
 463 the diagonal components in a system’s impedance matrix are equal (input impedance = output  
 464 impedance, Eq. 20c). In other words, the input force and flow are proportional to the output force  
 465 and flow, respectively. This postulate is only defined for the two-port network.

466

For the readers benefit, the six types of network symmetry are defined, as followed:

467

1. Reciprocal network: If  $z_{12} = z_{21} \Leftrightarrow \Delta_T = 1$  with  $C \neq 0$ .

468

2. Non-reciprocal network: all systems that are not reciprocal.

469

3. Anti-reciprocal network:  $-z_{12} = z_{21} \Leftrightarrow \Delta_T = -1$  with  $C \neq 0$ .

470

4. Reversible network:  $z_{11} = z_{22} \Leftrightarrow A = D, C \neq 0$ .

471

5. Reciprocal and reversible network:  $z_{11} = z_{12} \ \& \ z_{21} = z_{22} \Leftrightarrow A = D \ \& \ \Delta_T = 1$  with  $C \neq 0$ .

472

6. Anti-reciprocal and reversible network:  $-z_{12} = z_{21} \ \& \ z_{11} = z_{22} \Leftrightarrow A = D \ \& \ \Delta_T = -1$  with  
 473  $C \neq 0$ ,

474

where  $\Delta_T$  is the determinant of the transmission matrix. When  $C = 0$  or  $z_{21} = 0$ , conversion  
 475 between transmission matrix and impedance matrix is not possible.

476

Note that all categorized postulates are independent<sup>7</sup> including the reversibility (Carlin and  
 477 Giordano, 1964).

478

## 2.1 Additional postulates to include Brune’s impedance (Brune, 1931)

479

In addition to Carlin’s postulates for the one-port network (C1-C5), one should consider Brune’s  
 480 impedance as a highly limited extension of the one-port network properties. Otto Brune synthesized  
 481 the properties of one-port (or two terminals) PR networks in his Ph.D. thesis at MIT (Brune, 1931).  
 482 However the critical limitation of his network theory is that it assumes a quasi-static approximation.  
 483 This limitation has been addressed in Roger Serwy’s master thesis (Serwy, 2012).

484

B1 Positive-Real (PR):  $Z(s) = \Re(\sigma, \omega) + j\Im(\sigma, \omega)$ , where  $s = \sigma + j\omega$ . Then  $\Re(\sigma \geq 0) \geq 0$ . Note  
 485 that PR functions (i.e., impedances) are a subset of minimum phase functions. Therefore  
 486 impedance is a Positive-Definite (PD) operator. Moreover the order difference between num-  
 487 erator and denominator is  $\pm 1$  for PR. This concept is an expanded version of C1-C5.

488

B2 Quasi-static (QS) (*vs.* non quasi-static or ‘Einstein Causality’): Delay does not exist in the  
 489 QS system. The complement concept is ‘Einstein Causality’ meaning that the delay ( $\tau = \frac{x}{c}$ )  
 490 depends on a distance ( $x$ ) where ‘ $c$ ’ is the wave speed (sound or light,  $\delta(t - x/c)$ ). For a  
 491 quasi-static system,  $x = 0$ .

492

For further explanation of B1,  $Z(s)$  is represented as a rational polynomial fraction (pole-zero  
 493 pairs). It can be factored into first-order terms in  $s$  (Van Valkenburg, 1964)

$$Z(s) = \frac{\prod_{i=1}^L K_i(s - n_i)}{\prod_{k=1}^N K_k(s - d_k)} = \frac{|\rho| e^{j\theta_n}}{|r| e^{j\theta_d}} = \left| \frac{\rho}{r} \right| e^{j(\theta_n - \theta_d)}, \quad (21)$$

<sup>7</sup>It is not an absolute statement. There is an exception to this rule.

494 where  $K_i$  and  $K_k$  are scale factors. The  $s$  values for which  $Z(s)$  is zero ( $s = n_i$ ) and infinite  
 495 ( $s = d_k$ ) are called the system's zeros and poles. In the first definition of  $Z(s)$  in Eq. 21, any  
 496 poles and zeros that have the same complex location,  $n_i = d_k$ , (pairwise pole-zero, aka "removable  
 497 singularities") are canceled. Then, the product of zeros and poles can be represented in polar form  
 498 (middle definition in Eq. 21 with magnitude: $\rho$ ,  $r$ , phase: $\theta_n$ ,  $\theta_d$ ). Finally  $Z(s)$  has a reduced form  
 499 with its magnitude  $\frac{\rho}{r}$  and phase  $\theta_n - \theta_d$ . If a system satisfies the PR property, then the phase  
 500 difference  $|\theta_n - \theta_d|$  must be less than  $\frac{\pi}{2}$ . This means  $Z(s)$  is always positive in the Right Half Plane  
 501 (RHP). It follows that the difference in order between numerator and denominator cannot be more  
 502 than  $\pm 1$  or  $|L - N| \leq 1$  (Van Valkenburg, 1960).

503 This PR property is closely related to the positive definite (PD) matrix (operator property).  
 504 For an example, a  $(2 \times 2)$  impedance matrix  $\mathcal{Z}$  for a two-port network must have,

$$[\mathcal{I}_1 \quad \mathcal{I}_2] \begin{bmatrix} z_{11} & z_{12} \\ z_{21} & z_{22} \end{bmatrix} \begin{bmatrix} \mathcal{I}_1 \\ \mathcal{I}_2 \end{bmatrix} \geq 0, \quad \forall \mathcal{I}_1, \mathcal{I}_2, \quad (22)$$

505 or

$$\mathcal{I}^T \cdot \mathcal{Z}(s) \cdot \mathcal{I} \geq 0, \quad \forall \mathcal{I}(\omega). \quad (23)$$

506 Note this generalizes to a  $\mathcal{Z}_{2 \times 2}$  matrix, for example,  $\mathcal{Z}(s)$  and  $\mathcal{I}(\omega)$  are  $(2 \times 2)$  and  $(2 \times 1)$  matrices  
 507 respectively. And  $\mathcal{I}^T$  is the transpose of  $\mathcal{I}$ . Since  $\mathcal{Z}$  is PR, the matrix version of  $\mathcal{Z}$  is a PD operator.

508 The quasi-static property (B2) is an alternative way to specify C4. The definition of quasi-  
 509 static is "not having delay" ( $\tau[s] = \frac{\Delta_x[m]}{c[m/s]} = 0$ ) in a system. An equivalent definition inherently  
 510 exists in most classical circuit analysis such as KCL and KVL. Especially when we deal with an  
 511 electro-magnetic system, one or both of the time dependent terms in Maxwell's equation ( $\dot{\mathbf{B}}$  and  
 512  $\dot{\mathbf{D}}$ , where a dot represents the first-order time derivative) are zero. This point will be discussed  
 513 later in this study, section 5.2.

514 The antithesis of QS is non-QS, or "Einstein Causality," a delay existing in a system proportional  
 515 to a distance. The most relevant example is reflectance  $\Gamma$ , defined as

$$\Gamma(s) = \frac{Z(s) - 1}{Z(s) + 1}, \quad (24)$$

516 where  $\mathcal{L}^{-1}$  of  $Z(s)$  is  $z(t) \leftrightarrow Z(s)$ , such that  $z(t) = 0 \forall t < 0$ . Compared to C4, B32 limits the causal  
 517 boundary to be physical. Assuming, we live in a world within the theory of relativity of Einstein,  
 518 "Einstein Causality" is an appropriate characteristic to define a network when we talk about the  
 519 causality. All physical networks must obey B2.

520 Note that B1-B2 can be applied to both one and two port networks.

521 It is worth discussing the difference between 'static' and 'quasi-static'. The term 'quasi-static'  
 522 is different from 'static'. The 'static' system is not time-varying ( $\frac{d}{dt} = 0$ ). Serwy (2012) describes  
 523 two types of QS based on the definition of speed of light,  $c = \frac{1}{\sqrt{\mu_0 \epsilon_0}}$ ;  $\epsilon \rightarrow 0$  and  $\mu \rightarrow 0$  to realize  
 524  $c \rightarrow \infty$ . However this definition is inadequate since it conflicts with the definition of characteristic  
 525 impedance ( $\sqrt{\mu/\epsilon}$ ).

526 The concept of quasi-static still remains vague and needs a better definition. We claim that  
 527 it is necessary to move beyond quasi-static: one main reason is to handle the case of a physical  
 528 system, such as ear canal delay (i.e., the canal impedance needs to be factored into a delay and a  
 529 minimum-phase component and this means that it will not be a Brune impedance<sup>8</sup> (Robinson and  
 530 Allen, 2013). Details of this topic is discussed in section 5.1.

---

<sup>8</sup>The impedance at the probe can be fit to a Brune's form, but the ear canal is definitely better modeled as a delay line

531 **3 Generalization of the ABCD matrix using Möbius transformation**  
 532 **tion**

533 In this section, we explain how the Möbius transformation or bilinear transformation is an impor-  
 534 tant generalization of the ABCD transformation. In characterizing the ABCD transformation, a  
 535 cascading series of ABCD matrices is significant to simplify the algebra. It is equivalent to the  
 536 composition of Möbius transformations (Boas, 1987). This is a visual way of describing the ABCD  
 537 matrix.



Figure 9: Möbius strip sculpture at the Beckman Institute, UIUC. Möbius transformation matrix is presented underneath of the sculpture.

538 Equation 12 defines the relationship (conversion) between the impedance matrix and the ABCD  
 539 matrix. This formula maybe found in every electrical engineering text and is taught early in  
 540 undergraduate classes. The impedance matrix is a generalization of Ohm’s law. One side of each  
 541 equation has a force variable; the other side involves relation between two flows in the system. The  
 542 conversion to ABCD matrix results once the two equations are rewritten in terms of the first port’s  
 543 two variables, force and flow. The derivation is straightforward; however it is not completely clear  
 544 why the ABCD cascading method works. One can find the root of this method in the composition  
 545 of the Möbius transformation.

546 Let’s start with an example. The general form of a Möbius transformation is defined as a  
 547 rational function. We define two rational functions  $M_{a,b,c,d}(s)$  and  $M_{A,B,C,D}(z)$ ,

$$M_{a,b,c,d}(s) = \frac{as + b}{cs + d}, \text{ and } M_{A,B,C,D}(z) = \frac{Az + B}{Cz + D}. \quad (25)$$

548 where  $a, b, c, d, A, B, C$ , and  $D$  are any complex numbers satisfying  $AD - BC \neq 0$  and  $ad - bc \neq 0$ .  
 549 When  $ad = bc$  or  $AD = BC$ , Eq. 25 are not Möbius transformations.

550 For better visualizing of each Möbius function, 4 steps of transformations (compositions) are  
 551 introduced. Take one of the two formulas in Eq. 25,  $M_{a,b,c,d}(s)$  can be decomposed into 4 different  
 552 functions,

$$M_{a,b,c,d}(s) = M1_{a,b,c,d}(s) \circ M2_{a,b,c,d}(s) \circ M3_{a,b,c,d}(s) \circ M4_{a,b,c,d}(s), \quad (26)$$

553 where,

- 554 1.  $M1_{a,b,c,d}(s)$ :  $s + \frac{d}{c}$  translation by  $\frac{d}{c}$

- 555 2.  $M2_{a,b,c,d}(s)$ :  $\frac{1}{s}$  taking a inverse  
556 3.  $M3_{a,b,c,d}(s)$ :  $\frac{bc-ad}{c^2}s$  expansion and rotation  
557 4.  $M4_{a,b,c,d}(s)$ :  $s + \frac{a}{c}$  translation by  $\frac{a}{c}$

558 Composing the two functions in Eq. 25 leads the function  $Q(z)$ ,

$$Q(z) = M_{a,b,c,d}(s) \circ M_{A,B,C,D}(z) = \frac{as + b}{cs + d} \circ \frac{Az + B}{Cz + D} = \frac{a \left( \frac{Az+B}{Cz+D} \right) + b}{c \left( \frac{Az+B}{Cz+D} \right) + d}. \quad (27)$$

559 Finally we have

$$Q(z) = \frac{(aA + bC)z + (aB + bD)}{(cA + dC)z + (cB + dD)}. \quad (28)$$

560 Write two 2X2 matrix, based on the four coefficients in both  $M_{a,b,c,d}(s)$ ,  $M_{A,B,C,D}(z)$  in Eq. 25 and  
561 cascade the two matrix,

$$\begin{bmatrix} a & b \\ c & d \end{bmatrix} \begin{bmatrix} A & B \\ C & D \end{bmatrix} = \begin{bmatrix} aA + bC & aB + bD \\ cA + dC & cB + dD \end{bmatrix}. \quad (29)$$

562 It is therefore demonstrated that the composition of Möbius transformations (in Eq. 28 and Eq. 27)  
563 is equivalent (i.e., isomorphic) to the cascaded matrix of Eq. 29. It also applies to multiple matrix  
564 computation. As shown in Eq. 27, computational complexity will be increased as the order of the  
565 composition is increased. In such a case, the cascading matrix method is superior over composition.  
566 Cascading ABCD matrices in circuit theory is the best example of Möbius composition. When  
567 we compose a circuit system, we need lots of circuit components (e.g. Fig. 1). Therefore when  
568 analyzing a circuit using the ABCD matrix multiplication method, the algebra becomes trivial.

### 569 Example 1

570 Figure 10 depicts a circuit model with a series impedance  $Z$ . There are two inputs ( $\Phi_1, I_1$ ) and two  
571 outputs ( $\Phi_2, I_2$ ) to form this simple network. A well-known, ABCD matrix of a series impedance

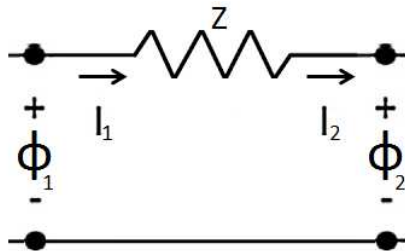


Figure 10: A series impedance ( $Z$ ) representation with inputs ( $\Phi_1, I_1$ ) and outputs ( $\Phi_2, I_2$ ). Note that, in this figure, all currents are defined as going out of the network.

571 ( $Z$ ) is given as  
572

$$\begin{bmatrix} \Phi_1 \\ I_1 \end{bmatrix} = \begin{bmatrix} 1 & Z \\ 0 & 1 \end{bmatrix} \begin{bmatrix} \Phi_2 \\ I_2 \end{bmatrix}, \quad (30)$$

573 where  $\Phi$  and  $I$  are the voltage and the current which is defined as going out of the network. And  
574 the subscripts 1 and 2 stand for the input port and the output port respectively. To form a rational

575 function using this relationship, take a ratio of the first and the second rows in Eq. 30 to have input  
 576 impedance  $Z_{in}$  as a function of the output impedance,  $Z_{out}$ ,

$$Z_{in}(Z_{out}) = \frac{\Phi_1}{I_1} = \frac{\Phi_2 + ZI_2}{0 + I_2} = \frac{\Phi_2/I_2 + Z}{0 + 1} = \frac{Z_{out} + Z}{0Z_{out} + 1}, \quad (31)$$

577 where the Eq. 31 may be changed by multiple of  $Z_{in}$  matrix itself. Representing Eq. 31 in Möbius  
 578 composition form,

$$M_{1,Z,0,1}(Z_{out}) = \frac{Z_{out} + Z}{0Z_{out} + 1} : [M] = \begin{bmatrix} 1 & Z \\ 0 & 1 \end{bmatrix}, \quad (32)$$

579 which is identical to the impedance matrix shown in Eq. 30. In summary, Eq. 30 is the matrix form  
 580 while Eq. 32 is the composition form.

581 As discussed early in this section, the parameter  $C$  (Eq. 10) for Eq. 31 is zero, therefore  $Z_{in}(\infty) =$   
 582  $\infty$ ; conversion to the impedance matrix is impossible for this case.

### 583 **Example 2**

584 This theory can be directly applied into any domain changing relationship such as the conversion  
 585 between reflectance  $\Gamma$  and impedance  $Z$ . The relationship between  $\Gamma$  and  $Z$  is

$$\Gamma_{1,-r_0,1,r_0}(Z) = \frac{Z - r_0}{Z + r_0} : [\Gamma] = \begin{bmatrix} 1 & -r_0 \\ 1 & r_0 \end{bmatrix}, \quad (33)$$

586 and its inversion relationship is

$$[\Gamma]^{-1} = Z = \frac{1}{2r_0} \begin{bmatrix} 1 & -r_0 \\ 1 & r_0 \end{bmatrix}, \quad (34)$$

587 where  $r_0$  is surge impedance.

588 In general we may show this as

$$Z_{A,B,C,D}(s) = \frac{As + B}{Cs + D} : [Z] = \begin{bmatrix} A & B \\ C & D \end{bmatrix}, \quad (35)$$

589 where  $s$  is Laplace frequency. It is standard to use round brackets  $Z(s)$  on the composition form  
 590 and square brackets  $[Z]$  on the matrix form. Composing Eq. 35 with Eq. 33,

$$\Gamma(Z) = \frac{\frac{As+B}{Cs+D} - 1}{\frac{As+B}{Cs+D} + 1} = \frac{(A-C)s + B - D}{(A+C)s + B + D}. \quad (36)$$

591 The coefficients in Eq. 36 are equivalently shown from the following matrix multiplication, cascading  
 592 Eq. 35 and Eq. 33 with  $z_0 = 0$  in Eq. 33,

$$\begin{bmatrix} 1 & -1 \\ 1 & 1 \end{bmatrix} \begin{bmatrix} A & B \\ C & D \end{bmatrix} = \begin{bmatrix} A - C & B - D \\ A + C & B + D \end{bmatrix}. \quad (37)$$

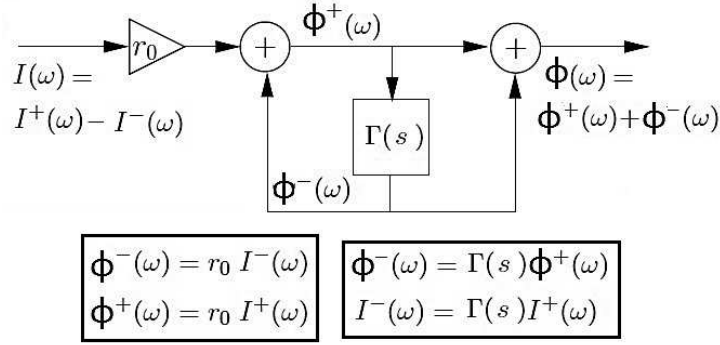
593 We have shown an example of the conversion relationship from  $Z$  to  $\Gamma$ . Now in Fig. 11 we consider  
 594 an inverted case, representing a relationship from  $\Gamma$  to  $Z$  with a simple diagram. We believe that  
 595 it will give us a better understanding of the composition method behind the algebra.

596 For the case of a lossless transmission line,

$$\Gamma(s) = e^{-s2L/c} \leftrightarrow \delta(t - 2L/c), \quad (38)$$

597 where  $L[m]/c[m/s]$  represents delay in the transmission line.

598 To summarize, multiplying 2X2 matrices is isomorphic to composition of the bilinear transfor-  
 599 mation.



$$\begin{aligned}
 Z(s) &\equiv \frac{\phi}{I} = \frac{\phi^+ + \phi^-}{I^+ - I^-} \\
 &= \frac{\phi^+}{I^+} \cdot \frac{1 + \Gamma(s)}{1 - \Gamma(s)} = r_0 \frac{\Gamma(s) + 1}{-\Gamma(s) + 1}
 \end{aligned}$$

$$Z(\Gamma)_{r_0, r_0, -1, 1} = r_0 \frac{\Gamma + 1}{-\Gamma + 1} : [Z](\Gamma) = \begin{bmatrix} r_0 & r_0 \\ -1 & 1 \end{bmatrix} (\Gamma)$$

Figure 11: Inverted relationship between reflectance ( $\Gamma$ ) and the wave impedance ( $Z$ ) shown in Eq. 37 where the conversion is made from  $Z$  to  $\Gamma$ . When we convert from  $\Gamma$  to  $Z$ , the matrix' diagonal elements are swapped compared to Eq. 37.

## 600 4 Motional Impedance ( $Z_{mot}$ )

601 Kennelly's first paper on  $Z_{mot}$  was published in 1912 (Kennelly and Pierce, 1912), it is referenced  
602 frequently in the extensive literature. The main point of this 1912 paper is that the impedance of  
603 a telephone receiver is different, when the diaphragm is free to vibrate, from when the diaphragm's  
604 motion is damped or blocked (Hunt, 1954). Kennelly defined  $Z_{mot}$  as the difference between the  
605 two (input) impedances with different boundary conditions, namely  $Z_{mot} = Z_{in}|_{free} - Z_{in}|_{blocked}$ .  
606 Details of the  $Z_{mot}$  definition maybe found in the next subsection (section 4.1)

607 Three years later, Kennelly published a second paper about  $Z_{mot}$  (Kennelly and Affel, 1915).  
608 In this paper,  $Z_{mot}$  is characterized in the  $Z$  plane (real and imaginary parts of the impedance,  $Z$ )  
609 as a circle shaped impedance passing through the origin of coordinates, with its diameter depressed  
610 through a certain angle (depressed compared to the circle in undamped impedance). Kennelly and  
611 Affel addressed these distinctive features in terms of the electrical and mechanical properties of  
612 the system. They described  $Z_{mot}$  using four constants,  $A$  (force factor),  $m$  (equivalent mass),  $r$   
613 (motional resistance), and  $k$  (stiffness constant). There are four unknowns, therefore four equations  
614 are needed to solve for  $Z_{mot}$ . Each of the four constants has the following relationship,

- 615 1. The resonant angular frequency  $\omega_0 = \sqrt{\frac{k}{m}}$ ,
- 616 2. The damping constant  $\Delta = \frac{r}{2m}$ , and
- 617 3. The magnitude of the  $|Z_{mot}| = \frac{A^2}{r}$ .

618 The missing fourth equation can be supplied by measuring any one of the four constants directly.  
619 In practice, what they actually did was to iterate for the four parameters (assuming one of the

620 constant is known) using least square method to estimate the  $Z_{mot}$  circle diagram. This is related  
 621 to Eq. 35 From the difference between two  $Z_{mot}$  circle diagrams, the last independent equation can  
 622 be found. The precise procedure may be found in Appendix E and in S. Ramo and Duzer (1965)  
 623 (section 11.07, pp.595).

624 Kennelly's third paper about  $Z_{mot}$  was published in 1919 (Kennelly and Nukiyama, 1919). In  
 625 this paper, he focused on power concept of  $Z_{mot}$ , and introduced the motional power diagram to  
 626 better physical understanding. The motional power diagram is drawn based on m.m.f. (magneto  
 627 motive force) generated by the vibration of the diaphragm in the permanent magnetic field. The  
 628 motional power can be regarded as a scaled motional impedance diagram. In their view, power is  
 629 a better concept to understand the system, compared to impedance.<sup>9</sup> He explained the motional  
 630 power circle by means of "active mechanical power ( $P_m$ )", which is defined as a difference between  
 631 electrical power ( $P_e$ ) and hysteresis power ( $P_h$ )

$$P_m = P_e - P_h. \quad (39)$$

632 The mechanical power observed from electrical side (the motional power circle) is depicted in  
 633 Fig. 12. This image is directly adapted from Kennelly and Nukiyama (1919), figure 27 in the  
 634 original paper. Based on the definition of  $P_m$  in Eq. 39, the negative real parts shown in motional  
 635 power diagram (Fig. 12) can be redefined as purely active mechanical power looking at the electric  
 636 part of the system.

637 Kennelly and Kurokawa published a fourth technical paper in 1921. The objective of this  
 638 paper is to describe some techniques to measure acoustic impedance including various constants  
 639 introduced in his three previous papers. Starting from definition of mechanical impedance, the  
 640 author explains specific ways of measuring the motional impedance, mechanical impedance, and  
 641 surge impedance. They also introduce a method to calculate the mechanical impedance ( $z_m$ ) from  
 642  $Z_{mot}$

$$z_m = \frac{A^2}{Z_{mot}} [\text{vector ohm}], \quad (40)$$

643 where  $A$  is a complex constant, representing the force factor. Note that this equation is presented  
 644 as equation 16 in the original paper (Kennelly and Kurokawa, 1921). This was before the anti-  
 645 reciprocal gyrator was invented. Dividing the complex constant  $A^2$  by the measured  $Z_{mot}$ ,  $z_m$  at  
 646 a single frequency (including the size and the slope) is obtained. Repeating this calculation for  
 647 several frequency points, the total  $z_m$  is determined. An example of  $z_m$  is shown in Fig. 13, along  
 648 with its theoretical value. The theoretical impedance for a shorted transmission line is defined as

$$z_0 \tanh(\beta l), \quad (41)$$

649 where  $z_0$ ,  $\beta$  are the surge impedance and wavenumber ( $\beta = 2\pi/\lambda$ ,  $\lambda$  is the wavelength), and  $l$  is  
 650 the length of the transmission line.

651 Acquiring values to calculate mechanical impedance ( $z_m$ , Eq. 40) seems somewhat troublesome  
 652 and inefficient. Historically, this work can be viewed as the first measurement of a mechani-  
 653 cal impedance  $z_m$  purely from electrical measurements. Four years later Kennelly published a  
 654 paper (Kennelly, 1925) specific to this idea based on the preliminary data from the work with  
 655 Kurokawa (Kennelly and Kurokawa, 1921), for measuring acoustic impedance electrically (Hunt,  
 656 1954).

---

<sup>9</sup>In 1919, impedance had not yet to be defined properly, which finally came about 12 years later in Brune's PhD thesis.

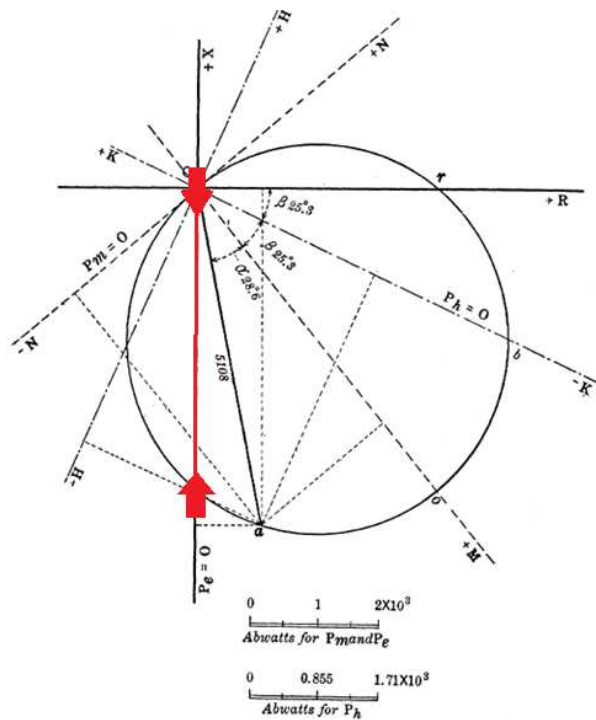


FIG. 27—MOTIONAL POWER DIAGRAM

Figure 12: The motional power diagram introduced by Kennelly and Nukiyama (1919). The x-axis and y-axis show resistive and reactive parts of the motional power respectively. When the resistance becomes negative (left part of the red line on the circle), power supplied from the electric part of the system no longer exists (It does not provide the mechanical power onto the diaphragm). Therefore (referencing at the electrical side) this part of the power is “active mechanical (motional) power”. All power in this region is consumed for hysteresis loss when the diaphragm is released (diaphragm is going back to its original position).

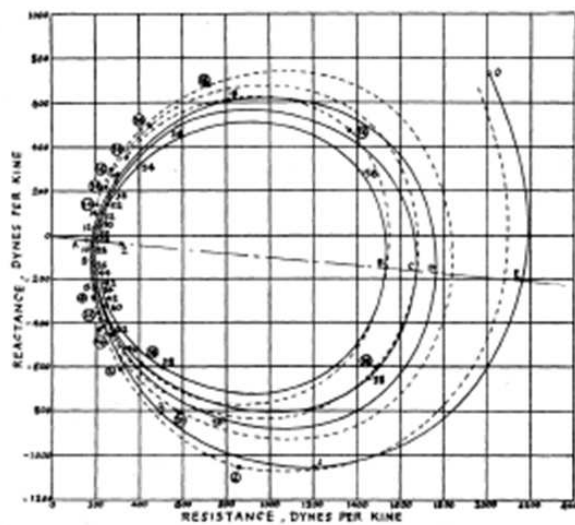


Figure 13: The calculated  $z_m$  (Eq. 40) graph by inverting  $Z_{mot}$  and then multiplying by the complex force factor  $A^2$  (Eq. 40). Solid curve is obtained by connecting observation values at each frequency point. The dotted line represents the computed (theoretical) values Eq. 41. Note that this image is shown as Figure 9 in the original manuscript (Kennelly and Kurokawa, 1921).

657 **Wegel 1921** Besides Kennelly, Wegel also considered  $Z_{mot}$  in his 1921 paper. This paper is  
658 credited by Hunt as the forefather of Hunt's 1954 two-port matrix representation (Eq. 5). Wegel  
659 takes account of the general theory of receiver structures using a simple schematic having four coils.  
660 As applications, he takes four different specific cases of a receiver: a simple receiver, a receiver with  
661 eddy currents in the core, a simple induction-type receiver, and an electro-dynamics receiver. One  
662 interesting point is he mentioned the effect of the eddy current, which decreases proportional to  
663 square root of the frequency when it flows around the core surface (page 797 on the last paragraph,  
664 Wegel (1921)). However the author did not derive any specific formula for this phenomenon, as it  
665 was simply an experimental observation. As a matter of fact, the observation of this phenomenon  
666 (the diffusion wave's impedance  $\propto \sqrt{\text{frequency}}$ ) has a long history. To fully appreciate this fact,  
667 the observation was related to the eddy current, the current flow from primary magnetic field, and  
668 finally analyzed using Maxwell's equation as carefully analyzed by Vanderkooy (1989), leading to  
669 the first definition of the semi-inductor with its impedance of  $Z_{semi} = K\sqrt{s}$ .

670 **Investigation of the circular shape of  $Z_{mot}$**  In terms of the "polar" impedance plane,  $Z_{mot}$  is  
671 a circle passing through the origin (Kennelly and Affel, 1915). Explaining the unusual shape may  
672 be explained in the physical nature of anti-reciprocal electro-mechanic system. The left side circuit  
673 (1) in Fig. 14 describes a (typical) mechanical electro-mechanic network. The series of a damper, a  
674 mass and a stiffness of the system are represented as circuit components  $R$ ,  $L$ , and  $C$  respectively.  
675 The  $Z_{mot}$  is defined as mechanical characteristic observed in electrical side, therefore simulation of  
676 these three main mechanical elements on the electrical side is our main concern.

677 Two circuits shown in Fig. 14 are functionally equivalent, (1) is physically intuitive due to using  
678 a gyrator, (2) is dual version of (1) via the mobility analogy (Firestone, 1938). Figure 15 simulates  
679 the two circuit cases in Fig. 14; blue line (1) without gyrator (purely mechanical case) and red line  
680 (2) decoding the gyrator using mobility method to see mechanical behavior on electrical input side.  
681 The upper and lower plots in left plane represent magnitude and phase of input impedance and the  
682 right polar plot shows real and imaginary parts of the impedance.

683 In Fig.15, the red circle on the polar plot ( $Z_{dual}$ ) shows  $Z_{mot}$  which is the dual of  $Z_M$  namely,

$$Z_M = R + \frac{1}{sC} + sL \Big|_{R,L,C=1} = 1 + \frac{1}{j\omega} + j\omega = \begin{cases} \infty & \omega \rightarrow \infty \\ 1 & \omega \rightarrow 1 \\ -\infty & \omega \rightarrow -\infty \end{cases}, \quad (42)$$

684

$$Z_{dual} = \frac{1}{R} || sC || \frac{1}{sL} \Big|_{R,L,C=1} = \frac{1}{1 + j\omega + \frac{1}{j\omega}} = \begin{cases} 0 & \omega \rightarrow 0 \\ 1 & \omega \rightarrow 1 \\ 0 & \omega \rightarrow \infty \end{cases}. \quad (43)$$

685 The reason we have a circle shape of  $Z_{mot}$  is because, we are observing mechanical behavior across  
686 the gyrator. Note that  $F_c$  stands for the transition frequency between  $C$  (low frequency) and  $L$   
687 (high frequency) for both original and dual of magnitude and phase plots. In polar plots, when  
688  $\Im Z \rightarrow +\infty$ ,  $Z$  is dominated by  $L$  and in case of  $\Im Z \rightarrow -\infty$ ,  $Z$  depends on  $C$ .

689 One may suggests a refined model of  $Z_{mot}$  based on Fig. 14. The only difference between real  
690 experimental data of  $Z_{mot}$  and the simulation in Fig. 15 is angular rotation of the circle (to clockwise  
691 direction) pivoted the circle at the origin, which will introduce the negative real part in  $Z_{mot}$ . One  
692 way to realize this model is to add a phase delay in the system ( $e^{-j\phi(\omega)}$ ) along with mechanical  
693 circuits.

694 Rotating the circle toward the negative real part is related to any shunt loss in electrical part  
695 of the system. The details are discussed in section 4.3.



Figure 14: The corresponding circuits for Fig. 15 (1) and (2), before (1) and after (2) mobility networking. Due to the gyrator, the mechanical components becomes dual when they are seen on the electrical side of the network. As investigated in Fig. 15, this makes the shape of the  $Z_{mot}$  circle.

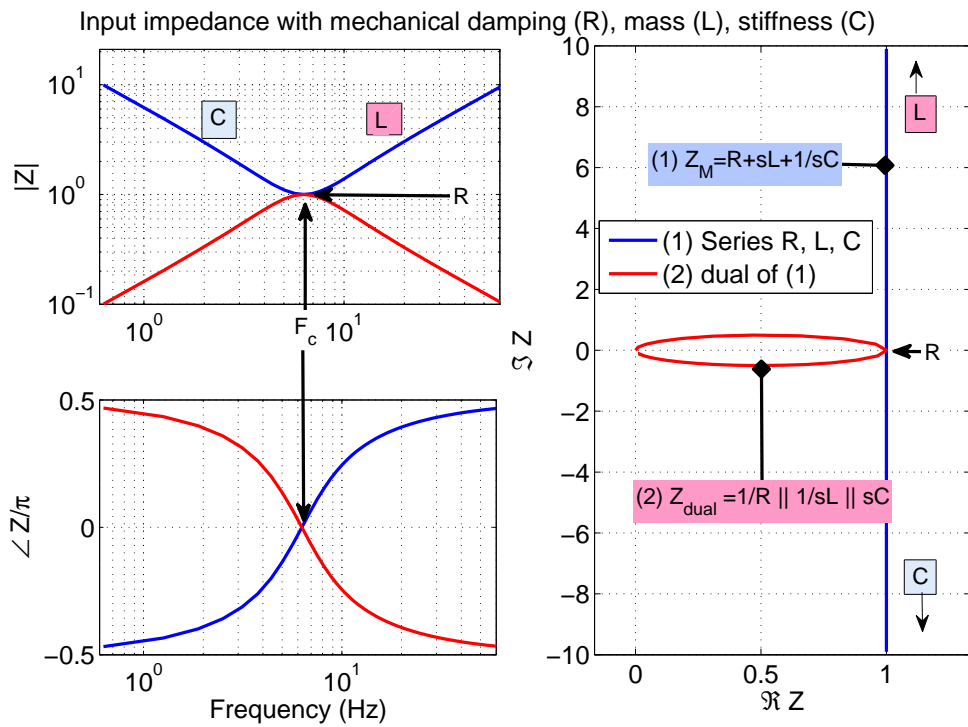


Figure 15: This figure explains the circular shape of  $Z_{mot}$  where the motion of the mechanical behavior (i.e., damping (loss), mass, and stiffness) projected to the electrical side defines  $Z_{mot}$ . When the mechanical behavior are seen on the electrical input side, due to the gyrator, the series mechanical network becomes a dual network based on the mobility analogy. The blue line shows input impedance based on the series relationship ((1) in Fig. 14 without considering the gyrator) while the red line represents the dual. The upper-left, lower-left plots show magnitude and phase of impedance and the right plot (polar plot) shows real and imaginary parts of the impedance. The red circle on the polar plot justifies the circular shape of  $Z_{mot}$ .  $F_c$  stands for the transition frequency between  $C$  (low frequency) and  $L$  (high frequency) for both original and dual of magnitude and phase plots. In polar plots, if  $\Im Z \rightarrow +\infty$ ,  $Z$  is dominated by  $L$  and in case of  $\Im Z \rightarrow -\infty$ ,  $Z$  depends on  $C$ . Note that this figure only discusses the shape of typical  $Z_{mot}$ , not its negative real parts. For simplification, values for  $L$ ,  $R$ , and  $C$  are '1' in this simulation.

696 **4.1 Definition of  $Z_{mot}$**

697 Physically,  $Z_{mot}$  can be interpreted as the impedance of the mechanical side of the system as seen  
 698 from the electrical input.  $Z_{mot}$  was first defined (Kennelly and Pierce, 1912) by taking a difference  
 699 between the mechanical open and the short circuit conditions, of electrical input impedance.

700 Starting from Hunt's impedance matrix (Eq. 5), we see that

$$\Phi = Z_e I + T_{em} U, \quad (44a)$$

701

$$F = T_{me} I + Z_m U. \quad (44b)$$

702 When the force 'F' is zero, i.e., "shorting out" the mechanical side, the electrical input impedance  
 703 is

$$\frac{\Phi}{I} = Z_e + \frac{T_{em} U}{I}, \quad (45a)$$

704 and

$$\frac{U}{I} = -\frac{T_{me}}{Z_m}. \quad (45b)$$

705 The "shorted" electrical input impedance is

$$Z_{in}|_{F=0} = \frac{\Phi}{I}|_{F=0} = Z_e - \frac{T_{em} T_{me}}{Z_m} = Z_e + Z_{mot}. \quad (46)$$

706 Thus  $Z_{mot}$  may be interpreted as the difference between the two mechanical boundary conditions  
 707 on the electrical impedance ( $Z_{in}$ )<sup>10</sup>:

- 708 1)  $Z_{in}$  with freely oscillating (vibrating) mechanical side (F=0: short circuit condition, Eq. 46),  
 709 2)  $Z_{in} = Z_e$  when the mechanical system is not allowed to move (U=0: open circuit condition,  
 710 Eq. 6),

$$\boxed{Z_{mot} = Z_{in}|_{F=0} - Z_{in}|_{U=0}}. \quad (47)$$

711  **$Z_{mot}$  definition using Hunt parameters** For the computational benefits, we can also define  
 712  $Z_{mot}$  from ABCD matrix parameters introduced in Eq. 10,

$$Z_{mot} = \frac{\Phi}{I}|_{F=0} - \frac{\Phi}{I}|_{U=0} = \frac{B}{D} - \frac{A}{C} = -\frac{\Delta_T}{DC} = \frac{1}{DC}, \quad (48)$$

713 where A, B, C, D are the transmission matrix parameters described in Eq. 10. Note that the  
 714 determinant of the transmission matrix ( $\Delta_T$ ) for an anti-reciprocal network is always '-1'.

715 To satisfy the positive real (PR) property of Brune's impedance (Brune, 1931),

$$\Re Z(s) \geq 0. \quad (49)$$

716 In Eq. 47, it is obvious the two individual terms  $Z_{in}|_{F=0}$  and  $Z_{in}|_{U=0}$  are PR functions as they are  
 717 physical, real impedances. A sum, or product of two PR functions has to be PR, but a difference,  
 718 which is  $Z_{mot}$ , will not be a PR function when  $\Re Z_{in}|_{U=0} > \Re Z_{in}|_{F=0}$ . Thus  $Z_{mot}$  is not a physically  
 719 realizable impedance. This because it is a transfer impedance, not a driving point impedance.

720 To be more detail on the problem, Eq. 47 may be written as

$$\boxed{Z_{mot} = -\frac{T_{em} T_{me}}{Z_m} = -T_{em} T_{me} Y_m}, \quad (50)$$

<sup>10</sup>The electrical conditions "open" and "short" are equivalent to the mechanical terms, "blocked" and "free", respectively. Electrically "open" means no current while "blocked" means no velocity.

721 where  $Y_m = \frac{1}{Z_m}$  is mechanical admittance, which is PR. Therefore the answer to our question  
 722 is reduced to investigation of the two transfer impedances' product  $T_{em}T_{me}$ . According to Hunt,  
 723  $T_{em} = B_0l$ , which is real and positive. We know that where  $T_{em} = T_{me}$  the system is reciprocal  
 724 and when  $T_{em} = -T_{me}$ , the system is anti-reciprocal.

725 The question here is, if  $Z_{mot}$  is PR. If the transfer impedances are real, then  $Z_{mot}$  must be PR.  
 726 However, if they are complex, then  $Z_{mot}$  could have negative real parts (negative resistance). It  
 727 has been observed (e.g., Fig. 12), the motional power has negative real parts.

## 728 4.2 $Z_{mot}$ interpretation with Eq. 50

729 If we define  $Z_{mot}$  using Eq. 50 (with Eq. 7, Eq. 8, and 9),  $Z_{mot}$  can be reinterpreted as

$$Z_{mot} = -\frac{\Phi_{I=0}}{U_{I=0}} \frac{F_{U=0}}{I_{U=0}} \frac{U_{I=0}}{F_{I=0}}, \quad (51)$$

730 where  $U_{I=0}$  terms are in both  $T_{em}$  and  $Z_m$  canceled out. This definition is interpreted based on  
 731 the system's signals, is quite different from Kennelly's experimental definition shown in Eq. 47. So  
 732 the remaining four terms represent  $Z_{mot}$ , which is

$$Z_{mot} = -\frac{\Phi_{I=0}}{I_{U=0}} \frac{F_{U=0}}{F_{I=0}}. \quad (52)$$

733 Lorenz force ( $\mathbf{F}_L$ ) is

$$\mathbf{F}_L = q(\mathbf{E} + \mathbf{U} \times \mathbf{B}), \quad (53)$$

734 where  $q$ ,  $\mathbf{E}$ ,  $\mathbf{U}$ , and  $\mathbf{B}$  represent a point charge, electric field, particle velocity, and magnetic field  
 735 respectively. From Eq. 53 one can infer the two terms  $F_{U=0}$ ,  $F_{I=0}$  in Eq. 52 are  $q\mathbf{E}$ , and  $q\mathbf{U} \times \mathbf{B}$   
 736 (or  $q\mu\mathbf{U} \times \mathbf{H}$ ,  $\mathbf{B} = \mu\mathbf{H}$ ).<sup>11</sup>

737 Also one may view  $\Phi_{I=0}$  in Eq. 52 is the Thevenin voltage ( $\Phi_{Th}$ ) considering only the electrical  
 738 side of the network (one-port system's open circuit voltage). And  $I_{U=0}$  is the electrical side's Norton  
 739 current ( $I_{No}$ ), as the  $U$  across the gyrator becomes  $\Phi$ , therefore the  $U = 0$  is equivalent to  $\Phi = 0$ ,  
 740 the shorted condition. The ratio of the Thevenin voltage and the Norton current is the Thevenin  
 741 electrical impedance ( $Z_{Th}$ ) representing the electrical side of the network ( $\frac{\Phi_{Th}}{I_{No}} = Z_{Th}$ ). Recall and  
 742 compare  $Z_{Th}$  to  $Z_e$  from Eq. 6, the open circuit electrical impedance.

743 To sum up: Eq. 52 can be rewritten as (scalars in frequency domain)

$$Z_{mot} = -\frac{\Phi_{I=0}}{I_{U=0}} \frac{F_{U=0}}{F_{I=0}} = -\frac{\Phi_{Th}}{I_{No}} \frac{q\mathbf{E}}{qU\mathbf{B}} \quad (54)$$

744 where  $\mathbf{B}$ ,  $\mathbf{E}$  represents scalar magnetic flux density and electric field in frequency domain respec-  
 745 tively.

746 Finally we have

$$Z_{mot} = -Z_{Th} \frac{q\mathbf{E}}{qU\mathbf{B}} = -Z_{Th} \frac{\mathbf{E}}{\mu U \mathbf{H}}, \quad (55)$$

747 where  $U$ ,  $\mathbf{H}$  are scalars in frequency domain.

748 From Eq. 55, we can consider the motional impedance as affected by the electrical impedance  
 749 ( $Z_{Th}$ ), as well as the mechanical velocity ( $U$ ).

<sup>11</sup>The current  $I = \int \mathbf{J} \cdot d\mathbf{S}$ . Based on Eq. 53,  $\mathbf{J}$  can be defined in two different ways,  $\mathbf{J}_e = \sigma\mathbf{E}$  and  $\mathbf{J}_m = q\mathbf{U}$ . The zero current specified in  $F_{I=0}$  is relevant to  $\mathbf{J}_e = 0$ , as the condition of  $U$  is still unspecified, therefore  $F_{I=0}$  indicates the magnetostatic force,  $q\mathbf{U} \times \mathbf{B}$ .

750 The semi-inductor (related to the magnetic diffusion wave) elaborated on Eq. 55 is part of  
 751  $Z_{mot}$ , causing the negative real parts. When the wave is diffusive, the diffusion time constant  
 752 (delay) can be characterized by the velocity  $\mathbf{U}$ . In Vanderkooy (1989, p.127), the author says  
 753 “physically, for an applied voltage step (i.e.,  $\underline{E}$  in Eq. 55), the coil will try to create a magnetic field  
 754 (i.e.,  $\underline{H}$  in Eq. 55) which takes a while to diffuse into the iron. Hence there will be no back emf for  
 755 the first instant, and the current waveform will rise sharply at the leading edge.” Highlighting the  
 756 words “takes a while,” may be interpreted as the delay resulting from the velocity  $\mathbf{U}$ . Thus the  
 757 voltage lags behind the current. When  $U = 0$ , there is no back emf. Note that  $\Phi = -B_0 l U$  is the  
 758 anti-reciprocal equation of the gyrator. Detail discussion may be found in section 5.3, Eq.86.

759 When the velocity  $U$  is zero, there is no magnetic force ( $q\mathbf{U} \times \mathbf{B} = q\mu\mathbf{U} \times \mathbf{H} = 0$  in Eq. 53).  
 760 Because the magnetic force is defined, when and only when, a charge is moving. However, the  
 761 electric force ( $q\mathbf{E} = 0$  in Eq. 53) exists with a stationary charge  $q$  (charge is not moving, zero  
 762 velocity). Therefore the denominator in Eq. 55 lags behind the numerator, and this phase shift can  
 763 make a part of  $Z_{mot}$ ’s real parts negative.

### 764 4.3 $Z_{mot}$ interpretation with Eq. 47

765 In this section, we search for a realizable (simple) circuit such that  $Z_{mot}$  has a negative real part.  
 766 Figure 16 demonstrates a case where a difference of two input impedances ( $Z_{in}$  with different  
 boundary conditions) goes negative.

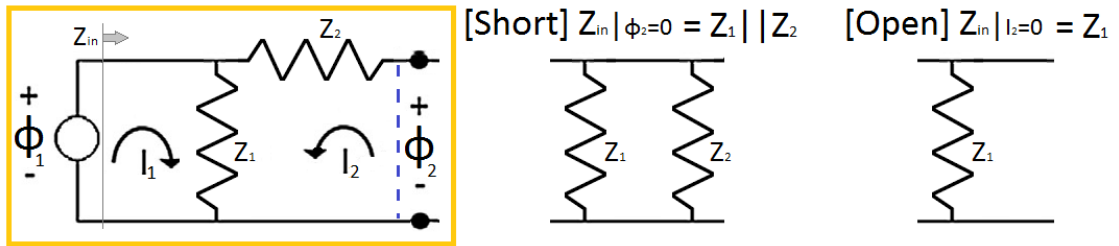


Figure 16: Demonstration of  $Z_{mot}$ ’s negative real part using a simple circuit example

767 For example, taking  $Z_1 = Z_2 = 100\Omega$ . Based on the definition of  $Z_{mot}$  (Eq. 47), subtracting the  
 768 open circuit impedance from the short circuit impedance results in  $-50\Omega$  ( $Z_{in}|_{\Phi_2=0} - Z_{in}|_{I_2=0} =$   
 769  $Z_1 || Z_2 - Z_1 = 50\Omega - 100\Omega$ ). This simplest example tells us a lot about the nature of  $Z_{mot}$ , as well  
 770 as modeling the electro-mechanic system.

771 Let’s consider a real example, an electro-mechanic system. If there is no **SHUNT** resistance  
 772 (i.e.,  $Z_1$ ) in a system,  $Z_{mot}$  cannot have negative real part, as may see from Fig. 16. The physical  
 773 meaning of the ‘shunt’ is this: any current through the shunted component cannot be seen from the  
 774 other components. The only physical place for this (shunt component) loss is in the eddy-current,  
 775 the diffusing current into magnetic core. It has been shown experimentally since Kennelly and  
 776 Pierce (1912), that  $Z_{mot}$  has negative real parts. This fact supports the view that a shunt loss in  
 777 the electrical side of the system must contribute to this loss (semi-inductor) when modeling the  
 778 system (Kim and Allen, 2013).  
 779

780 In the results (section 3), we study  $Z_{mot}$  from the physically based/simplified electro-mechanic  
 781 system. The real part of  $Z_{mot}$  (Eq. 47, Eq. 50) from the suggested two-port network is the target  
 782 of our investigation. Also in Appendix D, we reconsider  $Z_{mot}$  formula based on each parameter’s  
 783 spatial relationship.

## 5 Hidden, quasi-static assumptions in classic circuit theories

We revisit classic theories related to the anti-reciprocal circuit networks, such as KCL, KVL, the gyrator, and the semi-inductor. The purpose is to clarify quasi-static limitations in each well-known formula with derivations starting with Maxwell's equations.

### 5.1 Arguments about quasi-static approximation

The objective of this section is to devise another working definition of the quasi-static assumption. Starting from a physical example, such as the human ear, we claim that the key feature of the QS approximation is the absence of delay. To deal with this delay, one must use the reflectance  $\Gamma$ .

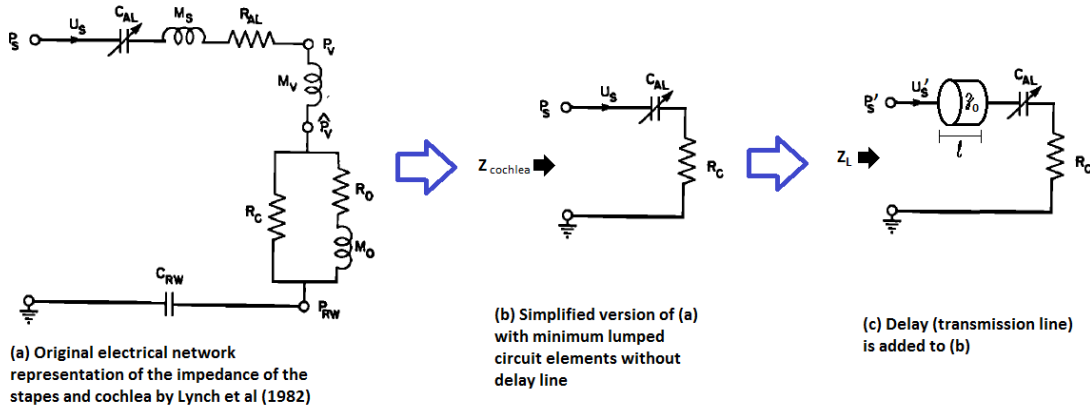


Figure 17: Electrical lumped circuit representations of the cochlea (adapted from Lynch et al. (1982)). (a) and (b) employ the quasi-static assumption where (b) is a simplified version of (a). A transmission line (length  $l$  and characteristic resistance  $r_0$ ) is used in (c), which introduces the delay  $\tau = l/c$  forcing  $Z_L$  to be non-quasi-static.

Figure 17 represents the acoustic impedance of the human ear in terms of electrical elements. Figure 17(a) is the network representations of the impedance of the stapes and cochlea (Lynch et al., 1982). In Fig. 17(b), we simplified this original model by considering only the significant components, the cochlear resistance  $R_C$  and nonlinear stiffness of the annular ligament  $C_{AL}$ . For this simplified version, the cochlear impedance is

$$Z_{cochlea} = R_C + \frac{1}{sC_{AL}}. \quad (56)$$

Note that both Fig. 17(a) and Fig. 17(b) use lumped (Brune's) circuit elements constituting a QS approximation, having no system delay.

To include the effect of the ear canal and ear drum delay (Puria and Allen, 1998), a transmission line (i.e., ear canal) is added, as shown in Fig. 17(c), with two extra parameters, length  $l$  and characteristic impedance  $r_0 = \frac{\rho c}{A}$ . Note that  $\rho$ ,  $c$ , and  $A$  are the air density, speed of sound, and area of ear canal, respectively. When  $l \rightarrow 0$ , the reflectance of this network is

$$\Gamma_0 = \frac{Z_{cochlea} - r_0}{Z_{cochlea} + r_0} = \frac{Z_0 - 1}{Z_0 + 1}, \quad (57)$$

where  $Z_0 = Z_{cochlea}/r_0 = \frac{R_C}{r_0} + \frac{1}{sC_{AL}r_0}$  is the normalized cochlear input impedance. Then reflectance at the measurement location  $L$  ( $\Gamma_L$ ) is

$$\Gamma_L = \Gamma_0 e^{-s\tau} = \Gamma_0 e^{-j\omega 2L/c}, \quad (58)$$

805 where  $s = \sigma + j\omega$  is the Laplace frequency and  $2L/c$  is the delay,  $\tau$ . Thus, the impedance at the  
 806 measured point  $L$  becomes

$$Z_L = r_0 \frac{1 + \Gamma_L}{1 - \Gamma_L}. \quad (59)$$

807 This model has been verified many times (Lynch et al., 1982; Puria and Allen, 1998; Parent and  
 808 Allen, 2010)

809 The final impedance does not obey the QS assumption (i.e., it is non-QS) due to the delay  $\tau$ .  
 810 It would require an infinite number of poles and zeros to form a QS approximation of this model,  
 811 due to the delay. Note that the difference between Eq. 56 and Eq. 59 is in the delay  $\tau = 2L/c$ .

812 The simulation comparison between Eq. 56 (QS) and Eq.59 (non-QS) is shown in Fig.18. The  
 813 very simple distinction between non-QS and QS is the number of poles and zeros. In the case of QS  
 814 ( $Z_{cochlea}$  red line), there is 1 pole and 1 zero, while in the non-QS case ( $Z_L$ , blue line), the system  
 has an infinite number of poles and zeros.

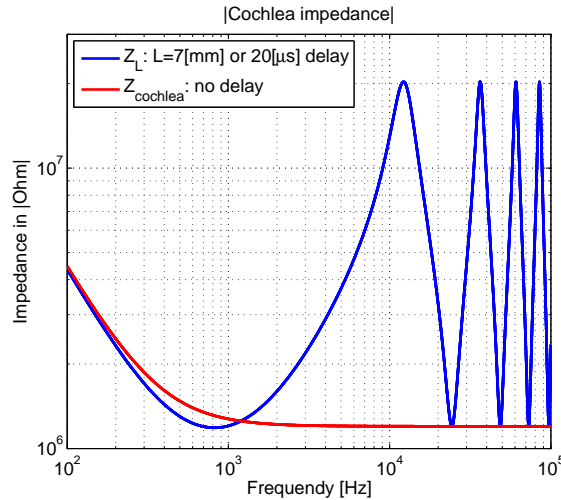


Figure 18: Input impedance simulation based on Fig.17. Values for the simulation are followed: Cochlea resistance  $R_c = 1.2e6[\text{dyn} - \text{s}/\text{cm}^5]$ , stiffness of the annular ligament  $C_{al} = 0.37e - 9[\text{cm}^5/\text{dyn}]$ , air density  $\rho = 1.14[\text{kg}/\text{m}^3]$ , speed of sound in room temperature  $c = 340[\text{m}/\text{s}]$ , area of ear canal  $A = r^2 * \pi[\text{m}^2]$  with  $r = 0.5[\text{cm}]$ , and length of ear canal  $L = 0.7[\text{cm}]$ .

815

816 Next, we will show how this example is equivalent to the traditional quasi-static description,  
 817 namely, the low-frequency or long-wave approximations.

### 818 5.1.1 Quasi-static in electromagnetism

819 The origin of QS approximation is not clear. However, the QS assumption has been widely used  
 820 in classic circuit analysis, such as Kirchhoff's circuit laws (KCL and KVL, 1845). Efforts to search  
 821 for the beginning of the QS in history can be found in Appendix A.

822 In 1865, James Clerk Maxwell completed his full mathematical description of electro-magnetic  
 823 fields using Michael Faraday's theory,<sup>12</sup>

$$\nabla \cdot \mathbf{D} = \rho \quad (60a)$$

824

$$\nabla \cdot \mathbf{B} = 0 \quad (60b)$$

<sup>12</sup>The original Maxwell's equations were written in 20 equations with 20 variables using quaternion. It was Oliver Heaviside who reformulated them into four vector equations having 4 variables by using curl and divergence vector operators (1884).

825

$$\nabla \times \mathbf{E} = -\frac{\partial \mathbf{B}}{\partial t} \quad (60c)$$

826

$$\nabla \times \mathbf{H} = \mathbf{J} + \frac{\partial \mathbf{D}}{\partial t}. \quad (60d)$$

827

828

829

830

831

832

833

834

835

836

837

838

839

840

841

842

843

844

845

846

Regardless of the appreciation for the QS theorem in Maxwell's time, the concept of QS can be applied to Eq. 60 by disregarding either the magnetic induction  $\dot{\mathbf{B}}$  (electro-quasi-static, EQS) or the electric displacement current  $\dot{\mathbf{D}}$  (magneto-quasi-static, MQS, Woodson and Melcher (1968)). With either of those terms removed, there can be no delay, since wave equation does not exist.

In EQS,  $\mathbf{E}$  is irrotational since  $\nabla \times \mathbf{E} = -\frac{\partial \mathbf{B}}{\partial t} \approx 0$  and  $\nabla \cdot \mathbf{D} = \nabla \cdot \epsilon_0 \mathbf{E} = \rho$ . Therefore, the curl and divergence of  $\mathbf{E}$  specify the charge density  $\rho$ . In the case of MQS,  $\mathbf{H}$  is rotational (solenoidal) as the divergence of  $\mathbf{H}$  is zero ( $\nabla \cdot \mu_0 \mathbf{H} = 0$ ) and  $\nabla \times \mathbf{H} = \mathbf{J} + \frac{\partial \mathbf{D}}{\partial t} \approx \mathbf{J}$ . Once the current density  $\mathbf{J}$  is known, the curl and divergence of  $\mathbf{H}$  can be solved in MQS.

To illustrate this, one can imagine a source distribution in each case (EQS with  $\rho$  or MQS with  $\mathbf{J}$ ). The solution for these equations ignores the delay between the source and measurement points (i.e., functionally,  $c \rightarrow \infty$ ). Thus, each field (EQS with  $\mathbf{E}$  or MQS with  $\mathbf{H}$ ) at a certain instant will be governed by its source,  $\rho$  or  $\mathbf{J}$ .

One interesting comparison is that in both the EQS and MQS situations, similar to Kirchhoff's circuit laws, the time-derivative terms are not considered. EQS ignores the  $\dot{\mathbf{B}}$  term (KVL) and MQS ignores the  $\dot{\mathbf{D}}$  (KCL). Sommerfeld (1964) explained this as "neglecting retardation of fields."

However, the QS definition used for MQS and EQS does not mean setting  $\frac{\partial}{\partial t} \rightarrow 0$ . For instance, impedance of lumped circuit elements (i.e., capacitors or inductors) cannot be defined if  $\frac{\partial}{\partial t} \rightarrow 0$ . Such elements are also known as the QS "Brune's impedance" (Brune, 1931; Van Valkenburg, 1960, 1964). Therefore, it is critical to search for a precise way to define QS systems.

### 847 5.1.2 Quasi-static descriptions

848 The QS assumption is loosely defined via the long wave approximation

$$kl \ll 1, \quad (61)$$

849 where  $k = \frac{2\pi}{\lambda} = \frac{2\pi f}{c}$  is the wave number ( $f$  is the frequency and  $c$  is the speed of sound or light) and  $l$  is the circuit dimension (Sommerfeld, 1964).

851 This QS description (Eq. 61) involves inequalities (i.e.,  $\gg$ , or  $\ll$  operator), which makes it  
852 confusing to specify each system's QS status. Moreover, when we deal with a physical system, such  
853 as the middle ear or a loudspeaker, it becomes even more difficult to properly characterize the QS  
854 system because of the relatively slow speed of sound. A more precise definition for QS is not based  
855 on inequalities. We shall shear that the proper definition depends on delay (The QS systems have  
856 no internal delay).

### 857 5.1.3 Transmission line and delay

858 Ohm's law (1781) represents the ratio of the voltage over the current as an impedance.<sup>13</sup> The now  
859 classical definition of QS impedance was first stated by Brune (1931).<sup>14</sup> He characterized a *point*

<sup>13</sup>At that time, the theory of impedance was applied only to resistance. It was Arthur Edwin Kennelly in 1893 who first suggested using the impedance concept in AC circuit.

<sup>14</sup>Brune's thesis was supervised by Wilhelm Cauer and Ernst Guillemin who were the top people in the field at the time.

860 impedance (Eq. 61) as a positive-real (PR) quantity (positive-definite operator in matrix version),  
 861 meaning that an impedance cannot have a negative resistance, i.e.,

$$Z(s) = \Re(\sigma, \omega) + j\Im(\sigma, \omega), \text{ then } \Re(\sigma \geq 0) \geq 0, \quad (62)$$

862 where  $s = \sigma + j\omega$ . This requires that the driving point impedance is defined as the ratio of two  
 863 polynomials, i.e.,  $Z(s) = N(s)/D(s)$ , such that the degree of difference in  $Z(s)$ 's numerator ( $N(s)$ )  
 864 and denominator ( $D(s)$ ) is  $\pm 1$ . This definition assures that the real part is positive in the right  
 865 half plane (RHP)(Brune, 1931). This is proved by Van Valkenburg (1960, 1964).

866 Brune's impedance is consistently studied with KCL and KVL under the QS condition because  
 867 it assumes no delay ( $\tau = 0$ ) in the system (Fig. 17 (a), (b)). For instance, wire delay in the  
 868 system is ignored. A Brune impedance network is represented using lumped circuit elements such  
 869 as resistors, inductors, and capacitors, but not delay. All Brune's impedances are minimum phase  
 870 (MP), because every PR function must be MP. Thus a Brune impedance is QS, PR, and MP. We  
 871 shall see that the more general "wave impedance" is PR but not QS (section 2).

872 A transmission line is a natural element to represent delay. Under the QS assumption, we as-  
 873 sume no delay (i.e., no transmission line). A transmission line is a two-port network, which can be  
 874 interpreted as the physical wire connecting the circuit components. As shown in Fig. 17, a trans-  
 875 mission line is required for physical modeling of the middle ear and electro-acoustic transducers,  
 876 especially where a delay plays a significant role in understanding the system (Kim and Allen, 2013;  
 877 Parent and Allen, 2010). The transmission line becomes critical when the signal's wavelength is  
 878 similar to or less than  $l$ . A delay ( $\tau$ ) is related to this  $l$ , defined as  $\tau = l/c$ , where  $c$  is the speed of  
 sound or light. Note that any system exhibiting modes requires a delay.

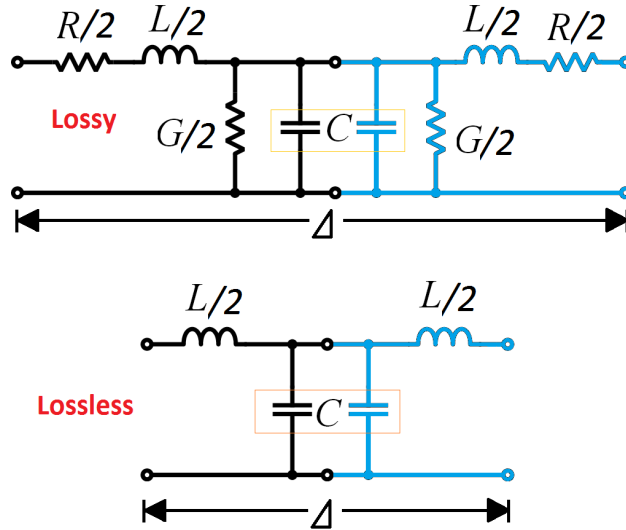


Figure 19: An infinitesimal unit of a transmission line (in the limit as  $\Delta \rightarrow 0$ ) having primary line constants,  $L$  (series inductance or mass per unit length [ $H/m$ ]),  $R$  (series resistance per unit length [ $\Omega/m$ ]),  $C$  (shunt capacitance or compliance per unit length [ $F/m$ ]), and  $G$  (shunt conductance per unit length [ $S/m$ ]). The upper figure represents a loss case while the lower figure is lossless case. Transmission segments are mirrored (shown in blue) to represent reversible transmission lines. By taking  $\Delta \rightarrow \infty$ , this goes from a QS to a true transmission line having a delay.

879

880

881

882

A low-frequency approximation of a transmission line, using lumped elements, is effectively a Brune approximation satisfying Eq.62. A popular and simple loss-transmission line approximation uses four elements:  $L$  (series inductance per unit length),  $R$  (DC resistance per unit length),  $C$

883 (shunt capacitance between the two conductors per unit length), and  $G$  (shunt conductance per unit  
884 length). In the lossless case,  $R$  and  $G$  can be ignored.<sup>15</sup> The remaining circuit elements,  $L$  and  $C$ ,  
885 represent an elementary unit of the lossless Brune (QS) transmission line. Usually infinite numbers  
886 of these units are cascaded when defining a transmission line. In terms of the transmission line  
887 per-length parameters (divided by the line length  $\Delta$ ), characteristic impedance  $r_0$  and propagation  
888 constant  $\kappa$  are computed as

$$r_0 = \sqrt{\frac{\mathcal{Z}}{\mathcal{Y}}}, \kappa = \sqrt{\mathcal{Z}\mathcal{Y}}, \quad (63)$$

889 where  $\mathcal{Z}|_{\Delta \rightarrow 0} = R + j\omega L$  and  $\mathcal{Y}|_{\Delta \rightarrow 0} = G + j\omega C$ . In the lossless case  $r_0 = \frac{L}{C}$ ,  $\kappa = s\sqrt{LC}$ . As shown  
890 in Fig. 19, the QS input impedance is

$$Z_{in, QS} = s(L/2) + \frac{1}{sC} \Big|_{@low\ freq} \approx \frac{1}{sC}. \quad (64)$$

891 However, the model for a true transmission line having delay, such as a coaxial cable, will differ  
892 from this QS transmission line segment (Eq.64). Cascading an infinite number of AS transmission  
893 line units and using Eq. 63, the input impedance of the transmission line becomes

$$Z_{in} = \frac{\Phi}{I}. \quad (65)$$

894 The voltage  $\Phi$  and current  $I$  are composed with outbound (+) and inbound (-) waves as

$$\Phi(x) = \Phi^+ e^{-\kappa x} + \Phi^- e^{+\kappa x}, \quad (66)$$

895

$$I(x) = \frac{1}{r_0} (\Phi^+ e^{-\kappa x} - \Phi^- e^{+\kappa x}). \quad (67)$$

896 Note that waves travel between  $x = 0$  and  $x = l$  based on each direction.

897 When we short the transmission line ( $\Phi = 0$  or  $Z_L = 0$ ),

$$Z_{in, short}(x) = r_0 \tanh(\kappa x), \quad (68)$$

898 and if it is opened ( $I = 0$  or  $Z_L = \infty$ ),

$$Z_{in, open}(x) = r_0 \coth(\kappa x). \quad (69)$$

899 Input impedance (magnitude) simulation results based on Eq. 64 and 69 are shown in Fig. 20.  
900 In this figure,

- 901 1. **Blue line:** Infinite numbers of poles and zeros exist with the exact transmission line formula  
902 (Eq. 69). These poles and zeros represent standing waves, based on the length of the line.
- 903 2. **Red line:** Number of poles and zeros is limited. There is one zero and one pole in this  
904 approximation. Compared to the blue line, this approximation works up to 2kHz.
- 905 3. **Green line:** One pole at the origin, and no zero is found. This approximation works under  
906 2kHz.

907 There is a finite number of poles and zeros in the QS (lumped circuit) approximation (red and  
908 green), while poles and zeros are infinite for the transmission line model (blue).

909 If a system is QS (having Brune's-type impedance), a finite number of poles and zeros exists  
910 and the number (degree) of poles and zeros is within  $\pm 1$ . If it is not QS (non-QS, having a delay),  
911 then the number of poles and zeros is infinite. It follows that any system having delay will have  
912 infinite numbers of modes without any exception. This is especially applicable for acoustical and  
913 mechanical systems.

---

<sup>15</sup>This transmission line model was created by Oliver Heaviside based on Maxwell's equations.

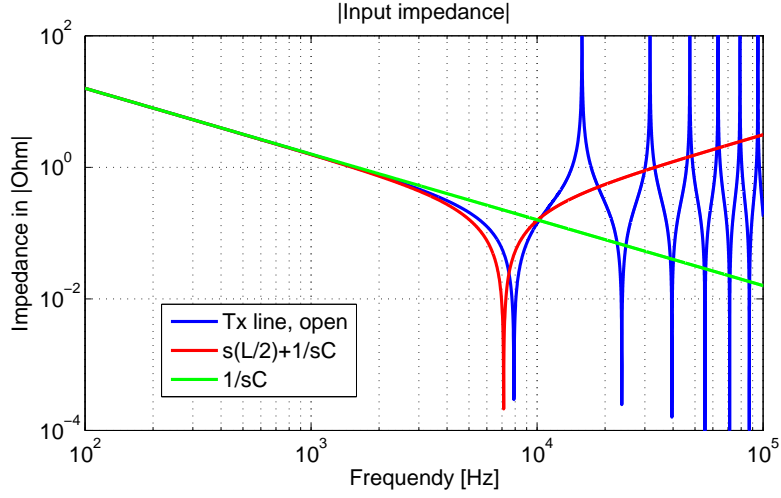


Figure 20: Simulation of transmission line input impedance from Eq. 64 and 68. Values for this specific example are  $L = 1e - 5$  [H/m],  $C = 1e - 4$ [F/m].

## 914 5.2 Kirchhoff's voltage and current laws (KVL, KCL)

915 **KVL** Equation 70 is the classical definition of KVL,

$$\sum_{k=1}^n \phi_k = 0, \quad (70)$$

916 where  $\phi_k$  is a voltage at each node  $k$  in a circuit.

917 Starting from Faraday's law

$$\nabla \times \mathbf{E} = -\frac{\partial \mathbf{B}}{\partial t}, \quad (71)$$

918 and applying Stoke's theorem, an electric potential (voltage) is defined as a line integral over an  
919 electric field.

$$\int (\nabla \times \mathbf{E}) \cdot d\mathbf{A} = -\frac{\partial}{\partial t} \int \mathbf{B} \cdot d\mathbf{A}, \quad (72)$$

920 it equals to

$$\oint \mathbf{E} \cdot d\mathbf{l} + \underbrace{\frac{\partial}{\partial t} \int \mathbf{B} \cdot d\mathbf{A}}_{\Psi, \text{ flux}} = 0. \quad (73)$$

921 The first term in Eq. 73 represents emf, the direction is opposite to the voltage.

$$\text{emf} \equiv \oint \mathbf{E} \cdot d\mathbf{l} = \int_a^b \mathbf{E}' \cdot d\mathbf{l} = -\phi(t), \quad (74)$$

922 where  $E$  is the electric field intensity measured by an observer moving with the contour of the  
923 conductor and  $\mathbf{E}' = \mathbf{E} - (\mathbf{u} \times \mathbf{B})$  (Woodson and Melcher, 1968) based on the quasi-static Lorenz  
924 force (Eq. 53). To arrive at the classical KVL, Eq. 70, the quasi-static assumption that  $\mu_0 \rightarrow 0$   
925 ( $-\frac{\partial \mathbf{B}}{\partial t} = -\mu_0 \frac{\partial \mathbf{H}}{\partial t} = 0$ ) must be assumed. In other words, the classic KVL is valid when the magnetic  
926 field is not time-varying (i.e., a constant  $\mathbf{B}_0$  or very slowly changing in time). The classic KVL  
927 equation deals with the quasi-static ( $\mu_0 \rightarrow 0$ ) electric field with a stationary charge and thus

928 assumes the electric field around a closed loop to be zero. Therefore Eq. 70 is a special, quasi-static  
 929 case of KVL, in general form of KVL is

$$-\sum_{k=1}^n \phi_k + \dot{\Psi} = 0, \quad (75)$$

930 where  $\dot{\Psi}$  is time derivative of the magnetic flux  $\Psi$ . In a frequency domain Eq. 75 becomes

$$-\sum_{k=1}^n \Phi_k + j\omega \underline{\Psi} = 0, \quad (76)$$

931 where  $\underline{\Psi} = L_m I$  represents the magnetic flux in frequency domain. Finally we have

$$\boxed{\sum_{k=1}^n \Phi_k = sL_m I}, \quad (77)$$

932 meaning that, the sum of the  $\Phi_k$  is the induced voltage (emf) in RHS is equal to the LHS which  
 933 represents the mutual inductance ( $L_m$ ). Typically the leakage flux is considered as an undesirable  
 934 effect (mutual inductive leakage flux).

935 **KCL** To derive KCL, Gauss's law and Ampere's law (Eq. 78 and Eq. 79 respectively) must be  
 936 used. Note that Eq. 79 and Eq. 107 are equivalent. The Gauss's law is

$$\nabla \cdot \mathbf{D} = \rho, \quad (78)$$

937 and the Ampere's law is

$$\nabla \times \mathbf{H} = \mathbf{J} + \frac{\partial \mathbf{D}}{\partial t}. \quad (79)$$

938 We apply a divergence theorem on Eq. 79, the left term ( $\nabla \cdot (\nabla \times \mathbf{H})$ ) becomes zero as divergence  
 939 of the curl is zero. Then assuming a quasi-static magnetic field, then  $\frac{\partial \mathbf{D}}{\partial t} = 0$  (Eq. 79),

$$\nabla \cdot \mathbf{J} + \frac{\partial(\nabla \cdot \mathbf{D})}{\partial t} = \nabla \cdot \mathbf{J} + \frac{\partial \rho}{\partial t} = 0. \quad (80)$$

940 Via the Divergence theorem,

$$\int (\nabla \cdot \mathbf{J}) \cdot d\mathbf{V} + \frac{\partial}{\partial t} \int \rho d\mathbf{V} = \int (\nabla \cdot \mathbf{J}) \cdot d\mathbf{V} + \frac{\partial Q}{\partial t} = \underbrace{\int \mathbf{J} \cdot d\mathbf{A}}_{i(t)} + \dot{Q} = 0. \quad (81)$$

941 One can deduce the classical KCL from the Eq. 81. The net flux of current at a point (node) is  
 942 zero (the classic KCL assumption, no accumulating current at a node) when we ignore the stray  
 943 capacitance  $\dot{Q}$ . Therefore the correct KCL is,

$$\sum_{k=1}^n i_k + \dot{Q} = 0, \quad (82)$$

944 and the frequency domain representation of Eq. 82 is,

$$\sum_{k=1}^n I_k + sQ = 0. \quad (83)$$

945 Note that  $Q = C\Phi$  is physically interpreted as stray capacitance ( $C$ ) related to current between two  
 946 adjacent inductors. Usually it is considered to be an undesirable effect (capacitive leakage current),

$$\boxed{\sum_{k=1}^n I_k = -sC\Phi}. \quad (84)$$

947 Note that the difference in the sign for Eq. 77 and Eq. 84 follows from Lenz's law.

948 **Extension of KCL/KVL to include flux coupling and time delay** When KVL and KCL  
 949 are derived from Maxwell's equations, electrostatic and magnetostatic assumptions (i.e., quasi-  
 950 static) are used respectively in section 5.2. In the KCL derivation, the coupling of a charge, due to  
 951 a stray capacitance ( $\frac{\partial \mathbf{D}}{\partial t}$ ), is ignored while for the KVL the magnetic flux coupling (stray mutual  
 952 inductance,  $-\frac{\partial \mathbf{B}}{\partial t}$  in Eq. 71) is ignored. That is, in both cases the time-dependent components in  
 953 the Maxwell's equations are assumed to be negligible, since

$$\lambda \left( = \frac{c}{f} \right) \geq \text{circuit size} \quad (85)$$

954 where 'c' is the speed of light, and 'f' is frequency of interest. This is a low frequency approximation  
 955 where the standard KVL and KCL apply under the quasi-static assumption.

956 However, the ignored terms in KVL or KCL have their own significance. For example, when  
 957 current flows through a wire, there is a magnetic field created around the wire. The flux in a KVL  
 958 loop has an induced flux ( $\Psi$ ) that induces an emf ( $\dot{\Psi}$ ). This term results in the anti-reciprocal  
 959 coupling terms that requires the gyrator in the Hunt matrix (Eq. 93 and Eq. 94), and it has been  
 960 ignored in the KCL/KVL analysis based on the time dependency of the magnetic field in the  
 961 system. Also in terms of the wave equation, both  $\dot{\mathbf{B}}$  and  $\dot{\mathbf{D}}$  terms allow us to derive the wave  
 962 equation describing delay, and without them we get diffusion equations.

963 This discussion can be extended to the limitation of general circuit theory, the quasi-static  
 964 assumption. Once we include time delay (elements that include the wires), one must consider the  
 965 finite transit time when describing circuits. To clearly relate the delay to a dimension, we defined  
 966 a term "Einstein causality" as a generalization of causality (B2 in section 2.1).

### 967 5.3 Gyrator

968 A two-port network, such as an electro-mechanic system has  $\Phi$ ,  $I$ ,  $\mathbf{F}$ , and  $\mathbf{U}$  as the system's  
 969 variables. A gyrator exists to couple the electric and mechanical sides. Specifically, through the  
 970 gyrator, the potential,  $\Phi$ , maps to the velocity  $-\mathbf{U}$  and the current  $I$  maps to the force  $F$ . To show  
 971 this property, one can employ the impedance matrix of the gyrator

$$Z_{gyrator} = \begin{bmatrix} 0 & -G \\ G & 0 \end{bmatrix}, \quad (86)$$

972 where  $G = B_0 l$  is the gyration coefficient,  $B_0$  is the DC magnetic field and  $l$  is the length of the  
 973 wire. Thus

$$\begin{bmatrix} \Phi(\omega) \\ F(\omega) \end{bmatrix} = \begin{bmatrix} 0 & -B_0 l \\ B_0 l & 0 \end{bmatrix} \begin{bmatrix} I(\omega) \\ U(\omega) \end{bmatrix}. \quad (87)$$

974 namely,

$$\Phi(\omega) = -B_0 l U(\omega) \text{ and } F(\omega) = B_0 l I(\omega). \quad (88)$$

975 When defining an impedance, the flow direction is defined as into the terminals, thus  $U$  is defined  
 976 as going into the network. Thus, the minus sign of  $U$  in Eq. 88 follows from the Lenz's law. Note  
 977 that Eq. 88 explains an ideal gyrator, considering only a DC magnetic field.

978 **The non-ideal gyrator** Here we derive the nature of the gyrator from the basics of electro  
 979 magnetism. Ulaby (2007) described the induced emf (voltage  $\phi$ ) as the sum of a transformer  
 980 component ( $\phi_{tr}$ ) and a motional component ( $\phi_{mot}$ ) namely,

$$\phi(t) = \phi_{tr} + \phi_{mot}. \quad (89)$$

981 The transformer voltage is  $\phi_{tr} = -(-\int \frac{\partial \mathbf{B}}{\partial t} \cdot d\mathbf{A}) = \frac{\partial \psi}{\partial t}$ , where  $\psi$  is magnetic flux. In the static  
 982 case ( $\frac{d}{dt} = 0$ ), the time-varying term is zero.

983 The  $\phi_{mot}$  represents the motion of electrical voltage as observed from the mechanical side  
 984 (motional voltage due to  $u$ ). Derivation of  $\phi_{mot}$  starts from the Lorentz magnetic force ( $\mathbf{f}_m$ ), acting  
 985 on a moving charge  $q$  inside a magnetic field  $\mathbf{B}$  with a velocity  $\mathbf{U}$ ,

$$\mathbf{f}_m = q(\mathbf{U} \times \mathbf{B}). \quad (90)$$

986 Then the motion of magnetic force from the electrical field  $\mathbf{E}_{mot}$  is  $\mathbf{f}_m = q\mathbf{E}_{mot}$ ,<sup>16</sup> therefore

$$\mathbf{E}_{mot} = \frac{\mathbf{f}_m}{q} = \mathbf{U} \times \mathbf{B}, \quad (91)$$

987 where  $\mathbf{E}_{mot}$  is the motional electric field seen by the charged particle  $q$  and its direction is perpen-  
 988 dicular to both  $\mathbf{U}$  and  $\mathbf{B}$ .

989 Thus the voltage  $\Phi_{mot}$  is defined as the line integral of the corresponding electric field which is  
 990  $\mathbf{E}_{mot}$  in this case,

$$\phi_{mot} = -\oint_C \mathbf{E}_{mot} \cdot d\mathbf{l} = -\oint_C (\mathbf{U} \times \mathbf{B}) \cdot d\mathbf{l}. \quad (92)$$

991 Note that only this term has been considered in an ideal gyrator.

992 Finally, the total voltage is

$$\phi = \phi_{tr} + \phi_{mot} = \int \frac{\partial \mathbf{B}}{\partial t} \cdot d\mathbf{A} - \oint_C (\mathbf{U} \times \mathbf{B}) \cdot d\mathbf{l}. \quad (93)$$

993 In the frequency domain with scalars, Eq. 93 is rewritten as

$$\Phi = s\Psi - BIU = sL_e I - BIU, \quad (94)$$

994 where  $L_e$  is a leakage inductance due to the leakage flux of a self-inductance in the electrical side,  
 995  $\Psi = L_e I$ .

996 Assuming a static DC magnetic field ( $B_0$ ), then  $s\Psi = 0$  and we find the ideal gyrator definition  
 997  $\Phi = \Phi_{mot} = -UB_0 l$  (Eq. 88). Note that the frequency dependant term shown in Eq. 94 ( $j\omega\Psi$  and  
 998  $j\omega L_e I$ ) is non QS term that is not considered in an ideal gyrator. The minus sign for the other  
 999 term  $-UBl$  is related to Lenz's law.

1000 Figure 21 shows a simple experiment to demonstrate Lenz's law, using a magnet and an amme-  
 1001 ter. Moving the north pole of a magnet towards the coil causes positive current  $I$ . The motion that  
 1002 the magnet is pushed into the coil reveals the negative direction of the  $\Psi$  or emf. If the magnet is  
 1003 pulled out from the coil (positive  $\Psi$  or emf), the direction (sign) of the current is reversed. When  
 1004 there is no motion of the magnet, then the current does not flow. A faster moving magnet creates  
 1005 a larger induced current.

---

<sup>16</sup>The unit of  $q$  is in coulombs[C],  $\mathbf{E}_{mot}$  is in [V/m]=[N/C] as  $1V \equiv 1J/C$  and  $1N = 1J/m$ . Therefore  $q\mathbf{E}$  stands for force with a unit of [N]. A positive charge ( $q > 0$ , proton) is  $1.602 \times 10^{19}$ [C], thus the charge of an electron (negative charge) is  $-1.602 \times 10^{19}$ [C]. One Coulomb of charge equals to the charge which can light a 120-watt-bulb for one second.

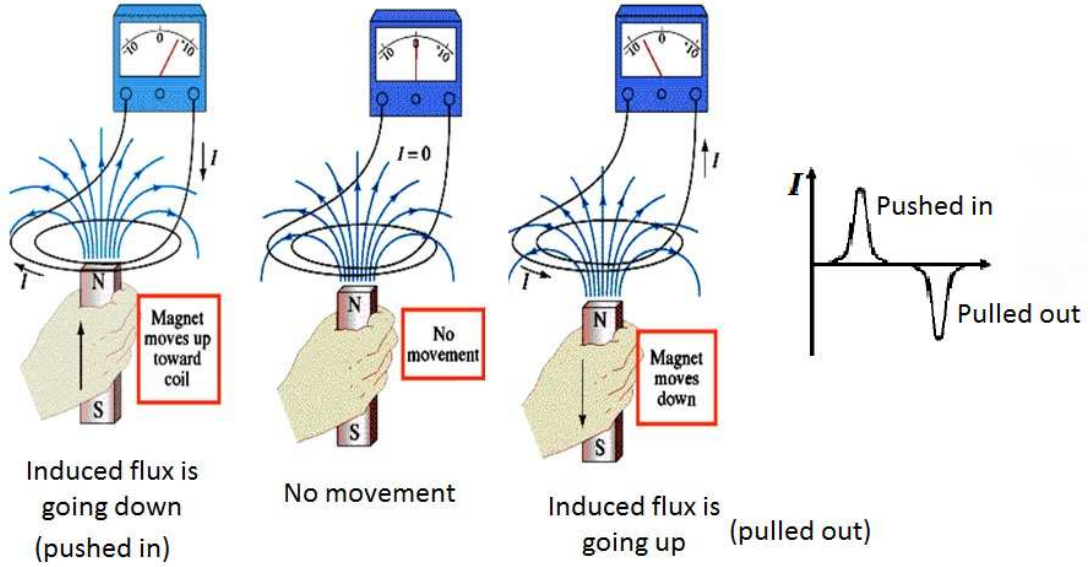


Figure 21: A simple experiment to display Lenz's law. The induced flux,  $\Psi$  (or emf), gives rise to a current  $I$  whose direction opposes to the direction of the  $\Psi$ . Moving the north pole of a magnet towards the coil causes positive current  $I$ . The motion that the magnet is “pushed into the coil” reveals the negative direction of the  $\Psi$  or emf. If the magnet is “pulled out from the coil” (positive  $\Psi$  or emf), the direction (sign) of the current is reversed. When there is no motion of the magnet, then the current does not flow. The image is retrieved and modified from [https://bearspace.baylor.edu/Walter\\_Wilcox/www/courses/phy2435/chap29xxa.pdf](https://bearspace.baylor.edu/Walter_Wilcox/www/courses/phy2435/chap29xxa.pdf)

1006 Considering a simple circuit of a moving coil loudspeaker, with a resistor  $R$  across the terminal,  
 1007 voltage  $-UBl$  (the induced emf grounded to zero), and current  $I$  which is moving across the  $R$ .  
 1008 By Ohm's law, the current satisfies

$$I(\omega) = \frac{0 - (-UBl)}{R} = \frac{UBl}{R} = \frac{U l}{R A} \Psi, \quad (95)$$

1009 where  $\Psi = BA$ , and  $l$ ,  $A$  are length and area of wire respectively. The direction of current is always  
 1010 opposite of the induced emf, this explains the Lenz's law.<sup>17</sup> Note the minus signs in Eq. 94 requires  
 1011 anti-reciprocity, Carlin's postulate C6.

1012 Similar to Eq. 93, one can examine the relation between the force and the current in Eq. 88,  
 1013 this force term also need two parts; transformer force and motional force,

$$f(t) = f_{tr} + f_{mot}. \quad (96)$$

1014 Reconsidering the magnetic force density in Eq. 90, the motion of force in electrical side,  $f_{mot}[\text{N}]$  is

$$\mathbf{f}_{mot} = i \oint_C \mathbf{dl} \times \mathbf{B}. \quad (97)$$

1015 Assuming that the magnetic field is uniform and the conducting wire is not closed, starting from  $a$   
 1016 ending at  $b$  (if it is closed then the net magnetic force is zero, in Eq. 98  $a$  equals to  $b$ .), then Eq. 97  
 1017 becomes

$$\mathbf{f}_{mot} = i \left( \int_a^b \mathbf{dl} \right) \times \mathbf{B}_0 = i \mathbf{l} \times \mathbf{B}_0, \quad (98)$$

<sup>17</sup>If we consider the emf with its positive sign ( $UBl$ ), consisting the fixed positive direction in the circuit, we will have  $-I$ .

1018 where  $\mathbf{l}$  is a vector, a piece of wire directing from  $a$  to  $b$ . In frequency domain, Eq.98 is  $F = B_0 l$ ,  
 1019 it is the ideal gyrator's equation discussed in Eq.88 which only considers motional behavior of the  
 1020 network.

1021 Based on the Lorentz force, the transformer force on mechanical side is defined as

$$f_{tr} = m_B \times a = m_B \frac{dU}{dt} \quad (99)$$

1022 where  $m_B$  is the leakage mass due to imperfect (frequency dependent) mass coupling in the me-  
 1023 chanical side, and  $a = \frac{dU}{dt}$  is acceleration. In frequency domain, this term becomes  $F_{tr} = sm_B U$ ,  
 1024 where  $s = j\omega$ .

1025 The final force for the non-ideal gyrator is

$$f = f_{tr} + f_{mot} = m_B \frac{dU}{dt} + i\mathbf{l} \times \mathbf{B}, \quad (100)$$

1026 in frequency domain with scalars, Eq. 100 is reconsidered as

$$F = sm_B U + B_0 l I. \quad (101)$$

1027 In conclusion, two types of magnetic fields exist in an electro-mechanic network; one is a DC  
 1028 magnetic field and the other is an AC magnetic field. In the ideal gyrator formula, only the  
 1029 motional parts (or the DC magnetic field) of the variables (voltage and force) are considered. The  
 1030 two modalities in the network (electrical and mechanical) share this DC magnetic field which is  
 1031 shown in the motional part of each variable. For the non-gyrator case one must use the transduction  
 1032 parts (or AC magnetic field) of variables along with the motional parts which do not contribute to  
 1033 the opposite modality.

1034 One can convert the impedance matrix form of the ideal gyrator in Eq. 86 into an ABCD matrix  
 1035 form using Eq. 12,

$$T_{i-gyrator} = \begin{bmatrix} 0 & G \\ G^{-1} & 0 \end{bmatrix}, \quad (102)$$

1036 where  $G = B_0 l$ . The ABCD matrix for of the non-ideal gyrator is,

$$T_{noni-gyrator} = \frac{1}{G} \begin{bmatrix} sL_e & s^2 L_e m_B + G^2 \\ 1 & sm_B \end{bmatrix}. \quad (103)$$

1037 The determinants ( $\Delta$ ) of both Eq. 102 and Eq. 103 are '-1' which define the anti-reciprocal network.  
 1038 When  $\Delta$  is '1', the network is reciprocal. Note that all of these relationships are in the Laplace  
 1039 complex frequency domain  $s = j\omega$ .

1040 Finally the suggested non-ideal gyrator's impedance matrix formula is

$$Z_{noni-gyrator} = \begin{bmatrix} sL_e & -G \\ G & sm_B \end{bmatrix}, \quad (104)$$

1041 a non-reversible and anti-reciprocal network (if  $L_e \neq m_B$ ).

1042 What provides the coupling between the electrical and mechanical sides? The only thing that  
 1043 matters in the electro-mechanic coupling is the magnetic field,  $\dot{\mathbf{H}}$ . This variable is hidden in terms  
 1044 of input and output variables of the system (voltage, current, force and velocity). The  $\dot{\mathbf{H}}$  generated  
 1045 by the conducting current from the coil affects the armature by inducing magnetic polarity on the  
 1046 armature surface. This induced  $\dot{\mathbf{H}}$  and the permanent magnet define the net force on the armature.  
 1047 Thus the armature moves based on the experienced total net force.

1048 It is intuitive that the electrical current leads to a force, because the system transforms the  
 1049 current signal into a force on the diaphragm, creating sound pressure waves. Followed by this  
 1050 logic, a gyrator equation relates the electrical current to the force,  $F = B_0 I$ .<sup>18</sup> Therefore we can  
 1051 conclude that the gyrator is a more physically intuitive convention.

#### 1052 5.4 Eddy currents and diffusion waves

1053 Along with the gyrator, the semi-inductor (due to eddy-current<sup>19</sup>) is one of key components to  
 1054 describe electro-mechanic system (Kim and Allen, 2013). If a magnetic field near a conductor is  
 1055 changing in time, the traveling magnetic field is described in terms of the diffusion equation. This  
 1056 is a physical phenomenon which can be observed in our daily life.

1057 There are two ways to examine Eddy current, (1) direct way and (2) in-direct way; (1) a magnet  
 1058 traveling inside of a copper pipe can be affected by this diffusive eddy-current. The magnet falling  
 1059 outside of a conductor does a free fall, while falling inside of the conducting pipe experiences a  
 1060 significant delay, due to the opposite force caused by the eddy current. Figure 22 describes this  
 phenomenon.

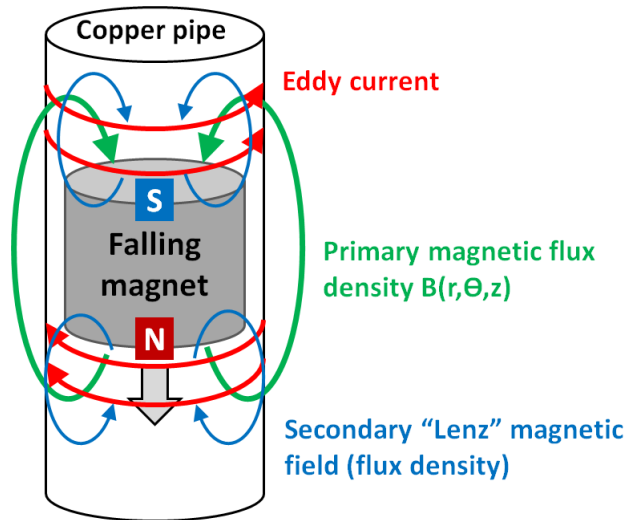


Figure 22: Eddy current with a falling magnet inside a conductor (falling from south to north). When the magnetic field is changed in time in a closed electric field (a falling magnet in a copper pipe), an “eddy current” is induced on the copper pipe (red). The direction of the eddy current is perpendicular to the primary magnetic field (green, it is static when velocity is zero. Also the field is not a function of  $\theta$ ) followed by right hand rule (thumb-force, 1<sup>st</sup> finger-electric field, 2<sup>nd</sup> finger - magnetic field). The eddy current creates the secondary magnetic loop (blue) whose force is opposite to the force of gravity. At the terminal velocity, the force of gravity equals the Lenz reactive force.

1061  
 1062 (2) starting from Ampere’s law, the current in the wire, namely driven (or conducting) current,  
 1063 induces magnetic field  $\mathbf{H}$ . Then, similar to the direct way (1), based on the Faraday’s law, the  $\mathbf{H}$   
 1064 creates Eddy current (induced current via  $\mathbf{H}$  on the surface of the adjacent ferromagnetic material).

<sup>18</sup>We may can relate the current to the velocity (transformer and mobility), which seems to be less intuitive.

<sup>19</sup>There are three types of currents in electro-magnetic system

1. Conducting current is created by moving charge in conducting medium (J term in Ampere’s law, i.e., current through wire).
2. Displacement current is current due to changing electric field (E) (D term in Ampere’s law, i.e., capacitors).
3. Eddy current is current due to changing magnetic field (H). It is directly related to Faraday’s (induction) law.

1065 Note that the magnitude of the eddy currents is a function of the drive current with opposite  
 1066 direction.

1067 Vanderkooy (1989) modeled the electrical impedance representation of the semi-inductor based  
 1068 on this concept (in-direct way to examine the eddy current). Impedance of the semi-inductor is  
 1069 proportional to  $\sqrt{s}$ , to realize a diffusive element in circuits. A simple impedance formula of the  
 1070 semi-inductor is derived with the assumption that the length of a coil sheet is infinite. Neglecting  
 1071 the radius of the coil and the air gap between the magnetic material and the wire,

$$Z_{semi} = n^2 \sqrt{\frac{\mu s}{\sigma}} = K \sqrt{s}, \quad (105)$$

1072 where  $K$  is semi-inductance per unit length in semi-Henrys,  $n$  is the number of coil winding turns  
 1073 of wire,  $\mu$  is the iron's permeability, and  $\sigma$  is the conductivity of the iron armature.

1074 Semi-inductors, which result from magnetic diffusion, are not commonly found in circuit analy-  
 1075 sis. However, it is a key element in characterizing the 'eddy-current' (skin effect) in electromagnetic  
 1076 models, such as loudspeakers. In a BAR, the eddy current is distributed through the surface of  
 1077 the armature, as well as in the cross section of the laminated iron box which surrounds the mag-  
 1078 nets (Fig. 2). In a dynamic loudspeaker, the coil is directly connected to the diaphragm and the  
 1079 eddy-current is distributed through the surface of an iron core (a pole-piece structure).

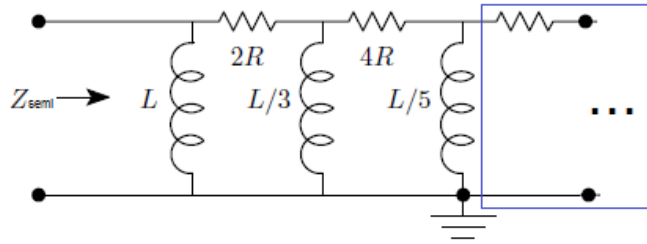


Figure 23: Semi-inductor approximate lumped circuit model via a truncated ladder network. Circuit diagram of the electrical impedance of the semi-inductor model is defined by the ladder network resistance factor  $R$  and shunt inductance factor  $L$  (Weece and Allen, 2010). This circuit follows from a continued fraction expansion of  $\sqrt{s}$ .

1080 Warren and LoPresti (2006) noted that the Bessel function ratio in the Vanderkooy model  
 1081 (1989) can be expanded as a continued fraction expansion, into a diffusion ladder network, so that  
 1082 the electrical impedance can be represented by the circuit shown in Fig. 23. The semi-inductor  
 1083 model includes two parameters: the diffusion resistance  $R$ , and the shunt diffusive inductance  $L$   
 1084 which can be represented by the physical characteristics of the transducer. The  $R$  and  $L$  are given  
 1085 by

$$R = \frac{4\pi n^2 l}{\sigma}, \quad L = \mu l n^2 \pi r_0^2, \quad (106)$$

1086 where  $n$  is the number of coil windings,  $l$  is the coil length,  $\sigma$  is the conductivity of the pole  
 1087 structure,  $\mu$  is the permeability of the pole structure, and  $r_0$  the coil radius.

1088 Although the combination of the resistor and the inductor should extend to infinity (more  
 1089 resistor-inductor pairs), these can only affect higher frequencies (i.e., Fig. 23 is a sufficient low  
 1090 frequency approximation). As shown in Fig. 23, Weece and Allen (2010) determined only 5 elements  
 1091 ( $L$ ,  $2R$ ,  $L/3$ ,  $4R$ , and  $L/5$ ), and compared the network to the demagnetized condition of their bone  
 1092 driver transducer. Demagnetizing the transducer ( $T = B_0 l = 0$ ) is mathematically equivalent to  
 1093 the open circuit condition (i.e.,  $V = 0$ ).

1094 Starting from Maxwell's equation, we derive two types of wave equations, normal and diffusive  
 1095 cases.

1096 Equation 107 has two terms, current from the source, and displacement current.

$$\nabla \times \mathbf{H} = \epsilon \frac{\partial \mathbf{E}}{\partial t} + \sigma \mathbf{E}, \quad (107)$$

1097 where  $\mathbf{D} = \epsilon \mathbf{E}$  and  $\mathbf{J} = \sigma \mathbf{E}$ . Via  $\mathbf{B} = \mu \mathbf{H}$ , Faraday's law (Eq. 71) for free space written as,

$$\nabla \times \mathbf{E} = -\mu \frac{\partial \mathbf{H}}{\partial t} = -\dot{\mathbf{B}}. \quad (108)$$

1098 Also since monopole magnetic charge does not exist, and  $\mu$  is independent of  $x$  (i.e.,  $\nabla \mu = 0$ ),

$$\nabla \cdot \mathbf{B} = \nabla \cdot \mathbf{H} = 0. \quad (109)$$

1099 Taking a curl of Eq. 107 using the following vector identity,

$$\nabla \times (\nabla \times \mathbf{H}) = \nabla(\nabla \cdot \mathbf{H}) - \nabla^2 \mathbf{H}. \quad (110)$$

1100 then using Eq. 108 and Eq. 109, Eq. 110 becomes

$$\nabla \times (\nabla \times \mathbf{H}) = \epsilon \frac{\partial(\nabla \times \mathbf{E})}{\partial t} + \nabla \times (\sigma \mathbf{E}) = -\mu \epsilon \frac{\partial}{\partial t} \frac{\partial \mathbf{H}}{\partial t} - \mu \sigma \frac{\partial \mathbf{H}}{\partial t} = 0 - \nabla^2 \mathbf{H}. \quad (111)$$

1101 Finally we have,

$$\nabla^2 \mathbf{H} = \underbrace{\mu \epsilon \frac{\partial^2 \mathbf{H}}{\partial t^2}}_{\text{loseless wave}} + \underbrace{\mu \sigma \frac{\partial \mathbf{H}}{\partial t}}_{\text{lossy wave}} \leftrightarrow \left( \frac{s^2}{c^2} + \mu \sigma s \right) \underline{\mathbf{H}} = \mu \sigma s (s \epsilon / \sigma + 1) \underline{\mathbf{H}}, \quad (112)$$

1102 where  $\underline{\mathbf{H}}$  is frequency variable of  $\mathbf{H}$ , and  $s = j\omega$ . When  $\omega \leq \sigma/\epsilon = \omega_c$  the wave is dominated by  
 1103 diffusion, otherwise we have lossy waves. Since the two waves satisfy superposition, we can separate  
 1104 the two solutions.

1105 **Lossless wave equation ( $\mathbf{J} = 0$  or  $\sigma = 0$ )** When there is zero conductive current density  
 1106 ( $\mathbf{J} = 0$ ),

$$\nabla \times \mathbf{H} = \frac{\partial \mathbf{D}}{\partial t} + \overset{0}{\mathbf{J}} = \epsilon \frac{\partial \mathbf{E}}{\partial t}. \quad (113)$$

1107 Going through same algebra from Eq. 108 to Eq. 111 we have the wave equation,

$$\nabla^2 \mathbf{H} = \mu \epsilon \frac{\partial^2 \mathbf{H}}{\partial t^2} = \frac{1}{c^2} \frac{\partial^2 \mathbf{H}}{\partial t^2}. \quad (114)$$

1108 **Lossy wave equation: diffusion equation (semi-inductor basics,  $\epsilon \rightarrow 0$ )** Similar step is  
 1109 used to derive the diffusion equation via Maxwell's equation. The fundamental difference is in the  
 1110 first step when the medium is conducted, we can ignore the displacement current term in Eq. 107  
 1111 as it is too small compared to the conducting current term. Therefore in this case we can set  $\frac{\partial \mathbf{D}}{\partial t}$   
 1112 to zero,

$$\nabla \times \mathbf{H} = \mathbf{J} + \frac{\partial \overset{0}{\mathbf{D}}}{\partial t} = \sigma \mathbf{E}. \quad (115)$$

1113 Based on Eq. 108 - Eq. 111, finally the diffusion wave equation is derived,

$$\nabla^2 \mathbf{H} = \mu \sigma \frac{\partial \mathbf{H}}{\partial t}. \quad (116)$$

1114 The normal wave equation in 3D wave form (Eq. 114) describes the propagation of electromag-  
 1115 netic (EM) waves through a medium whereas the diffusion wave equation (Eq. 116) describes the  
 1116 propagation of EM waves in a conducting magnetic medium. For both equations the Laplacian on  
 1117 left hand side is same. A diffusion case has a single time derivative term whereas a normal wave  
 1118 equation has a double time derivative term. Let's define  $\mathbf{H}(x, t)$  assuming a simple geometry,

$$\mathbf{H}(x, t) = H_0 e^{j(\omega t - kx)}, \quad (117)$$

1119 where  $H_0$  is the  $\mathbf{H}$ ,  $\mathbf{E}$  propagate in  $y$ ,  $z$  directions, respectively. Note that  $k$  is wave number. Then  
 1120 Eq. 116 in frequency domain

$$(jk)^2 = \mu\sigma j\omega, \quad (118)$$

1121 then the wave number  $k$  is

$$k = \sqrt{\mu\sigma\omega}(\cos 45^\circ - j \sin 45^\circ). \quad (119)$$

1122 Thus the wave propagation is proportional to the square-root frequency ( $\sqrt{s}$ ). Brief description of  
 1123 the exact impedance formula of a semi-inductor are followed; substitute Eq. 119 into Eq. 117 and  
 1124 calculate the magnetic flux  $\Psi$  per unit area, where  $\Psi = \int \mathbf{B} \cdot d\mathbf{S} = \mu \int \mathbf{H} \cdot d\mathbf{S}$ . Then the inductance  
 1125  $L$  per unit length with  $n$  numbers of turn with current  $I$  is

$$L = \frac{n\Psi}{I}. \quad (120)$$

1126 The impedance of an inductor is  $Z(s) = sL$ . Once we follow all these step, the square-root frequency  
 1127 dependency can be easily shown. Note that more details are discussed in Vanderkooy (1989)).

One can calculate a cutoff frequency of two waves in a medium. Convert Eq. 114 and Eq. 116 into frequency domain representation via Laplace transform, and set them equal to each other.

$$\mu\sigma \frac{\partial \mathbf{H}}{\partial t} = \mu\epsilon \frac{\partial^2 \mathbf{H}}{\partial t^2} \quad (121)$$

$$\mu\sigma(j\omega)\mathbf{H} = \mu\epsilon(j\omega)^2\mathbf{H} \quad (122)$$

$$\sigma = \epsilon(j\omega), \quad (123)$$

1128 the cutoff frequency( $f_c$ ) is

$$f_c = \frac{\sigma}{2\pi\epsilon}. \quad (124)$$

1129 The  $f_c$  of copper, for example, is about 4300[GHz] ( $\sigma = 5.96 \times 10^7$ ,  $\epsilon_r = 250,000$ ,  $\epsilon_0 = 8.854 \times 10^{-12}$ )  
 1130 meaning that wave below this frequency is diffusive. The corresponding wave length ( $\lambda_c$ ) can be  
 1131 calculated as

$$\lambda_c = \frac{c_{copper}}{f_c} = \frac{3 \times 10^8}{4.3 \times 10^{12} \sqrt{250,000}} \approx 0.14 \mu[m], \quad (125)$$

1132 where  $c_{copper} = \frac{c_0}{\sqrt{\epsilon_r}}$ .

## 1133 5.5 Reinterpretation of quasi-static

1134 Signals (usually in wave form) and systems are distinguished in terms of causality. Signals are  
 1135 defined over all time support,  $|t| \leq \pm\infty$ , whereas in systems, the support is restricted to  $t \geq 0$ . The  
 1136 forwarding waves are typically reflected back if the network has a finite length. A traveling time  
 1137 difference between the forward and backward waves represents the group delay  $\tau(\omega)$ . Regardless  
 1138 of the speed of the wave, there is a system delay given a finite system length  $l$ .

1139 The QS approximation is a classic tool used to simulate and analyze electrical systems, assuming  
1140  $\lambda \geq l$ . However, this assumption does not always describe the physical reality. Critical examples  
1141 include electro-acoustic networks, where the system's speed transits from one to the other (i.e.,  
1142 from the speed of light to the speed of sound). The ED7045 receiver (Knowles balanced armature  
1143 receiver) has a  $4.29 \times 6.5 \times 3$  [mm] dimension. Considering the frequency range of human hearing  
1144 (20Hz to 20kHz) with the speed of sound (345[m/s]), the wave length  $\lambda$  calculated at 20kHz is  
1145 17 [mm], which is compatible with the width of the receiver ( $l = 6.5$ [mm]). It does not, however,  
1146 satisfy the rule of thumb for  $\lambda \geq l$ ; the calculated  $\lambda$  is less than 10 times that of  $l$ . Also, acoustic  
1147 networks having a fairly slow system speed compared to their frequency regions of interest is another  
1148 example, such as the speed of sound on the eardrum relative to the speed of sound in air.

1149 Assume a train (1 mile in length, a very long train) has a speed of 60mph and someone slowly  
1150 moves inside the train at a speed of 1mph for at least an hour. The QS approximation may be  
1151 applied in this scene; an observer outside the train may think that the train and he are in the same  
1152 border until he hits the end of the train. The observer feels that the speed is 60mph for at least  
1153 an hour. When he hits the train wall, the QS approximation breaks. After one hour (if he breaks  
1154 out the train wall), he and the train will be separated. The outside observer no longer thinks that  
1155 he and the train are in the same location or have the same speed. The circumstance becomes  
1156 non-QS when the two subjects are physically separated. Then, what is the meaning of relating the  
1157 QS to delay? It means that the outside observer can discern his exact location inside the train at  
1158 each time frame when he is moving around the train. This interpretation does not depend on the  
1159 position of the person, whether inside or outside the train. The previous portion on the train is  
1160 similar to the phase across the object where the phase is due to the delay (i.e.,  $90^\circ$  is  $\lambda/4$  while  
1161  $180^\circ$  is  $\lambda/2$ , half way down the train).

1162 In summary, we propose a more fundamental way to characterize the QS approximation. In  
1163 describing a system as QS or non-QS, delay is the critical parameter as it determines the pole-  
1164 zero frequency density. This definition does not violate the traditional descriptions of QS such as  
1165 long-wave approximation; rather, it provides a precise analysis of the system.

## Part III

# Experimental Methods

## 1 Measurements for BAR modeling

Three different experiments were conducted for modeling the BAR. First, we calculate the Hunt parameters of a BAR from electrical input impedance measurements (Appendix E). The calculation of Hunt parameters may be considered as a two-port Thevenin calibration of the receiver, since  $Z_e$ ,  $T$ , and  $Z_a$  characterize the initial electrical, acoustical and transfer properties of the unloaded receiver. Second, we measure of the receiver's diaphragm velocity in vacuum using a laser. This procedure was needed to verify the mechanical and electrical parts of the model. The last step is the pressure measurement of the receiver using an ER7C probe microphone, (Etymotic Research). The resulting Thevenin pressure of the receiver from our transducer model and Hunt parameters is compared with this experimental pressure data. The detail of this result is discussed in chapter IV (model verification).

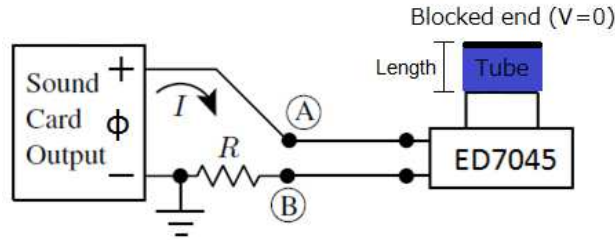


Figure 24: Experimental setup for the electrical input impedance measurement. Where  $\Phi$  is the voltage,  $I$  is the current, and  $R$  is a reference resistance. We varied the experimental acoustical load impedance by changing Length of a blocked tube and measured the voltage at two points (A, B) denoted as  $\Phi_A$  and  $\Phi_B$ .

### 1.1 Electrical input impedance measurements for the Hunt parameter calculation

Step 1 of calculating the Hunt parameters of the receiver requires a system for measuring electrical impedance as a function of frequency. As shown in Fig. 24, all stimulus signals were generated using a laptop sound card so that voltages could be recorded. The stimulus waveform was a 24-bit, 2048-point frequency-swept chirp with a sampling rate of 48[kHz]. The signal-to-noise ratio (SNR) was improved by looping the chirp and averaging between 10 and 1000 consecutive frames, depending on the required SNR. The  $\leq 1$  volt chirp signal from an Indigo sound card (Echo Audio) was sent to the receiver, which was in series with a known reference resistor  $R$  (1000[ $\Omega$ ], Fig. 24). The resistor was located between one of the receiver's terminals and the sound source ground. The measured electrical input impedance is expressed as:

$$Z_{in} = \frac{\Phi_A - \Phi_B}{I} = \frac{\Phi_A - \Phi_B}{\Phi_B/R} = R \left( \frac{\Phi_A}{\Phi_B} - 1 \right). \quad (126)$$

As shown in Fig. 25, eight different acoustic loads were attached to the end of the receiver output and eight corresponding electrical input impedances were recorded. Six of the seven tubes (excluding the longest length 6.11[cm]) were used in the experiments: 0.25, 0.37, 0.88, 1.24, 2.39 and 3.06[cm]. The inner diameter of the tubes was about  $\approx 1.5$ [mm], which is similar to the outer

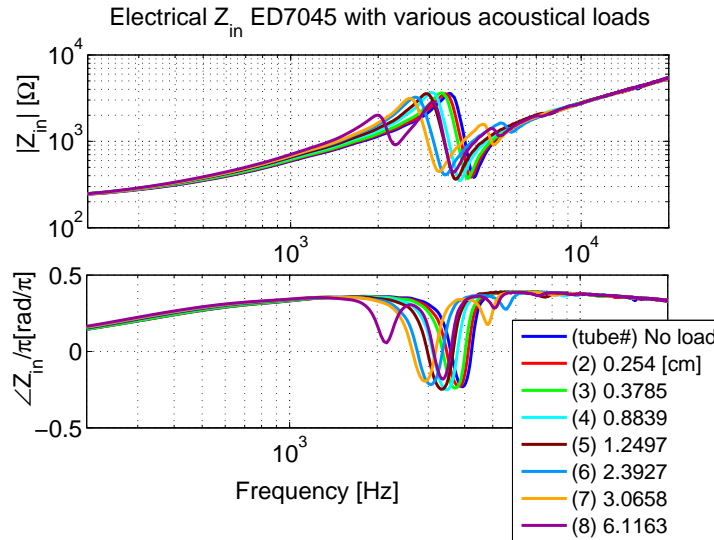


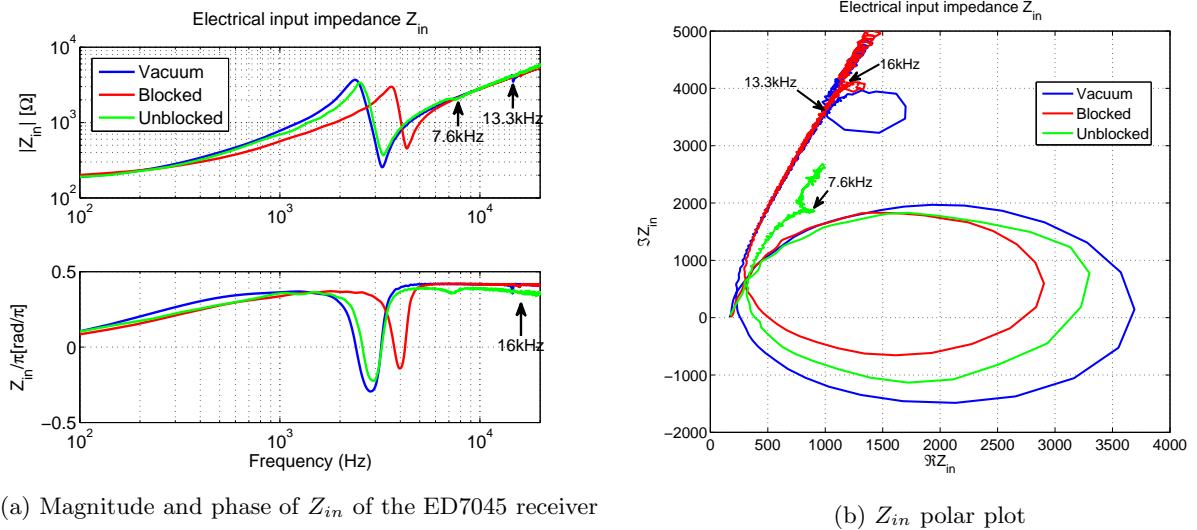
Figure 25: Measured  $Z_{in}$  of ED7045 with the eight acoustical load conditions, blocked cavities. Different lengths of the tubes are used to vary the acoustical load. Three different known electrical input impedances are selected to calculate Hunt parameters.

1194 diameter of the ED receiver port. As three different measurements were required to calculate the  
 1195 three unknown Hunt parameters ( $Z_e, Z_a, T_a$ ) (Weece and Allen, 2010), three out of six tubes with  
 1196 different lengths were selected, resulting in  ${}_6C_3 = 20$  possible combinations of the Hunt parameters.  
 1197 The results from every possible combination are not discussed in this paper; rather, we focus on  
 1198 the four calculated sets of Hunt parameters. We categorized our testing tube lengths into short,  
 1199 medium and long tubes, and picked one of each to make a set of three tubes. An open circuit  
 1200 condition (the volume velocity,  $V$ , is zero.) was applied, as the ends of the tubes were blocked  
 1201 for the experiment. The characteristics of the resulting derived Hunt parameters are discussed in  
 1202 Section 1.1.

1203 When the acoustic load impedance is unblocked, a small second resonance (SR)<sup>20</sup> appears  
 1204 around 7.6[kHz], following the first resonance (FR)<sup>21</sup> at 2.5[kHz], as shown in Fig. 26 (a) (green).  
 1205 In fact, a very small SR appears in *every* case in the figure, as clearly seen in the polar plot, Fig. 26  
 1206 (b). The SR of the blocked case (red) is not obvious in the magnitude plot, but one sees the SR  
 1207 location from the phase in the polar data. Note that a ‘loop’ in the polar data corresponds to  
 1208 the SR in the magnitude data. The vacuum data (blue) shows the biggest FR in magnitude (the  
 1209 largest circle in the polar plot), and the FR locates at the lowest frequency among all the other  
 1210 cases. Compared to the unblocked case (red), the SR frequency of the other two cases (blocked and  
 1211 vacuum) is above the frequency range of reliable measurements. In detail, it has almost an octave  
 1212 difference ( $SR_{unblocked} \approx 7.6[kHz]$ ,  $SR_{vacuum} \approx 13.3[kHz]$ ,  $SR_{blocked} \approx 15.7[kHz]$ ). In addition,  
 1213 the size of  $SR_{blocked}$  is insignificant. For these reasons, we have ignored the SR effect in our model  
 1214 analysis of the BAR model.

<sup>20</sup>SR: Second Resonance

<sup>21</sup>FR: First Resonance



(a) Magnitude and phase of  $Z_{in}$  of the ED7045 receiver

(b)  $Z_{in}$  polar plot

Figure 26: This plot shows the electrical input impedance of the ED7045 receiver in blocked/unblocked port, and vacuum conditions. In the unblocked receiver port case, the FR moves to lower frequency (2.5[kHz]) compared to the blocked case, 3.8[kHz]. The FR in vacuum is at the lowest frequency, 2.3[kHz]. The frequency locations of SR for each curve are indicated by arrows in the figures. (a) Magnitude and phase of the electrical input impedance, (b) Polar plot of the electrical input impedance ( $\Re Z_{in}$  vs  $\Im Z_{in}$ ). Note that above 5[kHz], the phase of  $Z_{in}$  in (a) approaches  $\approx .4\pi$ [rad]. Thus in (b), the curves merge at a fixed angle as  $\omega \rightarrow \infty$ .

## 1.2 Laser vacuum measurements

Figure 27 describes the experimental setup of the laser mechanical velocity measurement in the vacuum environment. In preparation for the laser measurement, a portion of the transducer's case was carefully removed using a dental drill, to expose the diaphragm. A thin plastic window was glued on, to reseal the case. The laser beam is finely focused on the diaphragm through the

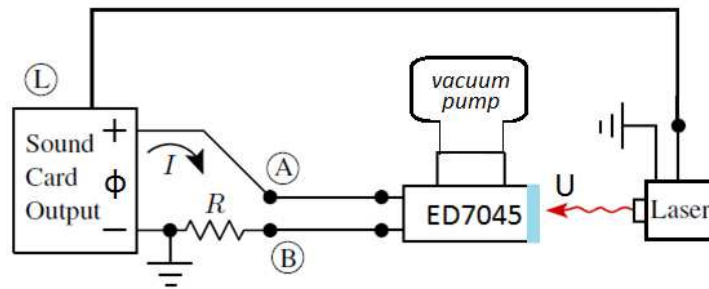


Figure 27: Experiment setup for the laser mechanical velocity measurement in vacuum. The circled 'L' means an input from the laser system. The laser beam is focusing on the plastic window of the transducer to measure the diaphragm velocity ( $U$ ).

1219

1220 window. The measurement was made where the driver rod (Fig. 2) connects to the diaphragm. For  
 1221 the vacuum condition, air inside the receiver was evacuated prior to measurement. The ambient  
 1222 pressure was maintained at less than 0.003[atm] during these measurements. The custom built  
 1223 vacuum system was used with a 'Sergeant Welch' vacuum pump and a 10-inch bell-shaped jar. A  
 1224 'Polytec OFV-5000 Vibrometer controller' was used with a 10x-lens on the laser. The calibration  
 1225 factor for the laser velocity was 125[mm/sec/volt]. As before, a chirp was used to measure the

1226 complex velocity frequency response.

### 1227 1.3 Pressure measurements

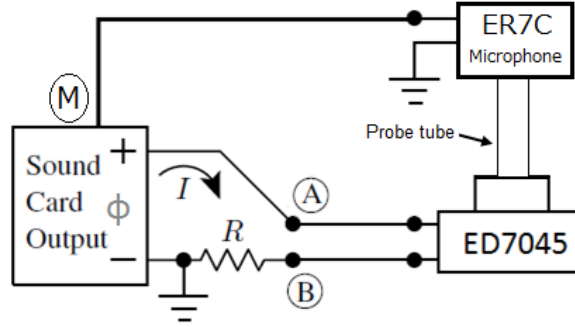


Figure 28: Experiment setup for pressure measurement. The circled ‘M’ means an input from the ER7C microphone.

1228 The purpose of experiment three is to compare the output pressure to the model with  $V = 0$ . An  
 1229 ER-7C probe microphone (Etymotic Research) was used for the transducer pressure measurement.  
 1230 The probe tube was .95 OD x .58 ID x 76[mm], and made of medical grade silicon rubber. In fact,  
 1231 it is impossible to connect a microphone probe with a perfectly blocked receiver ( $V = 0$ ) due to  
 1232 the finite load impedance of the microphone. The space between the microphone’s tube and the  
 1233 port of the receiver is minimized, so the tube and the port do not touch each other. The real part  
 1234 of the characteristic impedance of a tube,  $Z_{c_{tube}}$ , (without loss) is given by

$$Z_{c_{tube}} = \frac{\rho c}{Area_{tube}}, \quad (127)$$

1235 where  $\rho$  is the air density and  $c$  is the speed of sound ( $1.21[kg/m^3]$  and  $342[m/s]$  at  $20^\circ[C]$ , respec-  
 1236 tively). The diameter,  $d$ , of the receiver’s port and the microphone’s tube are  $d_{receiver} = 1.4[mm]$   
 1237 and  $d_{mic} = 0.58[mm]$ , thus the area of the receiver’s port is about 5.8 times larger than the mi-  
 1238 crophone’s. Adding more consideration of the length of both cases,  $Z_{c_{mic\_tube}}$  is much greater  
 1239 than  $Z_{c_{receiver\_port}}$ . Thus we assume that  $Z_{c_{mic\_tube}}$  has a negligible loading effect on the source  
 1240 impedance of the receiver. Recognizing these experimental limitations prior to comparing the mea-  
 1241 surement data to theoretical results should give us better understanding of the Thevenin pressure  
 1242 of the BAR.

1243 Utilization of this experiment can be found in section 2.4 for comparing the model calculated  
 1244 Thevenin pressure (per voltage) to the experimental pressure measurement.

## 1245 2 Technical analysis of an OAE hearing measurement probe

1246 In this section, we introduce several experimental methods to investigate an existing hearing mea-  
 1247 surement probe system, the ER10C by Etymotic Research, for otoacoustic emission (OAE) mea-  
 1248 surements. The ER10C system consists of two parts; a probe and an amplifier box (Fig. 29(a)).  
 1249 The ER10C probe has built-in sound sources (receivers), which eliminate the need for having ex-  
 1250 ternal speakers (Fig. 29(b)). The amplifier box contains special circuits for each probe to meet the  
 1251 unified and standard performance specification of the ER10C system.

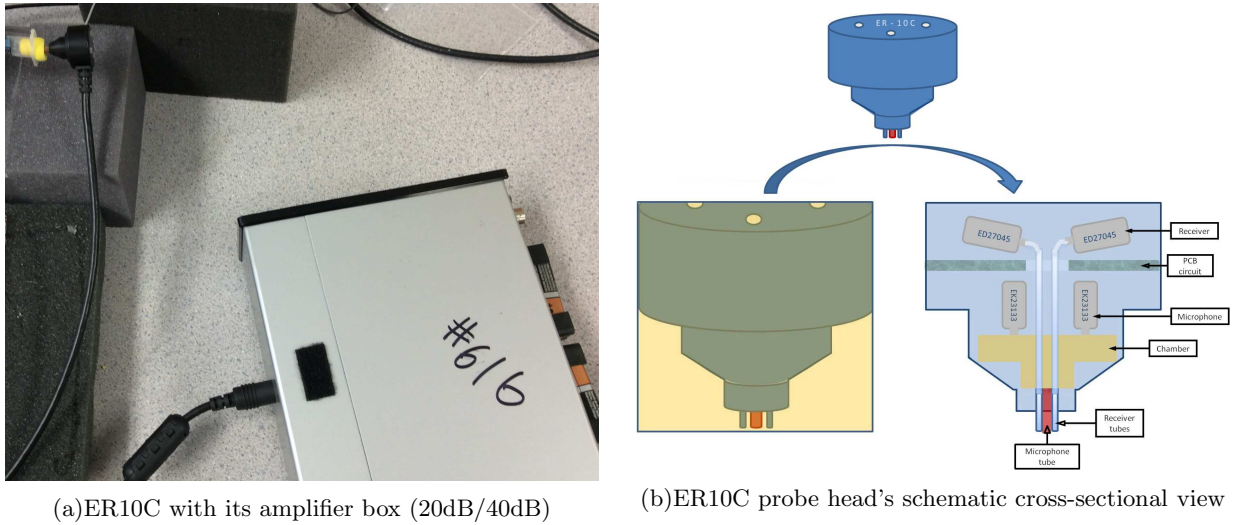


Figure 29: (a) A yellow foam tip (14A) is attached to the probe’s head. Note that numbers on the box indicates the system’s serial number. (b) Schematic representation of the ER10C probe. Two speakers and microphones are separated internally across the PCB circuit, microphones are placed ahead of the receivers (speakers).

1252 For the last decade, the system (or the probe alone with other software such as HearID or  
 1253 OtoStat by Mimoso Acoustics) has been widely used in clinics for hearing screening and diagnostics  
 1254 by measuring DPOAEs, and middle ear reflectance. Following the probe’s Thevenin calibration,  
 1255 OAE stimuli may be calibrated to have constant forward pressure levels (FPL).

1256 Because of the small number of competitors in the market, users have not had many alternatives  
 1257 to the system, even though the ER10C has several drawbacks. First, the size of the probe is too  
 1258 big for infants. Second, because the probe is such a delicate device, handling it without extreme  
 1259 caution may lead to malfunction of the probe. Finally, the result of the measurement depends too  
 1260 much on the condition of the foam tip that is inserted in the subject’s ear canal.

1261 Appreciating these facts, we believe that investigation of the properties of the ER10C will  
 1262 provide fundamental and operational understanding of not only the ER10C system but also hearing  
 1263 measurement devices in general.

## 1264 2.1 Physical structure of ER10C

1265 In this section, we report detailed observations of the ER10C by opening up the device. Figure 30  
 1266 shows the internal structure of the ER10C probe, which has been carefully disassembled into two  
 1267 parts; a holder with microphones (Fig. 30(a)) and a circuit board (PCB) with speakers (Fig. 30(b)).  
 1268 The microphone holder part has a chamber in the middle, holding steel tubes to construct the  
 1269 input (microphone) and the output (speakers) sound paths to each transducer. The microphones  
 1270 are firmly attached to the chamber while the speakers are attached to steel tubes via a soft rubber  
 1271 tubes, floated in the air. As the air acts as a best damper, in this way, any vibrational nonlinear  
 1272 effect (crosstalk) from the speakers can be reduced.

1273 Detailed shape of this chamber (alone) is introduced in Fig. 31. The front side of the chamber  
 1274 has three holes; two small holes are for the two outputs, and one large hole is for the input. The  
 1275 back side has four holes; two microphone’ ports are directly plugged into the larger two upper holes,  
 1276 and thin steel tubes (for the speakers) are passing through the small two lower holes.

1277 It may note from the structure of the brass cavity (Fig. 31) that a unique point about the  
 1278 input structure of the ER10C (compared to the other hearing measurement probes) is that it has

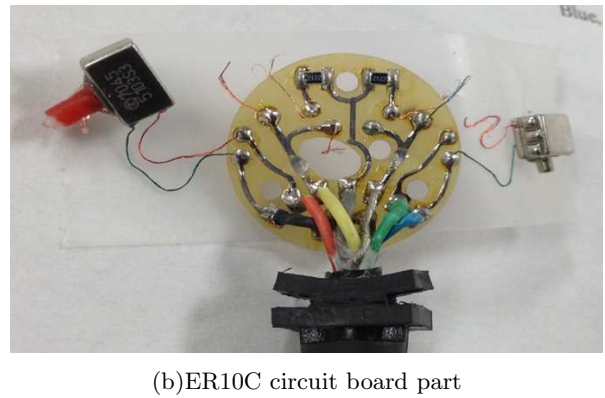
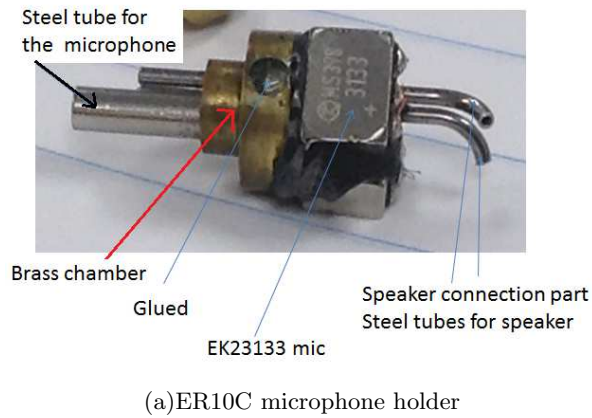


Figure 30: Disassembled ER10C. Two parts are inside; (a)microphone holder and (b)circuit board parts. Note that lots of care were needed to see the part (a) as it was permanently attached to the probe's case.

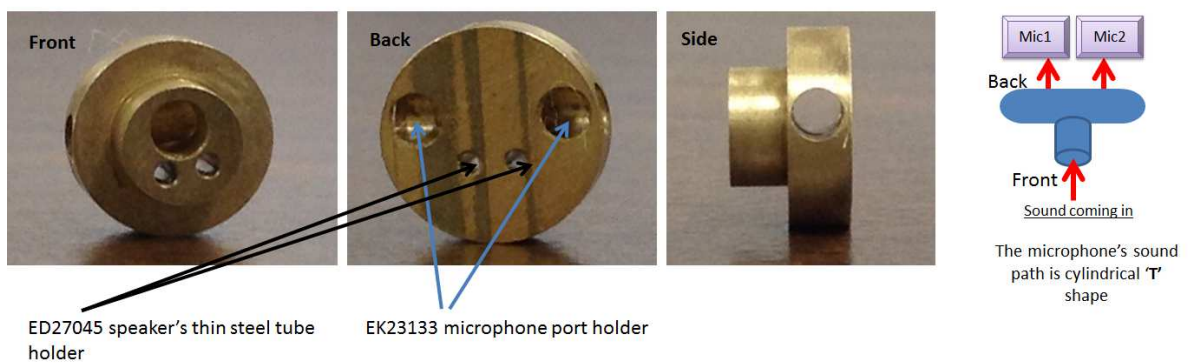


Figure 31: Details of the brass chamber in Fig. 30. The recent design of ER10C, an aluminum material chamber is used maintaining the same shape.

1279 two internal microphones which acts as one input. The electrical terminals of two microphones  
1280 are connected with a two-diode package (i.e., MMBD7000), but only one diode is used, set up to  
1281 be reverse biased in series with a capacitor (between the nominal microphone’s “output” and the  
1282 “ground” terminals, Fig. 32). This is a traditional approach in the hearing aid industry, to protect  
1283 the input from spark discharge. The capacitor is to filter out the very large spark discharge, and  
1284 take it out (clip it) with the diode. There are two parallel 22K ohm resistors for two microphones  
1285 as shown in Fig. 30 (black squares with 2122 written on it). But as this system has a single input  
1286 (this input channel may be separated as two inputs externally), the resistance of the input channel  
reads 11 k $\Omega$ .

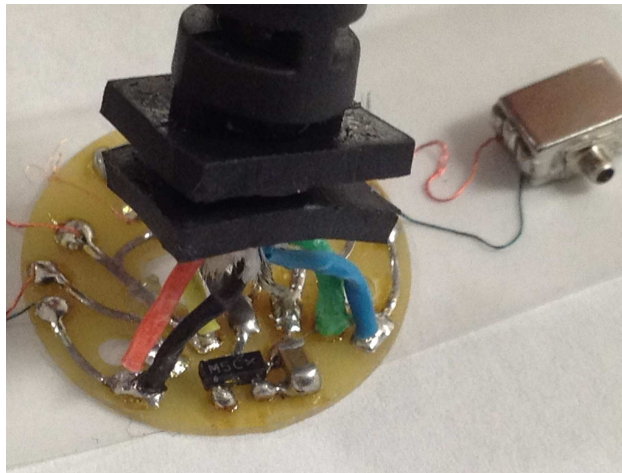


Figure 32: ER10C circuit board details. A diode package and a capacitor are shown under the wire soldering ends. Only one diode is used to set up to be reverse biased, in series with a capacitor between the microphone’s “output” and the “ground” terminals. It is a traditional approach in the hearing aid industry, to protect the input from spark discharge.

1287

1288 Figure 33 explains the connection details of the two probe parts shown in Fig. 30. The speakers  
1289 are connected to the curved steel tubes (right side of the upper right picture) via red rubber tubes  
1290 attached on speaker port (upper left).

## 1291 2.2 Crosstalk measurement

1292 In this part, we investigate a critical topic to design a hearing measurement probe: “crosstalk.”  
1293 Starting from categorizing various types of crosstalk, we describe each crosstalk measurement.

1294 In an electro-acoustic system, crosstalk is undesired signal that is observed in the system’s  
1295 response. It may contaminate system’s signal to and from both the speaker and the microphone.  
1296 Our main concern is the crosstalk in the microphone, which may be categorized into three types,

- 1297 1. Electrical: Coupling of the input signals via the electrical wires, usually affecting the output  
1298 at high frequencies. To measure this, we may block the probe’s microphone and generate a  
1299 signal from the speaker, then measure the probe’s microphone response. Ideally, as we blocked  
1300 the microphone, the signal from the probe’s microphone should be similar to the noise floor.  
1301 If any signal is greater than the noise floor, it is the electrical crosstalk.
- 1302 2. Mechanical: vibrational coupling to microphone’s diaphragm. Any physical vibration through  
1303 probe’s body, not through the main input path, the port of the microphone (i.e., touching the  
1304 probe’ head during measurement can affect the microphone’s diaphragm). To prevent this  
1305 crosstalk, the probe should be placed with a ‘hands-free’ condition during experiments.

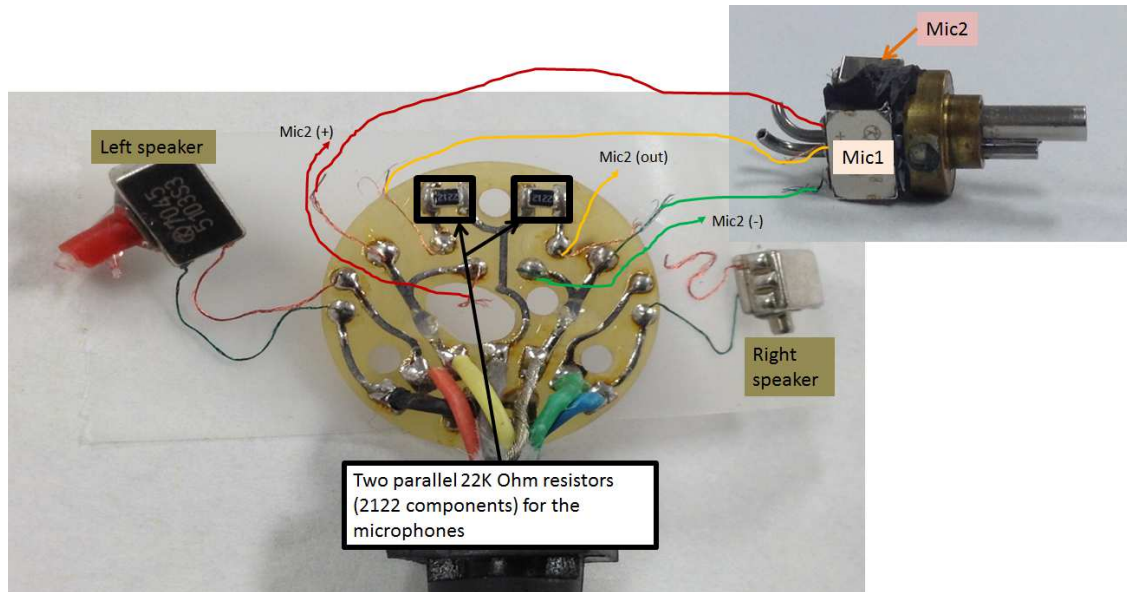


Figure 33: ER10C circuit board (Fig. 30(b)) and connection details with microphone holder part in Fig. 30(a). Note that the speakers are connected to the curved steel tubes via red rubber tubes.

1306 3. Acoustical: any signal coming into the system from outside of the region of measurement  
 1307 (i.e., noise). Typically this is related to poor acoustic seals in the system, and affects low  
 1308 frequency measurements, increasing the noise floor. To measure this acoustic crosstalk, we  
 1309 may stimulate output channel 1 (connected to input channel 1) with a signal and measure  
 1310 the input of channel 2. Ideally, input channel 2 should have no signal, if the device has zero  
 1311 crosstalk (or similar to noise floor). However if the acoustic crosstalk is present, some signal  
 1312 that corresponds to the output of channel 1 will be observed at the channel 2 input.

### 1313 2.3 Calibration issues

1314 Figure 34 describes calibration details of the ER10C. The ER10C probes may be categorized into  
 1315 three types based on their calibration pass/fail frequency range.

1316 With careful investigation to find out the reason of the calibration failure both physically and  
 1317 theoretically, we hypothesized that the problem is in the electrical crosstalk based on the exper-  
 1318 imental data shown in Fig. 35. When we blocked the ER10C microphone, sound signal cannot  
 1319 pass through the acoustic sound path of the microphone. Therefore the acquired data from the  
 1320 microphone should be similar to noise floor. The result that we had in Fig. 35 does not agree with  
 1321 this point, meaning that it is experiencing electrical cross talk. One might assume that imperfectly  
 1322 blocking the hole may cause this result, but the signal would have been shown in low frequency,  
 1323 not in high frequency.

1324 The long electric wire attached on ER10C probe head is the source of the electrical crosstalk.  
 1325 One ER10C was specially modified as requested to eliminate, the capacitive coupling in blocked  
 1326 ER10Cs microphone response, approximately 20dB per octave or 60dB per decade curve in high  
 1327 frequency (Fig. 35). To remove the capacitive coupling caused by the ER10Cs long wire, we put  
 1328 the amplifier near the probe head. A theoretical explanation of this can be found in Eq. 79,  $\frac{\partial D}{\partial t}$   
 1329 term in Ampere's law, which is underestimated in the probe's design process.

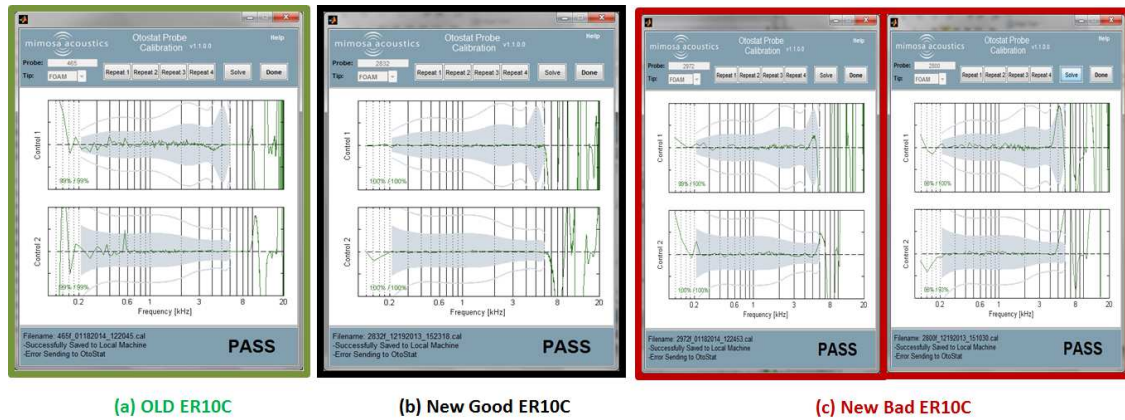


Figure 34: (a) Brass material for the middle tube holder part (the brass holder). RTV silicon is used to block the holder’s side hole. Calibration passes up to 9-10kHz (ER10C with 3 digits serial number) (b) Aluminum material for the chamber. RTV silicon is not used to block the holder’s side hole, but some of black material seals the side hole. Calibration passes up to 6kHz (ER10C with 4 digits serial number). (c) Aluminum chamber is used. None of material seals the holder’s side hole, a portion of the hole could be sealed randomly. Calibration totally fails or sometimes it passes but is unstable usually above 4kHz (ER10C with 4 digits serial number). Also (based on the manufacturer), the type of wire used in ER10C has been changed.

### 3 A new probe design

Motivated by the published transducer model (Kim and Allen, 2013) as well as the experimental investigation of ER10C, we have designed improved measurement probes to extend middle ear diagnostics. These new acoustic probes, the MA16 and MA17, have been considered to enhance characteristics of the ER10C, such as sensitivity, frequency response, noise floor and linearity.

We explain how we designed our hearing measurement probe based on the theoretical understanding of probe’s functions as well as trials and errors from experiments.

#### 3.1 Choice of transducers

Two kinds of transducers are needed, a microphone and receiver. Based on the linearity of the receiver, (usually) we may need two receivers in a probe to measure such as DPOAE.

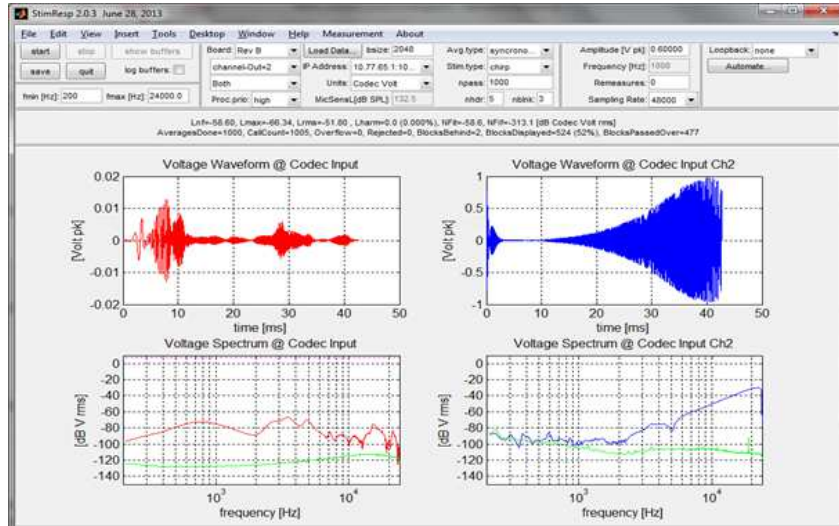
Using an absolute microphone (i.e., BK2137 or ER7C), sensitivities of both microphone and receivers should be measured in mV/Pa and Pa/mV. The industry standard for the microphone sensitivity is 50 [mV/Pa] at 1kHz.

Dynamic range (or linearity) of the probe defines the usable range of the probe in terms of both frequency range and the level of the signal.

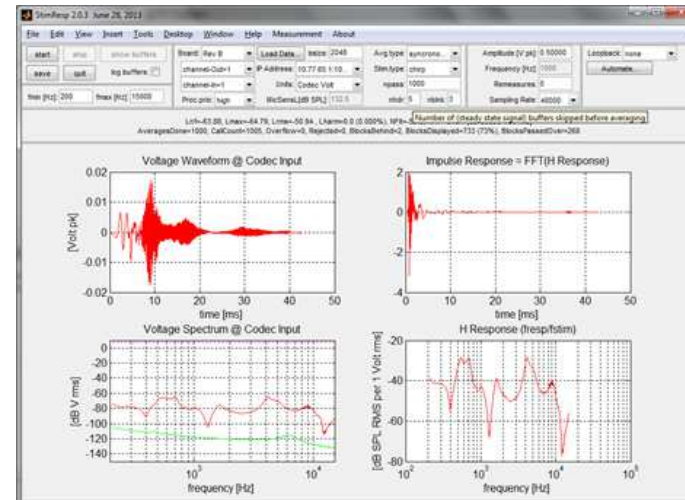
Based on the all of the above, we can choose the right combination of microphone and receiver.

#### 3.2 Sound delivery path for the microphone

The microphone picks up the sound inside a space such as a testing cavity, ear canal, or artificial ear. Though there are many modes in the spreading waves, namely higher order modes (HOMs) in the space, what we really consider is the plane wave, which is easy to analyze especially for the source calibration procedure; the HOMs may be ignored if there is a sufficiently large distance in the system over which they will die out exponentially. Here are some tips for performing a simple calibration procedure assuming the microphone is used to measure an ideal cylindrical cavity.



(a) Original ER10C crosstalk (blue) with ER7C response (red)



(b) ER10C crosstalk (blue) after the modification

Figure 35: (a) The sound (0.6V chirp, zero to peak, not RMS) was generated by one of the internal ER10C speakers. The right (blue, ch2) shows the blocked ER10C (serial: 2928) microphone response, and the left (red, ch2) shows the E7C microphone response as a reference of the sound level. Note that we used a small cut syringe with a tiny volume to connect both ER7C microphone and ER10C probe. We blocked the microphone hole on the attached ER10C foam tip for decoupling the microphone path from the sound in the cavity generated by the internal ER10C speaker. Physically and theoretically, internal ER10C's sound paths for the microphones and the receivers are separated. Therefore if the microphone hole is blocked, none of the acoustic signal can go through the microphone's diaphragm. any signal that is shown on the right side of this figure (blue) is internal crosstalk of the probe. We read that in high frequency it is approximately increasing proportion to 20dB/octave (capacitive coupling), based on this observation, we hypothesize the source of this crosstalk is in wire of ER10C. This was the motivation of modifying ER10C, including the preamp on the ER10Cs head. Note that this measurement was made on May 14 2014 at Mimosa Acoustics by NK using Stimresp software (Mimosa Acoustics) (b) Crosstalk measurement after the modification, the rising crosstalk behavior in high frequency is apparently reduced. The modified ER10C is inserted in a short cavity with blocked microphone. The probe is connected to the specially modified APU for the modified ER10C.

- 1353 1. centering the microphone port, pointing the cavity end.
- 1354 2. about 3[mm] of tube is needed in front of the microphone's port to pick up the plane wave.  
1355 Note that the HOMS die out within a few mm once the wave starts to spread from the source.
- 1356 3. when the frequency response of the microphone is not flat (dividing the microphone response  
1357 to an ideal microphone), introducing peaks, it usually means the microphone tube is too long.  
1358 You may use a loosely packed cotton or acoustic resistor, to minimize the tube effect.

### 1359 3.3 Sound delivery path for the receiver

1360 When sound is generated from a receiver, it is guided by its port and then spreads out. An ideal  
1361 speaker has a flat frequency response regardless of the signal level, maintaining a constant level  
1362 across all frequencies. But the reality is that distortions are observed due to high peaks (in pressure)  
1363 at certain frequencies. There is not a linear relationship between the level of the distortion and the  
1364 level of signal, due to the hysteresis effect of electro-magnetic system. Indeed it is a really noisy  
1365 device to deal with. Here are some useful tips to handle this device when we make a probe.

- 1366 1. Finding out the linear region of this transducer (dynamic range) based on the given sensitivity  
1367 is critical.
- 1368 2. A small piece of cotton (loosely packed) can be applied to the sound spreading area inside  
1369 the probe. This will help not only to damp out the pressure peak at the certain frequency  
1370 point but also to design the wave spreading space close to the ideal shape (i.e., cylinder).

### 1371 3.4 Probe evaluation

1372 The following is a list of specifications to evaluate a hearing measurement probe:

- 1373 1. Frequency responses of both microphone and speaker should be as flat as possible, especially  
1374 within the frequency range of human hearing (ideally up to 20kHz for the microphone and  
1375 up to 16kHz for the speaker)
- 1376 2. Thevenin parameters must be stable over time. This can be evaluated via source calibration  
1377 (i.e., 4 cavity calibration, Allen (1986))
- 1378 3. Output levels for loudspeakers should be higher for amplification of signal, especially for  
1379 measuring hearing impaired ears. (i.e., 85dB SPL desirable)
- 1380 4. Dynamic range as large as possible. Dynamic range is defined as the subtraction between  
1381 the first harmonic level and the total harmonic level at each frequency (i.e., 50-60dB is  
1382 acceptable).
- 1383 5. Linearity superior to current probes. Dynamic range should be linear across the frequency  
1384 range of interest.
- 1385 6. Impulse response should be short and exact. The duration of impulse ringing should be less  
1386 than 1 ms. This result is critical to TEOAE measurement.
- 1387 7. Crosstalk issues including all noise sources must be addressed - microphone, loudspeaker,
- 1388 8. Good seal and stability in the ear canal. This needs good earplug design to fit a range of  
1389 adult ear-canal sizes and shapes easily.

1390 The size of the probe is an especially critical factor in the clinic for measurements of infant ears,  
1391 due to their very small ear canals. There are other serious issues relevant to manufacturing a probe,  
1392 such as handling ear tips, removing ear wax, etc, which must take into account in the probe design.

1393 A general acoustic measurement setup (to test the itemized evaluation categories) is found in  
1394 Fig. 36.

1395 The ‘cavity or free field’ block can be DB100 or B&K4157 artificial ear coupler, a cut-off syringe,  
1396 any tube, or any rigid cavity in which the probe may be sealed. The ‘probe’ block can be any probe  
1397 containing a loudspeaker and a microphone (or two microphones). The probes we have used include  
1398 the ER10C and MA probes. We also use a probe simulator<sup>22</sup> to evaluate the electronic part of the  
1399 system, in order to provide a baseline for the probe’s performance characteristics.

1400 In our specific experiments, two audio processing units were used, an APU and MU (‘Audio  
1401 Processing Unit’ and ‘Modified Unit’ by Mimosa Acoustics). The APU is built for use with the  
1402 ER10C probe. The other, the MU, is built to by-pass the internal RC of the ER10C probe, setting  
1403 the gain to unity. The MU is used for the other probes, such as the MA probes (and ILO probe  
1404 from Otodynamics). When using the MU with these other probes, an external RC circuit and  
1405 pre-amp can be added for evaluation.

1406 Several microphones can be used for calibration of the transducers used in the probe, to measure  
1407 the receiver and microphone sensitivities, frequency responses, and other characteristics. The  
1408 microphone (‘Mic’, the previous stage of the ‘Sound Level Meter’ in Fig. 36) and ER7C microphone  
1409 (‘Mic ER7C’ in Fig. 36) are reference microphones, which are supposed to have wide and flat  
1410 frequency responses. When both the reference microphones and the tested probe microphone pick  
1411 up the response from the test cavity, the tested microphone’s response is divided by the reference  
1412 microphone’s response to obtain the test microphone frequency response.

1413 An oscilloscope, spectrum analyzer, or multi-meter can be used to monitor the voltage at various  
1414 points of the setup. In this setup, the specific points of interest are at

- 1415 1. the input to the tested probe speaker for computing the receiver sensitivity,
- 1416 2. the output of the tested probe microphone, and
- 1417 3. the output of the external gain for computing the microphone sensitivity.

1418 To check the frequency response of the transducers, it is necessary to calibrate the transducers  
1419 (receivers and microphone inside the probe). Once we calculate the sensitivity of the transducer,  
1420 we can compute the frequency response of the probe by applying a chirp signal and normalizing  
1421 the response with the sensitivity at 1kHz.

---

<sup>22</sup>a package of circuit elements to simulate electrical part of the probe excluding the acoustic elements

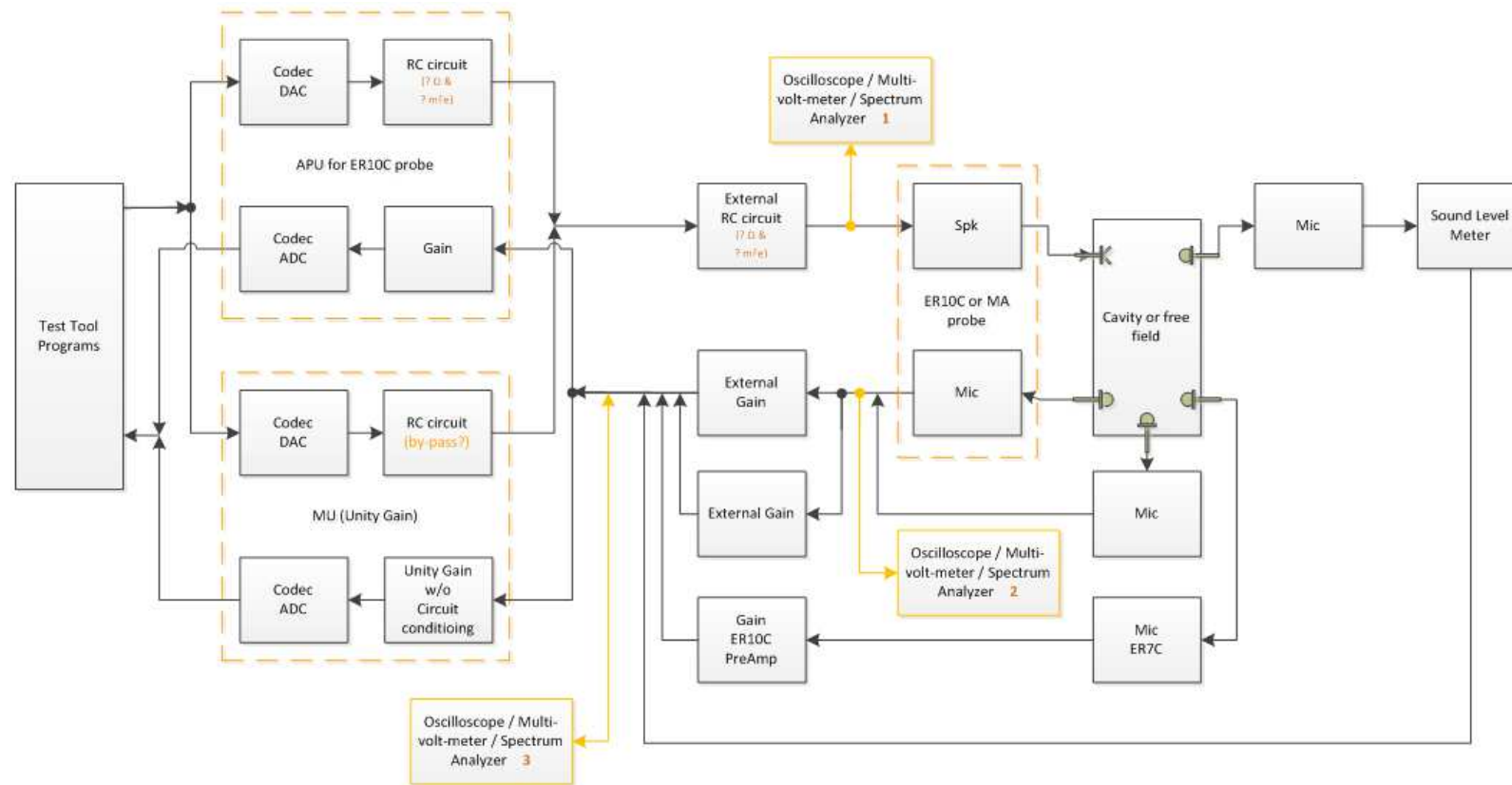


Figure 36: Basic acoustic testing setup

1422 **Part IV**  
 1423 **Results**

1424 In this section, we represent key results based on our theoretical and experimental study (chapter II  
 1425 and III). Details of modeling BAR and its calibration results using Hunt parameters are discussed.  
 1426 Then, we reduce the BAR model to a simple electro-mechanic system, only involving essential  
 1427 circuit components for composing the system. This minimized model is used for  $Z_{mot}$  simulations  
 1428 to justify our theory discussed in chapter II.

1429 **1 Hunt parameter calibration**

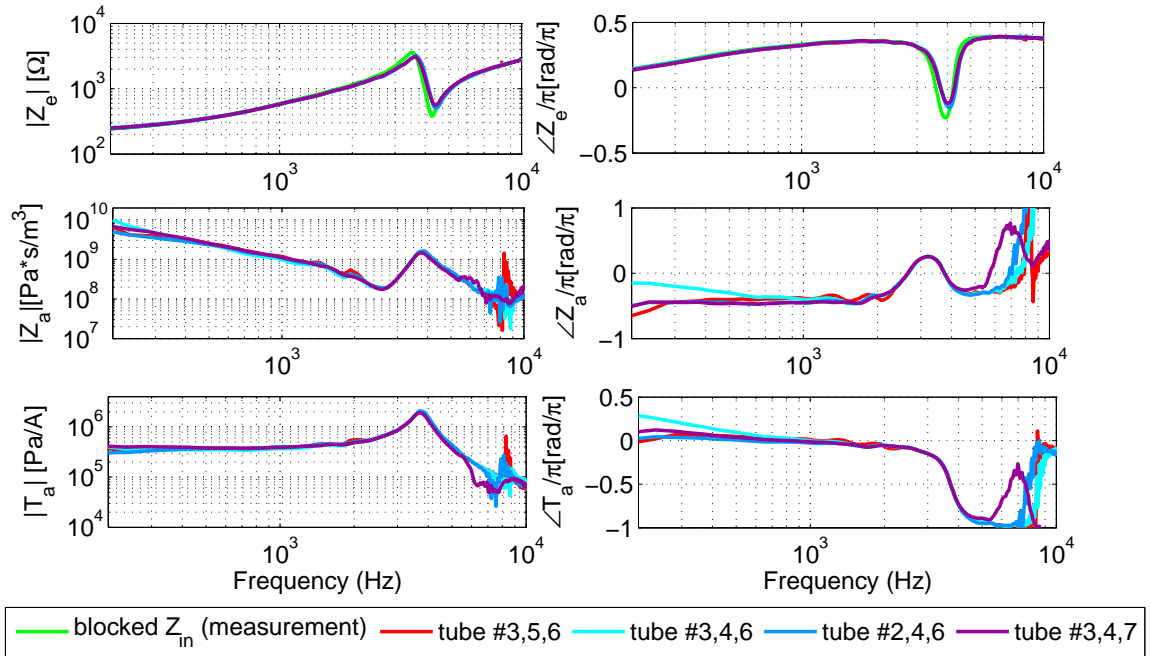


Figure 37: Calculated Hunt parameters ( $Z_e$ ,  $Z_a$ , and  $T_a$ ) of the ED7045. Three measurements of  $Z_{in}$  with acoustic loads (indicated by number as shown in the legend) are required to find one set of the three Hunt parameters. The length of each numbered tube is described in Fig. 25.  $Z_{in}$  which is measured by blocking the receiver's port ( $V = 0$ ) is plotted with  $Z_e$  (green line).

1430 The calculated Hunt parameters of the BAR derived from various  $Z_{in}$  (Fig. 25) are shown in  
 1431 Fig. 37. Some considerations for the Hunt parameters of the BAR are as follows:

- 1432 1.  $\mathbf{Z_e}$ : Compared to  $Z_a(s)$  and  $T_a(s)$ ,  $Z_e(s)$  has the smallest dependency on the choice of load  
 1433 cavities (the three of six chosen load impedances: loads (2)-(7) in Fig. 25). Below 200[Hz],  
 1434  $Z_e(s)$  converges to a fixed resistance (ED7045:  $\approx 195[\Omega]$ ). The frequency range between  
 1435 0.5-2.5[kHz] is proportional to 's' ( $Z_e$  shows a slope of 1 in this frequency range). It is not  
 1436 clearly shown at frequencies below 10[kHz], however when the frequency increases, the slope  
 1437 of  $Z_e$  approaches that of ' $\sqrt{s}$ '. More precise evidence of ' $\sqrt{s}$ ' domination at high frequency  
 1438 is shown in Fig.26 in the polar plot. These frequency dependant impedance behavior (e.g.,

- 1439 proportional to a constant, ‘s’ and  $\sqrt{s}$ ) is determined by the coil properties, which are closely  
1440 related the DC resistance, inductance and the semi-inductance. Note that  $Z_{in}$  (measured)  $\rightarrow$   
1441  $Z_e$  (calculated) as  $V \rightarrow 0$ .
- 1442 2. **Z<sub>a</sub>**: For frequencies below 2.5[kHz],  $Z_a$  is stiffness dominated (i.e., a capacitance), and between  
1443 2.5-4[kHz] it is dominated by the mass of the diaphragm and armature. Those properties  
1444 determine the first anti-resonance (zero, near 2.5[kHz]). The resonance (pole) at 3.7[kHz]  
1445 is the frequency where the transfer impedance,  $T_a$ , is maximum. The pole of  $Z_e$  is also  
1446 introduced in this same frequency. As  $T_a$  and  $Z_a$  are tied more closely, they move together  
1447 when the set of Hunt parameter is changed while  $Z_e$  is almost identical over every set of  
1448 the Hunt parameters (Fig. 38). Above 4[kHz] the transmission line and acoustic properties  
1449 dominates given the small volume inside the receiver. The error above 6-7[kHz] is primarily  
1450 caused by the experimental limitations, such as the manual manipulation of the tubes.
  - 1451 3. **T<sub>a</sub>**: It is nearly constant below 2-3[kHz] and is  $4 \times 10^5$ [Pa/A] at 1[kHz]. The phase shift in  
1452  $T_a$  is due to acoustic delay. Although the frequencies above 6[kHz] are obscured by the noise,  
1453  $T_a$  seems to behave as an all-pole function, which depend on the system delay  $\tau$ . To account  
1454 for this delay, a transmission line (Tx line) is added to the acoustic model, as shown in Fig. 1.

## 1455 2 Receiver model

1456 In this section, we discuss details of our refined BAR model introduced in Fig. 1. The electrical  
1457 circuit elements are shown to the left of the gyrator.  $R_e$  is approximated to the DC resistance. The  
1458 source of the armature movement is the Lorentz force ( $F = \int J \times BdA$ ) due to the interaction of  
1459 the current in the coil and the static magnetic field  $B_0$  of the magnets. The current in the coil and  
1460 the core of the E-shaped armature give rise to the inductance  $L_{em}$ , while the penetration of the  
1461 magnetic field into the core induces an eddy current, depicted by a semi-inductor element  $K_1$  in  
1462 Fig. 1 Vanderkooy (1989).  $L_e$  represents any leakage flux, in air gap, which explains an additional  
1463 small stored energy.

1464 There should be a transition frequency,  $f_t = \frac{1}{2\pi} \left( \frac{K_0}{L_0} \right)^2$ , between the inductor ( $L_0$ ) and the  
1465 semi-inductor ( $K_0$ ). Since we used two inductors and one semi-inductor (total 3) for our receiver  
1466 model, it is unclear exactly how to calculate the  $f_t$  from these components as we discussed in section  
1467 1. However as shown in Fig. 39 (polar plot), the slope of the impedance is approaching  $\sqrt{s}$  ( $45^\circ$ )  
1468 as  $\omega$  increases. Based on Thorborg et al. (2007), the  $f_t$  of a dynamic loudspeaker is 100-200[Hz],  
1469 which means the  $f_t$  for the balanced armature receiver is much higher than for the moving coil  
1470 loudspeaker.

1471 The gyrator relates the electrical and the mechanical sections with parameter  $T = B_0 l$ . The  
1472 wire inside the ED7045 receiver is made of 49 AWG copper, which has a resistivity of 26.5[ $\Omega$ /m].  
1473 Since the measured DC resistance of the receiver is around 190[ $\Omega$ ] we can calculate the length of  
1474 the wire is approximately 7.1[m]. In general, the dynamic moving-coil speaker’s  $l$  is shorter than  
1475 the BAR’s. Therefore we can expect a larger ‘T’ value for the BAR ( $n \propto l, 1/d_{coil}$ ).

1476 To the right of the gyrator are the mechanical and acoustical sections of the transducer. We can  
1477 simply describe the mechanical section as composed of a series combination of the armature and  
1478 the diaphragm’s stiffness, mass and damping. The transformer’s coupling ratio of the acoustic side  
1479 to the mechanical side is related to the diaphragm’s area. The capacitor ( $C_a$ ) and a transmission  
1480 line in the acoustical part account for the back (rear) volume and sound delay. Because we are  
1481 using a gyrator, the mobility analogy method is not used (Beranek, 1954; Hunt, 1954).

<b>Electrical elements</b>
$R_e = 195 [\Omega]$ ,
$L_e = 9 [\text{mH}]$ ,
$K_1 = 27.5 [\text{Semi-Henry}]$ , $L_{em} = 52 [\text{mH}]$
<b>GYR</b> = 7.5
<b>Mechanical elements</b>
$C_m = 1.25\text{e-}3 [\text{F}]$ , $L_m = 4.3\text{e-}6 [\text{H}]$ , $R_m = 0.003 [\Omega]$
<b>TRF (1/Area)</b> = $1/(2.4\text{e-}6)$
<b>Acoustical elements</b>
$C_a = 4.3\text{e-}15 [\text{F}]$
Tx Line: $z_0 = 1\text{e}9 [\text{kg/sec}]$ , $l_t = 1\text{e-}4 [\text{m}]$
<b>Radiation impedance</b>
$L_{rad} = 10^{10} [\text{Acoustic-Henry}]$ , $R_{rad} = 10^{11} [\text{Acoustic-Ohm}]$

Table 2: Specific parameters that are used for the suggested model (Knowles BAR ED7045).  $c$  is the speed of sound in the air (334.8[m/s]),  $j\omega/c$ ,  $z_0$ , and  $l_t$  are the propagation function, specific characteristic resistance and length of the transmission line, respectively. GYR and TRF stand for the gyrator and the transformer. All model parameters were found by minimizing the RMS error between the model and electrical input impedance measurements of the receiver.

The Thevenin pressure of the BAR is defined given that the volume velocity ( $V$ ) at the port is zero ('blocked' port), meaning the load impedance is set to  $\infty$ .

Several comparisons are made to verify that the transducer model (Fig. 37, 1). First, the Hunt parameters are calculated from the model to support the transfer relation between electrical and acoustical parts (Section 1.1). The mechanical part of the transducer model was verified by conducting laser mechanical velocity measurements in a vacuum condition (Section 1.2). Along with these results, we simulated the Thevenin pressure of the transducer from our model and compared the result to the pressure measurement (when  $V=0$ ) (Section 1.3). These three comparisons (electrical, mechanical, and acoustical) justify and verify the transducer model (Fig. 1).

## 2.1 Hunt parameters comparison

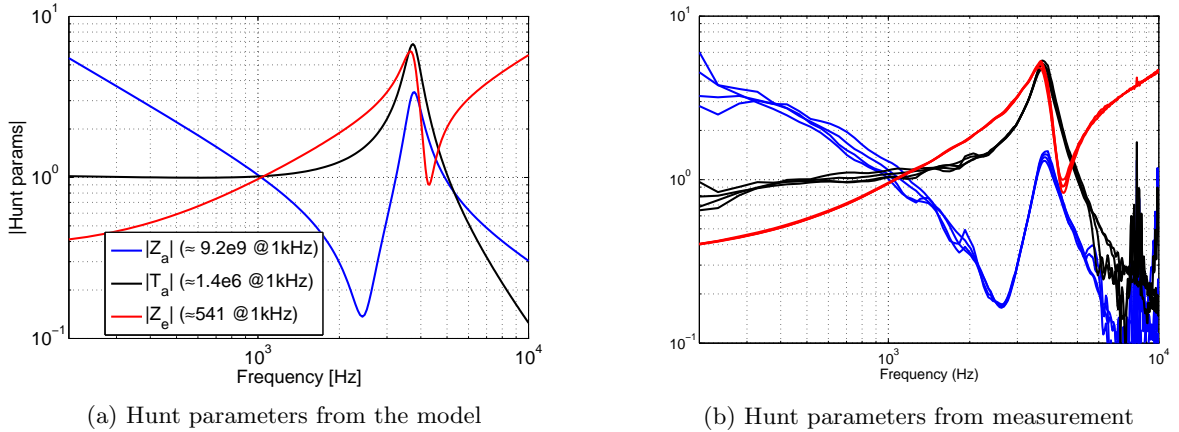


Figure 38: Comparison of Hunt parameters ( $Z_e$  (red),  $T_a$  (black), and  $Z_a$  (blue)) from the model (a) and the measurements (b). Any significant differences between the model and the data occur above 6[kHz]. All parameters are normalized to their 1[kHz] values.

1492 The Hunt parameters, from the model and the experimental calculation, are compared in Fig. 38.  
1493 The discrepancies of  $Z_a$  above 6 - 7[kHz] are presumably caused by the manual adjustment of the  
1494 experimental conditions. This error is insignificant in  $Z_e$ . However the small noise in electrical  
1495 impedance impacts the parameter estimation far from the electrical side. In other words, we can see  
1496 the largest variation in acoustical parameter ( $Z_a$ ), as the transition order goes from  $Z_e \rightarrow T_a \rightarrow Z_a$ .  
1497 Another interesting parameter is the resonant frequency (3-4kHz). The frequency of the pole  
1498 ( $f_p$ ) for in Fig. 38 looks almost identical:  $Z_e$ ,  $Z_a$  and  $T_a$  slightly differ by the set, but the  $f_p$  of the  
1499 three parameters occurs priorly at the same location for the same set of Hunt parameters. The three  
1500 parameters assume the zero-loaded condition which means, in theory, the  $f_p$  should be identical  
1501 for all cases. Because of small measurement differences, this is not exactly the case. This resonant  
1502 frequency can thus be interpreted as one of the most fundamental characteristics (eigenmode) of  
1503 an electro-magnetic transducer.

## 1504 2.2 Verification 1: Electrical impedance *in vacuo*

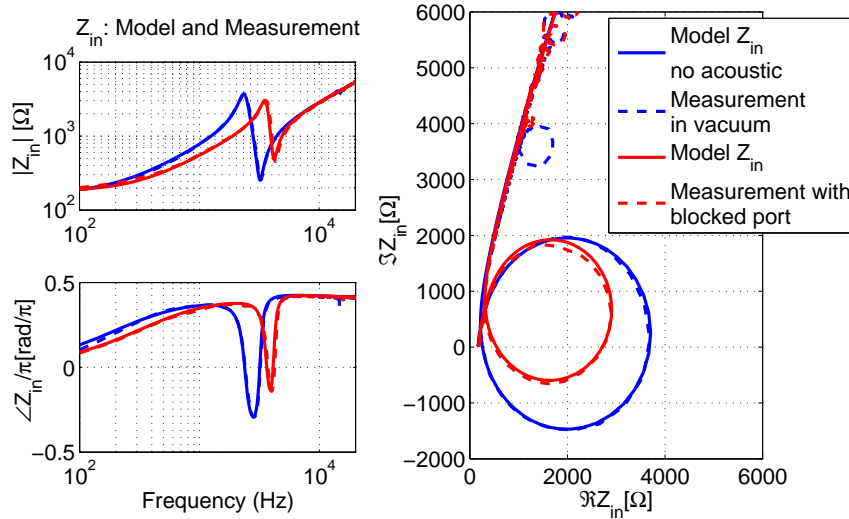


Figure 39: Comparison the suggested model of Fig. 1 and real electrical input impedance measurement of a balanced armature hearing-aid receiver (Knowles, ED7045). Blue and red colors represent vacuum and non-vacuum (ambient) conditions respectively. And the dashed lines represent the experimental result, whereas the single lines show the model results. For the vacuum experiment, the static pressure is less than 0.003[atm]. The left panel shows the magnitude and the phase of each condition while the real and imaginary parts of the same data are plotted in the right panel. Up to 23[kHz], the experimental data is in good agreement with the modeling result (The sampling rate is 48[kHz], therefore the maximum measured frequency is 24[kHz]). In the polar plot, above 8[kHz], the impedance behaves as  $\sqrt{s}$ .

1505 The acoustical part in the transducer model is removed for the vacuum case, while all the  
1506 electrical and mechanical parameters in Fig. 1 during the experiments remain the same as the  
1507 no-vacuum condition.

1508 In Fig. 39, the simulated electrical input impedance results are expressed in two ways; the  
1509 magnitude-phase and the polar plot (real vs. imaginary parts). For both the vacuum and the  
1510 blocked port condition, the model (solid lines) and the experiment result (dashed lines) show

1511 reasonable agreement below  $\approx 12$ [kHz].

1512 The transducer model, including acoustical elements ('blocked' output port) is in red, and the  
 1513 model excluding acoustical elements (vacuum condition) is in blue. Both cases give similar shape, a  
 1514 pole, followed by a zero, with increasing frequency ( $\approx 890$ [Hz] in vacuum,  $\approx 750$ [Hz] in blocked case).  
 1515 We conclude that the trapped air (between the diaphragm and the port of the receiver) influences  
 1516 the resonance by pushing it to higher frequencies due to the increased stiffness to mass ratio. Also  
 1517 because of the acoustical properties (including mechanical-acoustical coupling), the magnitude of  
 1518 the vacuum resonance is reduced by 1.9dB compared to the blocking the receiver's output port (in  
 1519 air).

1520 By looking at the polar plot (the right panel in Fig. 39), we can clearly see that the high  
 1521 frequency impedance is dominated by  $\sqrt{s}$ , clear evidence of the eddy-current, in the BAR. The  
 1522 many small loops appearing above 16[kHz] may be a measurement artifact, however the second  
 1523 resonance at 15[kHz] is real.

### 1524 2.3 Verification 2: Mechanical velocity measurement using Laser *in vacuo*

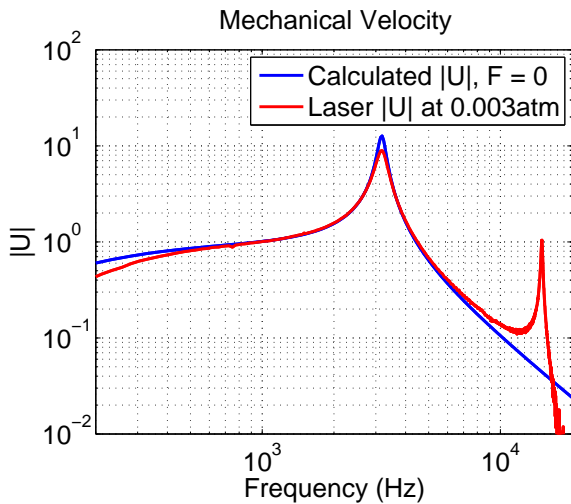


Figure 40: Comparison of the diaphragm (mechanical) velocity between the transducer model and the laser measurement in vacuum, the pressure  $P$  is zero. For the model simulation, the acoustical part in Fig. 1 is not included. The laser measurement was performed after pumping out the air in the receiver. All values are normalized to one at 1[kHz].

1525 As shown in Fig. 40, the mechanical velocity is also calculated from the transducer model and  
 1526 compared with the laser velocity measurement result. The model and the experiment are well  
 1527 matched below 10[kHz].

1528 However small magnitude difference is observed; the laser measured data has about 1[dB] higher  
 1529 velocity at the FR and the low frequency area. There are some possible solutions to improve the

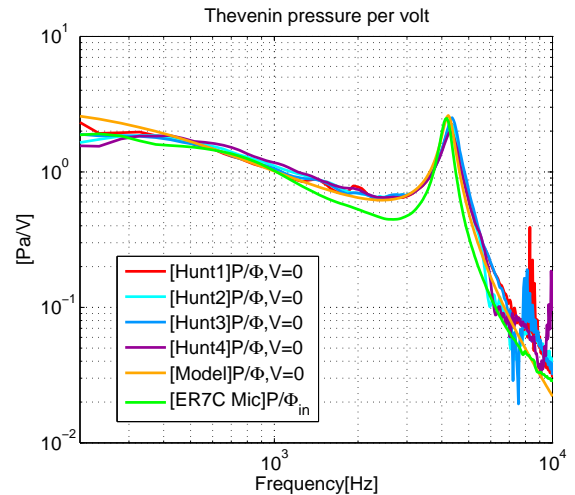


Figure 41: Comparison of Thevenin pressure (per voltage) data from various sources. There are 6 different lines, the first 4 lines are calculated from the electrical experiments (Hunt parameters), and the orange colored line is estimated from the model. The last pressure data (in light-green) are taken from the pressure measurement and are divided by the electrical input voltage of the receiver. All data assume the blocked condition,  $V=0$  (see text). Every value is normalized to one at 1[kHz].

1530 model. First, as explained in section 1.2, when we make the measurement, we put the laser’s  
 1531 focus near at the rod (where the armature and the diaphragm is connected). And secondly, when  
 1532 modeling the data, we could add or remove mechanical damping in the transducer model (i.e.,  
 1533 increasing or decreasing the value of  $R_m$  in our model Fig. 1) relative to the present value. The  
 1534 problem below 200[Hz] is due to a very small hole that is burned into the diaphragm, to act as a  
 1535 very low frequency leak.

1536 The mechanical velocity is calculated by assuming the force (F) in vacuum is zero. In reality, it  
 1537 is impossible to reach an absolute vacuum condition. Our experiment condition of 0.003[atm] seems  
 1538 adequate to understand the nature of the mechanical velocity of the transducer as the measurement  
 1539 gives a reasonable agreement with the model.

## 1540 2.4 Verification 3: Thevenin pressure comparison

1541 The model and measured Thevenin pressure are plotted in Fig. 41. Two indirect pressure estimation  
 1542 methods are used; one using the Hunt parameters, and the other using the simulation of our  
 1543 transducer model. There is a reasonable agreement among these measures up to 6-7[kHz]. The  
 1544 mathematical definitions of these data are the Thevenin pressure per unit voltage ( $P/\Phi$ ), with a  
 1545 zero volume velocity ( $V = 0$ ),

$$\frac{P}{\Phi} \Big|_{V=0} = \frac{T_a}{Z_e} \Big|_{V=0}. \quad (128)$$

1546 Note that  $\frac{P}{T}$  and  $\frac{P}{\Phi}$  differ in the theoretical meaning as well as in the definition;  $T_a \equiv \frac{P}{T} \Big|_{V=0}$  is  
 1547 one of the Hunt parameters, while the Thevenin pressure (per volt) in Eq. 128 is a more realistic  
 1548 experimental function, when one uses a voltage drive. For the comparison, the pressure data is  
 1549 divided by the voltage ( $\Phi_{in}$ ) across the two electrical terminals of ED7075 (A and B in Fig. 28)  
 1550 when  $V = 0$ . The data from section 1.1 is imported for  $\Phi_{in}$ , assuming  $V = 0$  at the port in the  
 1551 pressure measurement.

1552 The green line in Fig. 41 shows the Thevenin pressure data derived from the ER-7C probe  
 1553 microphone. Other than the direct pressure measurement (green), all responses are derived from  
 1554 the Hunt parameter calculation introduced in the Appendix E, using the ‘electrical input impedance  
 1555 measurements’ for acoustical loads.

## 1556 3 $Z_{mot}$ simulation of simplified electro-mechanic systems

1557 For further application, we will investigate a simple electro-mechanic network model including a  
 1558 semi-inductor. The goal is to demonstrate some condition that  $\Re Z_{mot} < 0$  based on the simplified  
 1559 electro-mechanic model. The simple electro-mechanic model has been reduced from the Kim and  
 1560 Allen’s original work (Fig. 1: the electro-acoustic network model, Kim and Allen (2013)). Related  
 1561 theories are discussed in section 4 and Appendix B.

1562 Left sided figure in Fig. 42 shows a oversimplified two-port network from Fig. 1 containing only  
 1563 essential components for better and easier understanding of the physical electro-mechanic system.  
 1564 In this simple model, any acoustic or resistive components are eliminated.

1565 In this figure we have four components: a semi-inductor, an inductor in the electrical port, a  
 1566 mass in the mechanical port, and a gyrator that links two ports.

1567 The two circuits in Fig. 42 represent equivalent circuits via the mobility (dual) analogy. In both,  
 1568 very low and high frequencies the capacitor ‘m’ is opened. The parallel relation of semi-inductor  
 1569 and inductor enables the semi-inductor’s high frequency dominance Vanderkooy (1989). The mid  
 1570 frequency is governed by the inductor L and the capacitor m. If we ignore the semi-inductor in

1571 Fig. 42, the system looks like a Helmholtz resonator with neck mass  $L$  and barrel compliance  $m$ .  
 Therefore these two components act like a resonator in the system.

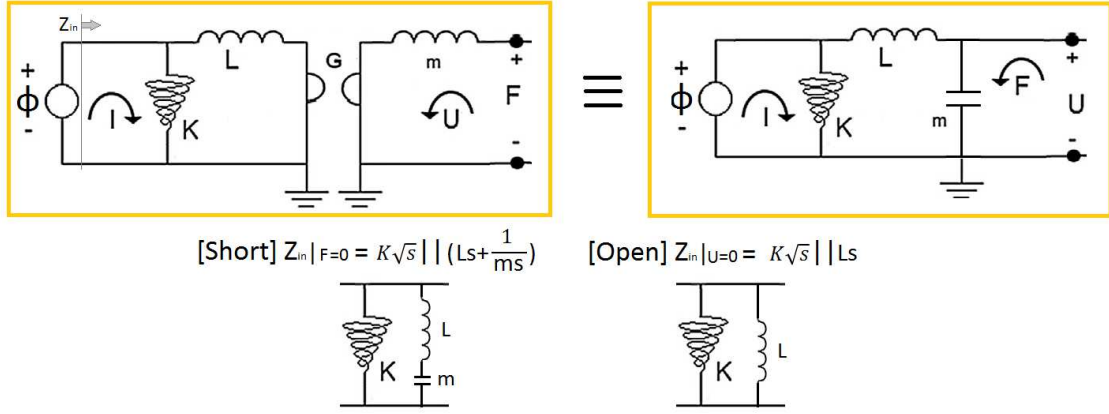


Figure 42: The top left circuit: A simple anti-reciprocal network with a semi-inductor presence. The top right circuit: The dual representation of the left circuit (equivalent) by applying mobility analogy beyond the gyrator.  $Z_{mot}$  is reconsidered based on Eq. 47. The frequency dependent real parts (shunt loss) of the semi-inductor in  $Z_{in}|_{F=0}$  (short) experience positive phase shift when the open condition impedance ( $Z_{in}|_{U=0}$ ) is subtracted from it.

1572

1573

1574

To realize this system into a matrix form, we can use ABCD matrix cascading method which results in Eq. 129.

$$\begin{bmatrix} \Phi(\omega) \\ I(\omega) \end{bmatrix} = \begin{bmatrix} 1 & 0 \\ \frac{1}{K\sqrt{s}} & 1 \end{bmatrix} \begin{bmatrix} 1 & sL \\ 0 & 1 \end{bmatrix} \begin{bmatrix} 0 & G \\ \frac{1}{G} & 0 \end{bmatrix} \begin{bmatrix} 1 & sm \\ 0 & 1 \end{bmatrix} \begin{bmatrix} F(\omega) \\ -U(\omega) \end{bmatrix}, \quad (129)$$

1575

1576

1577

1578

where  $s$  is the Laplace frequency ( $\sigma + j\omega$ ) and ' $L$ ', ' $K$ ', ' $G$ ', and ' $m$ ' are the inductance, the semi-inductance, the gyration coefficient, and the mass of the system respectively.

Let's isolating the ABCD matrix part in Eq. 129 and setting ' $L$ ', ' $K$ ', ' $G$ ', and ' $m$ ' to be '1' for a simple to make the algebra simple calculation, the equation is reduced to

$$\begin{bmatrix} 1 & 0 \\ \frac{1}{\sqrt{s}} & 1 \end{bmatrix} \begin{bmatrix} 1 & s \\ 0 & 1 \end{bmatrix} \begin{bmatrix} 0 & 1 \\ 1 & 0 \end{bmatrix} \begin{bmatrix} 1 & s \\ 0 & 1 \end{bmatrix} = \begin{bmatrix} 1 & s \\ \frac{1}{\sqrt{s}} & \frac{s}{\sqrt{s}} + 1 \end{bmatrix} \begin{bmatrix} 0 & 1 \\ 1 & s \end{bmatrix} \quad (130)$$

1579

Finally the ABCD matrix of the system in Fig. 42 is

$$\begin{bmatrix} \Phi(\omega) \\ I(\omega) \end{bmatrix} = [T_1] \begin{bmatrix} F(\omega) \\ -U(\omega) \end{bmatrix} = \begin{bmatrix} A(s) & B(s) \\ C(s) & D(s) \end{bmatrix} \begin{bmatrix} F(\omega) \\ -U(\omega) \end{bmatrix} = \begin{bmatrix} s & 1 + s^2 \\ \frac{s}{\sqrt{s}} + 1 & \frac{1}{\sqrt{s}} + \frac{s^2}{\sqrt{s}} + s \end{bmatrix} \begin{bmatrix} F(\omega) \\ -U(\omega) \end{bmatrix}, \quad (131)$$

1580

where  $\Delta_{T_1} = -1$ . Converting Eq. 131 into an impedance matrix, Eq. 11 is used to give us

$$Z_1 = \begin{bmatrix} z_{11} & z_{12} \\ z_{21} & z_{22} \end{bmatrix}, \quad (132)$$

1581

where

$$z_{11} = \frac{s}{\frac{s}{\sqrt{s}} + 1} = \frac{s\sqrt{s}}{s + \sqrt{s}} (\equiv s||\sqrt{s}), \quad (133)$$

1582

$$z_{12} = \frac{-1}{\frac{s}{\sqrt{s}} + 1} = -\frac{\sqrt{s}}{s + \sqrt{s}}, \quad (134)$$

1583

$$z_{21} = \frac{1}{\frac{s}{\sqrt{s}} + 1} = \frac{\sqrt{s}}{s + \sqrt{s}}, \quad (135)$$

1584

$$z_{22} = \frac{\frac{1}{\sqrt{s}} + \frac{s^2}{\sqrt{s}} + s}{\frac{s}{\sqrt{s}} + 1} = \frac{1 + s^2 + s\sqrt{s}}{s + \sqrt{s}}. \quad (136)$$

1585 By substituting ‘ $s$ ’ with ‘ $j\omega$ ’ one can easily find that all impedances of this system (Eq. 133, 134,  
1586 135, and 136) are complex quantities, meaning that all have both real and imaginary parts in each  
1587 frequency point. The results shown in Eq. 133 - Eq. 136 are a counter example that does not follow  
1588 the traditional approach of a lossless LC network. In the other words, a lossy network has been  
1589 realized without having a resistor in a system. We will show in the next section that this is due to  
1590 existence of the semi-inductor in a system by comparing a case where the semi-inductor does not  
1591 exist.

1592

Using Eq. 50,  $Z_{mot}$  of this system can be calculated as

$$Z_{mot1} = \frac{1}{\left(\frac{s}{\sqrt{s}} + 1\right)\left(\frac{1}{\sqrt{s}} + \frac{s^2}{\sqrt{s}} + s\right)} = \frac{s}{\sqrt{s} + s + s^2 + 2s^2\sqrt{s} + s^3} \quad (137)$$

For computational benefits, we can convert Eq. 137 to an admittance ( $Y_{mot}$ ) to investigate the real part of  $Z_{mot}$ ,

$$\begin{aligned} Y_{mot1} &= 1 + (\sqrt{s})^{-1} + s + 2s\sqrt{s} + s^2 = 1 + (\sqrt{j\omega})^{-1} + j\omega + 2j\omega\sqrt{j\omega} + (j\omega)^2 \\ &= \left(1 - \omega^2 - \frac{2\omega\sqrt{\omega}}{\sqrt{2}} + \frac{\sqrt{\omega}}{\sqrt{2\omega}}\right) + j\left(\frac{2\omega\sqrt{\omega}}{\sqrt{2}} - \frac{\sqrt{\omega}}{\sqrt{2\omega}} + \omega\right). \end{aligned} \quad (138)$$

1593

Since  $\omega$  is always greater than 0, the real part of Eq. 138 can have negative real parts if the equation  
1594 satisfies

$$1 - \omega^2 - \frac{2\omega\sqrt{\omega}}{\sqrt{2}} + \frac{\sqrt{\omega}}{\sqrt{2\omega}} < 0. \quad (139)$$

1595

For example, if we have an angular frequency  $\omega=1$ [rad/sec], Eq. 139 is satisfied ( $1 - 1 - \sqrt{2} - \frac{\sqrt{2}}{2} =$   
1596  $-\frac{1}{\sqrt{2}} < 0$ ). We can generalize if  $Y_{mot}$  is none positive then  $Z_{mot}$  is also not positive. In this  
1597 specific example, any angular frequency ( $\omega$ ) which satisfies Eq. 139 can have negative resistance in  
1598  $Z_{mot}$ . This  $Z_{mot}$  is not a positive definite quantity, which means it does not conserve energy of the  
1599 network. Something is missing here or should be explained further.

1600

Figure 43 represents the simulated Hunt parameters (Eq. 133-136). All impedances are complex  
1601 meaning both real and imaginary parts have frequency dependance. The two transfer impedances  
1602 have same magnitude but have 180 degree angle difference in complex domain. The input impedance  
1603 is inductive, but as frequency increases the angle approaches 45 degree. The output impedance  
1604 behaves like a resonator with damping. Figure 44 shows the motional impedance and input  
1605 impedances with both open and short circuit conditions. To help understand better, one can  
1606 think the open circuit impedance when a system is demagnetized, and the short circuit condition  
1607 is the system’s (i.e., a transducer) free oscillation in vacuum.

1608

## 4 Calibration results from both the modified and the manufactured probes

1609

1610

The probe’s source calibration is the first and perhaps most critical step to characterize the probe  
1611 system. Stable and accurate source parameters enable precise computation of the acoustic load

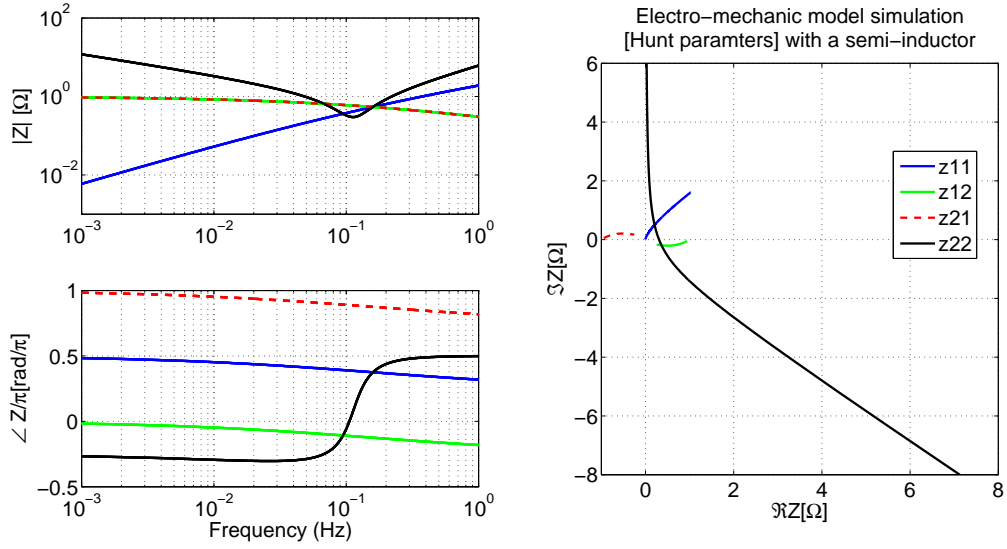


Figure 43: Computed Hunt parameters based on a simple electro-mechanic network shown in Fig. 42 (Eq. 133-136). All parameters  $K$ ,  $L$ ,  $G$ , and  $m$  are set to be 1 for a simple computation.

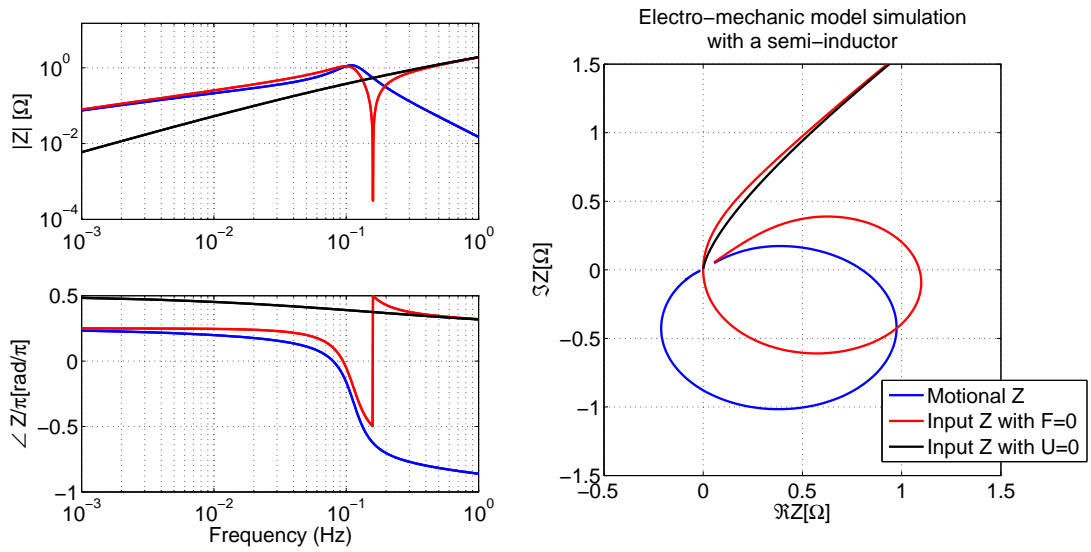


Figure 44: Computed motional impedance (Eq. 137), and input impedances with both open (Eq. 133) and short circuit conditions (Eq. 137+Eq. 133) based on a simple electro-mechanic network shown in Fig. 42.

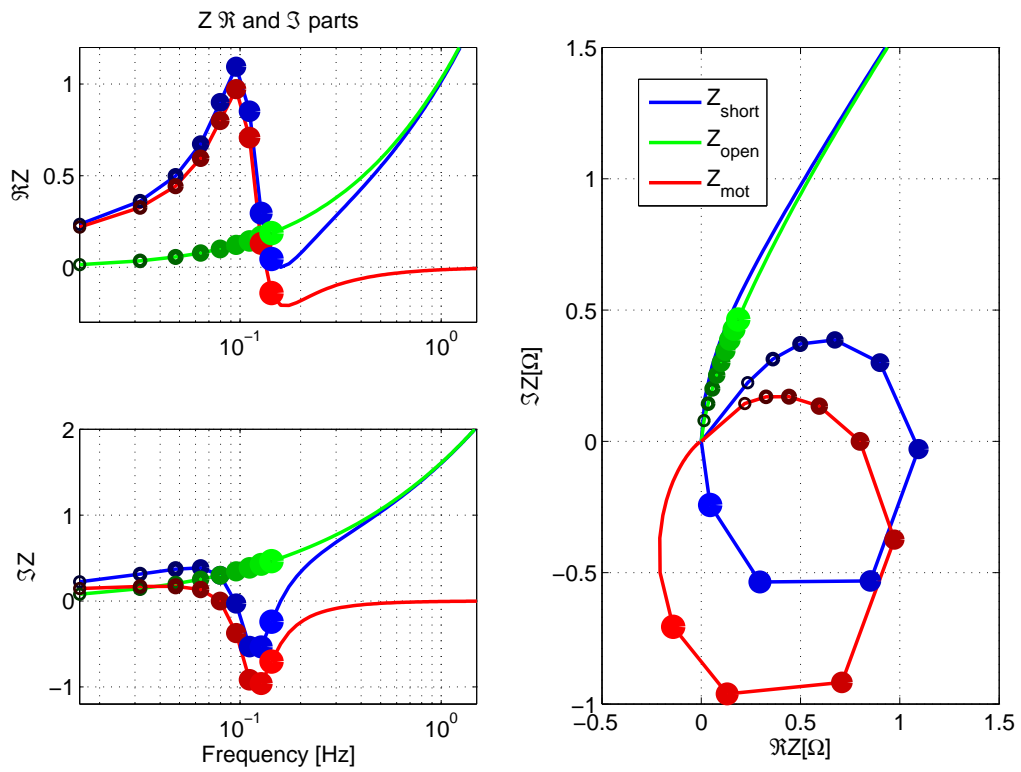


Figure 45: Real and imaginary parts of a simple electro-mechanic network shown in Fig. 42. The the marker's size indicates increment in frequency. Between 8<sup>th</sup> and 9<sup>th</sup> frequency points, the real parts of  $Z_{mot}$  goes to negative.

1612 such as a human ear. In the previous experiment section, we discussed several issues of existing  
 1613 probes and found the most common reason for calibration failure was crosstalk. Based on a solid  
 1614 understanding of the problem in the system, we physically modified and manufactured the probes  
 1615 to minimize the crosstalk effect in the system to calibrate the system above 6 kHz. As a result,  
 1616 the modified system can pass 4C calibration (Allen, 1986) above 10 kHz. The 4C calibration  
 1617 computes the 4C lengths ( $L_k$ ) and Norton parameters  $P_s(f)$ ,  $Y_s(f)$  based on the measured four  
 1618 cavity pressures, using a least-squares procedure.

1619 Also the MA16 and the MA17 (our manufactured prototype probes) have comparable perfor-  
 mance to the modified ER10C as shown in Fig. 46.



Figure 46: (Left figure) Source parameter calibration result from the modified ER10C to diminish the crosstalk effect. The probe can be calibrated above 10 kHz. Based on this result, we concluded that the crosstalk was interfering with the calibration procedure. (Middle figure) MA16 calibration result. This result demonstrates that we made our own system which can pass the 4C calibration above 10 kHz as well, for the first time. (Right figure) MA17 simulator calibration result. To overcome some drawbacks of the MA16, especially the size, we have proposed a new probe design, namely MA17. Before manufacturing the probe, we simulated acoustics of the probe’s structure to support the basic idea of the suggested design.

1620

1621 We believe that this study shows the electrical crosstalk may be a general problem for OAE  
 1622 hearing probe devices, which needs to be carefully addressed in the design process. This solution  
 1623 supports the importance of the  $\dot{\mathbf{D}}$  neglected in classical KCL as discussed in section 5.2, the dis-  
 1624 placement current due to time varying electrical field. The capacitive coupling in the wire should  
 1625 be carefully considered to design a probe.

#### 1626 4.1 The modified ER10C

1627 The modification includes the modified ER10C containing a +14dB differential amplifier, and a  
 1628 modified APU (Mimosa Acoustics) with a +20dB differential amplifier whose output is fed directly  
 1629 into the APU’s codec buffer amplifier. This modified system picture is shown in Fig. 47.

1630 Compared to the original ER10C, this modified probe showed better performance as demon-  
 1631 strated in Fig. 48. This figure investigates before and after characteristics of the ER10C modifica-  
 1632 tion compared to the theoretical values, particularly the change in sharpness of the acoustic null in  
 1633 each cavity (raw pressure data in a cavity with four different lengths). For example, if crosstalk is  
 1634 present at high frequencies, the pressure data around its corresponding null for the shortest cavity  
 1635 will be contaminated as shown (noisy notch in Fig. 48), hard to match by theoretical computation.  
 1636 With the low crosstalk probe, cleaner and sharper pressure acoustic nulls are detected, especially



Figure 47: The purpose of this modification is to reduce crosstalk due to the long wire of ER10C probe. This reveals that small changes in the wire may lead significant property changes of the probe. The key idea is to amplify the microphone signal before it passes through the long wire. Near the probe's head we placed amplifier as shown in this picture.

1637 for the shortest cavity. One can also calculate the reflectance  $\Gamma$  of each cavity theoretically (Keefe,  
 1638 1984), assuming that the load cavities have perfect cylindrical shape.

1639 This results will provide fundamental and operational understanding of not only ER10C system  
 1640 but also hearing measurement devices in general.

#### 1641 4.2 Prototype probes: MA16 and MA17

1642 Some efforts to make our own probe to substitute the ER10C can be found in the series of pro-  
 1643 totype probes that were made (i.e., MA4-8,6,12,13,14,16,17 series). Each series has 4-6 probes to  
 1644 demonstrate the strategy or idea highlighted at each stage. Finally we have demonstrated that  
 1645 our manufactured MA16 probe has a compatible performance to the modified ER10C probe which  
 1646 has the best performance on the market. Design of the MA17 is currently in progress to overcome  
 1647 drawbacks observed in the previous series, MA16. Compared to the our target size specification,  
 1648 the size of MA16 is too large. Figure 49 (a) shows the MA16 probe when it is inserted in the MA  
 1649 cavity. The inside structure of the MA16 head is shown in Fig. 49 (b).

1650 Based appreciation of the fundamental theories relevant to the design of a hearing measurement  
 1651 probe, we proposed the MA17. Before manufacturing the probe, the probe's acoustic characteris-  
 1652 tics were simulated using the MA17 simulator (Fig. 50). The Knowles FG23652 microphone and  
 1653 ED27045 receiver were used for the simulator. The ER7C was used as a reference microphone.  
 1654 To hold the transducers in a syringe, a piece of cut-foam was used, and cotton was used to center  
 1655 the microphones. The key idea of this structure is to line up all transducers inside of the probe.  
 1656 Also for the 4C calibration, when we change cavity lengths, the junction between probe's head and  
 1657 the cavity entry is smooth. Therefore the acoustic load (cavity) can be more similar to the ideal  
 1658 cylinder shape. To change the length using a piston, we need to open and close a small hole (using  
 1659 a piece of putty) to adjust the pressure inside the syringe every time we change the cavity length.

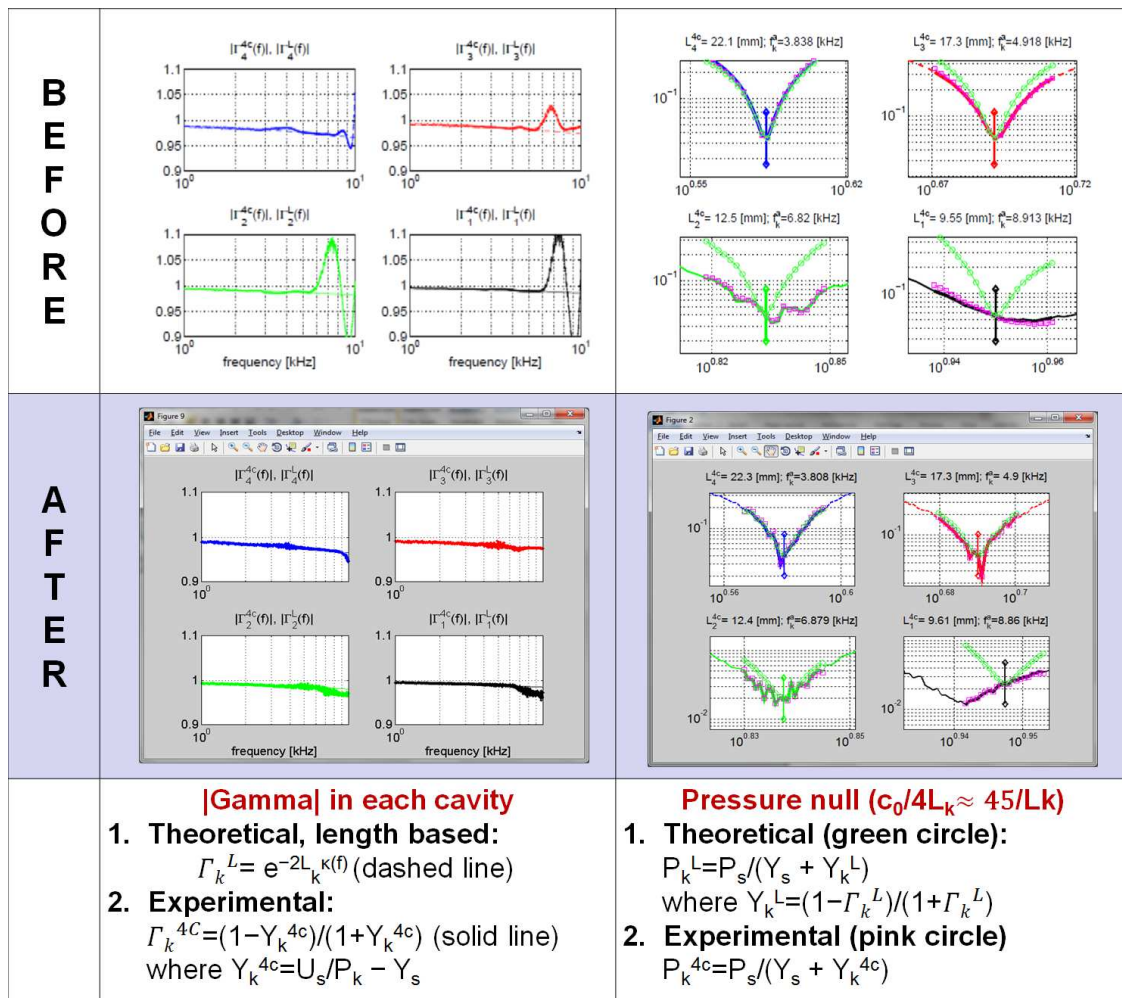
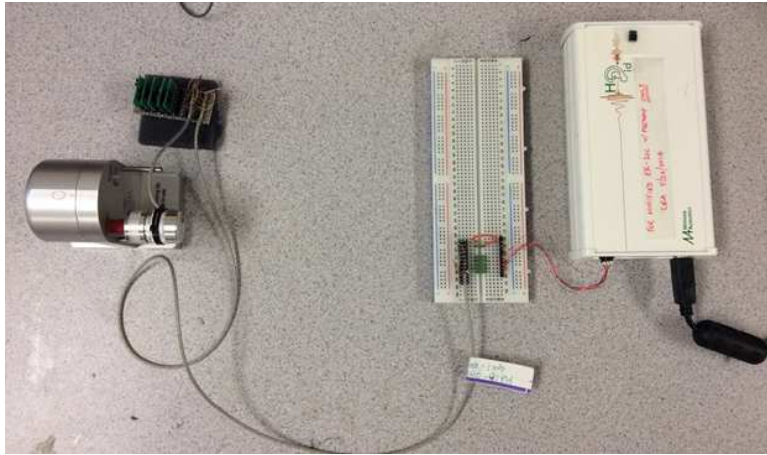
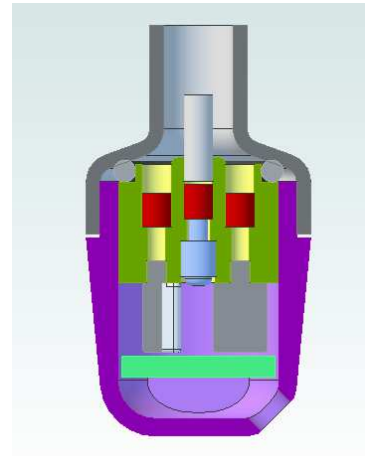


Figure 48: This figure shows improvement caused by the ER10C modification before and after. It gives a clear evidence that crosstalk was the source of the problem in the ER10C which has kept users from calibrating the probe above 6 kHz. Now the system can pass 4C calibration above 10 kHz. Note that all data and results are from preliminary tests. Some of the details are Mimosa Acoustics confidential information which will not be addressed here.



(a) The MA16 inserted in MA cavity



(b) Schematic representation of MA16.

Figure 49: (a) MA16 is used with the modified APU (right side white box) is used for audio processing. (b) Two speakers (lower two sided) and one microphone (in the middle) are used. The red parts represent acoustic resistors.

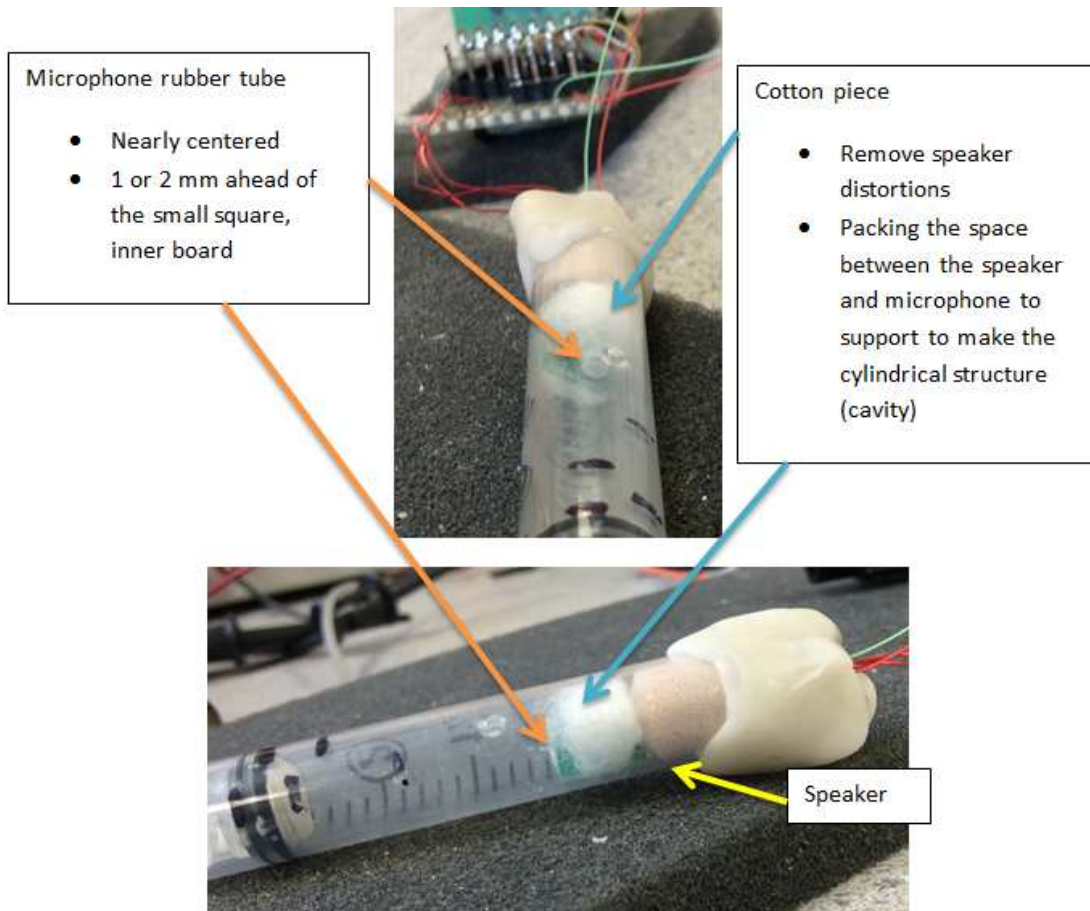


Figure 50: The MA17 simulator was made to simulate proposed design of the MA17. Due to the lined up transducers, the size of the probe can be greatly minimized.

## Part V

# Conclusions and Contributions

In this study, we have discussed the critical elements of a BAR including a gyrator, and a semi-inductor along with the two-port network properties. Starting by solving for the Hunt parameters of the receiver, we have proposed a new circuit model which contains these elements, the gyrator and the semi-inductor. An intuitive design of an electromagnetic transducer has been enabled by using the gyrator thereby avoiding the mobility method, which can be confusing to explain or teach. Moreover, we have shown an improved high frequency matching by using the semi-inductors, especially for the electrical impedance,  $Z_{in}(s)$ .

The model has been verified by comparing the experimental data (obtained from laser, vacuum, and pressure measurements) to theoretical data (obtained through model simulations). All the comparisons are in excellent agreement with the experimental results. The electrical input impedance data matches up to 23[kHz] (Fig. 39). A major advantage of the proposed receiver model is that the acoustic Thevenin pressure can be calculated directly from electrical input impedance measurements.

Several other contributions from this study beyond the BAR model are

1. The uniqueness of our BAR model includes i) extending the circuit theory to include anti-reciprocal networks, ii) semi inductor networks, and iii) non quasi-static networks by means of transmission line in the refined circuit model (Fig. 1). These are uniquely necessary components of the BAR transducer.
2. In-depth investigation of the gyrator's impedance matrix form. Reinterpreting the formula via electromagnetic basics and explaining the anti-reciprocal characteristic due to Lenz's Law.
3. Explaining the "matrix composition method", which are characterized by the Möbius transformation. This appears to be a generalization of the ABCD (Transmission) matrix cascading method, one of the most powerful computational analyzing tools in circuit theory.
4. A demonstration that  $Z_{mot}$  is not a physically realizable PR impedance, supporting by PR property Using a simplified electro-mechanic model simulation. Historical analysis of the concept of impedance, such as development of AC impedance by Kennelly, also contributes to understanding nature of the  $Z_{mot}$ .
5. The derivation of KCL, KVL from Maxwell's equations. This follows from a Galilean transformation of ME, which is an approximation to Einstein's theory of special relativity.

In summary, this analysis puts the electro-magnetic transducer's theory on a firm theoretical basis since its invention by A. G. Bell in 1876.

1693 **Part VI**

1694 **Appendix**

1695 **A Definition of Energy Conservation, Starting from Modality**

1696 In the field of engineering or physics, each bears an analogy to the others. If someone asks the  
 1697 meaning of the field in this context, answer would be ‘an area with a specific way of how a particle  
 1698 feels a force’. This means that there is a generalization with differences in each area. At this point,  
 1699 we can define the difference as a modality which refers a status of having characteristics in a given  
 1700 condition.

1701 Two general variables are used to describe a modality by their product, and their ratio. The two  
 1702 conjugate variables come in pairs; a generalized force and a flow. They could be either a **vector** ( $\mathbf{v}$ ,  
 1703 in bold) or a scalar ( $s$ ), and also can vary spatially. And a product of these two variables defines the  
 1704 power, while a ratio of them defines the impedance, which is usually defined in frequency domain.

1705 Some examples of the conjugate variables in each modality are described in table 3, and examples  
 of power and impedance are described in table 4. An frequency (phasor or time-harmonic) domain

Modality	Conjugate variables (vector in bold)	
	Generalized force [unit]	Flow [unit]
Electric	Voltage ( $\Phi$ ) [V]	Current ( $I$ ) [A]
Mechanic	Force ( $\mathbf{F}$ ) [N]	Particle velocity ( $\mathbf{U}$ ) [m/s]
Acoustic	Pressure ( $P$ ) [ $N/m^2$ ]	Volume velocity ( $\mathbf{V}$ ) [ $(ms)^{-1}$ ]
Electro-Magnetic	Electric field ( $\mathbf{E}$ ) [V/m]	Magnetic field ( $\mathbf{H}$ ) [A/m]

Table 3: Example of modalities and their conjugate variables. Upper case symbols are used for the frequency domain variables. The time domain representation of each variable can be described using the lower case of the same character, except in the EM case. But general Electro-Magnetic (EM) theories consider the time domain and its traditional notation uses capital letter for the time domain analysis. Note that in the electric field,  $\mathbf{E} = -\nabla\Phi$ , where  $\Phi$  is scalar potential, the voltage.

1706 of EM expressions are also common. In this case, a different notation (i.e., *under – line* or *italic*) is  
 1707 used based on the author’s choice. The EM wave can be decomposed into the sum of the sinusoidal  
 1708 waves. The EM wave phasor form is to analyze the waves’ propagation if they are oscillating at a  
 1709 single frequency.

Modality	Product in time domain	Ratio (Impedance $Z$ ) in frequency domain
Electric	$\phi(t)i(t)$	$Z_e = \Phi/I$
Mechanic	$\mathbf{f}(t) \cdot \mathbf{u}(t)$ (inner product)	$Z_m = F/U$
Acoustic	$p(t)\mathbf{v}(t)$ (intensity)	$Z_a = P/V$
Electro-Magnetic (EM)	$\mathcal{P} = \mathbf{E} \times \mathbf{H}$ (Poynting vector)	$\eta = \underline{\mathbf{E}}/\underline{\mathbf{H}}$

Table 4: Power and impedance definitions for each modalities in table 3. In general, power concept (a product of conjugate variables) can be used in time domain, however the impedance (a ratio) is thought of in the frequency domain. Assuming causality, the Laplace transformation can be applied to convert the impedance to the time domain.

1710 One can define a system using single modality or a combination of them. For the combination  
 1711 of the modalities, ‘n’-port network concept is required. (This discussion will be followed in next.)  
 1712 Independent from how many modalities exist in a system, there is a well-known law that one can  
 1713

1714 apply to every system. The law of the energy conservation is expressed as (Van Valkenburg (1960);  
1715 Cheng and Arnold (2013))

$$e(t) \equiv \int_{-\infty}^t power(t)dt \geq 0, \quad (140)$$

1716 where the total delivered energy  $e(t)$  which is an integration of the power over time should be than  
1717 greater than (or equal to) zero, and  $power(t)$  is work done per unit time defined as a potential  
1718 times a net flow. Simply speaking, Eq. 140 means we cannot have more energy than we supply.

1719 Let's take an example of an electric modality case in time domain power ( $power_e$ ).

$$power_e(t) = \phi(t)i(t) = (i(t) \star z(t))i(t), \quad (141)$$

1720 where  $i(t)$  is the net current (the current flow integrated by its affected area therefore it is a scalar)  
1721 in time domain which is not zero,  $z(t)$  is an inverse Laplace transform of an impedance ( $Z=\Phi/I$ )  
1722 in frequency domain,  $e(t)$  is a voltage in time, and  $\star$  denotes a convolution operator.

1723 In EM, a Poynting vector ( $\mathcal{P}$ ), represents the power density, a rate of energy transfer per unit  
1724 area,

$$\mathcal{P} = \mathbf{E} \times \mathbf{H}. \quad (142)$$

1725 Note that a cross product is used to consider the spatial variation of each variable. The units for  
1726  $\mathcal{P}$ ,  $\mathbf{E}$ , and  $\mathbf{H}$  are  $[W/m^2]$ ,  $[V/m]$ , and  $[A/m]$  respectively. The directions of  $\mathcal{P}$ ,  $\mathbf{E}$ , and  $\mathbf{H}$  vectors  
1727 follow the right hand rule. By integration of this Poynting vector over the effective surface area  $A$ ,  
1728 we have a scalar power in unit of  $[W]$  in electro-magnetic field ( $power_{EM}$ ),

$$power_{EM} = \int_s \mathcal{P} \cdot d\mathbf{A} = \int_s (\mathbf{E} \times \mathbf{H}) \cdot d\mathbf{A}. \quad (143)$$

1729 In the field of acoustic, the power is a measure of sound energy per unit time which is defined  
1730 as intensity times area  $\mathbf{A}[m^2]$  ( $power_a$ ),

$$power_a = p(t)\mathbf{u}(t) \cdot \mathbf{A}, \quad (144)$$

1731 where  $p(t)\mathbf{u}(t)$  defines the intensity.

1732 To take into account the power concept in frequency domain, one must use the Laplace transform  
1733 ( $\mathcal{L}$ )'s convolution theorem. Therefore a proper way to describe the instantaneous power in Laplace  
1734 frequency domain extending from Eq. 141 is

$$power_e(t) = \phi(t)i(t) \xleftrightarrow{\mathcal{L}} Power(s)|_{s=j\omega} = \Phi(\omega) \star I(\omega) \quad (145)$$

1735 where  $j = \sqrt{-1}$ ,  $\omega$  is the angular frequency and 's' is the Laplace frequency. Compared to an usual  
1736 power definition  $P = \Phi I$ , this is an unusual expression. However based on Eq. 141, a product  
1737 relationship becomes a convolution via Laplace transform.<sup>23</sup>

---

<sup>23</sup>If it is not true, then more explanation should be followed to make that point clear

## B Tellegen's Theorem & KCL/KVL

Tellegen's theorem (Eq. 146) states that the complex power,  $\mathcal{S}$ , dissipated in any circuit's components (or branches) sums to zero,

$$\sum \mathcal{S}_i = 0, \quad (146)$$

where 'i' is branches in a circuit and,  $\mathcal{S} = \Phi I^* = R + jQ$  is complex power measured. The  $\mathcal{S}$  has both real ( $R$ ) and imaginary ( $Q$ ) parts.

$$R = \Re \mathcal{S} = \Re(\Phi I^*), \quad (147a)$$

$$Q = \Im \mathcal{S} = \Im(\Phi I^*) \quad (147b)$$

where 'R' represents the average power measured in Watt [ $W$ ], and 'Q' shows the reactive power measured in Volt-Amps Reactive [ $VAR$ ].

Therefore the total power ( $P_{total}$ ) of the electro-mechanic system (Fig. 8) can be described as

$$P_{total} = \Phi I^* + FU^* = \Re(\Phi I^*) + \Re(FU^*) + j\Im(\Phi I^*) + j\Im(FU^*) = P_{avg} + jP_{reactive}, \quad (148)$$

where

$$P_{avg} = \Re \Phi I^* + \Re FU^* = \frac{1}{2}(\Phi I^* + \Phi^* I) + \frac{1}{2}(FU^* + F^* U) \quad (149a)$$

$$P_{reactive} = \Im \Phi I^* + \Im FU^* = \frac{1}{2}(\Phi I^* - \Phi^* I) + \frac{1}{2}(FU^* - F^* U). \quad (149b)$$

For any lossless network, the  $P_{avg}$  goes to zero. McMillan (1946) describes an elementary two-port network to generalize the system's total power using the impedance components of the system. Here, we revisit the steps using Hunt parameters introduced in 1954.

The total averaged input power ( $P_{avg}$ ) of an electro-mechanic system can be calculated from Eq. 5,

$$\begin{aligned} P_{avg} &= \frac{1}{2}[\Phi I^* + \Phi^* I + FU^* + F^* U] \\ &= \frac{1}{2}[(Z_e I + T_{em} U)I^* + (Z_e I + T_{em} U)^* I + (T_{em} I + Z_m U)U^* + (T_{me} I + Z_m U)^* U] \\ &= \frac{1}{2}[(Z_e + Z_e^*)II^* + (Z_m + Z_m^*)UU^* + (T_{em} + T_{me}^*)I^*U + (T_{em}^* + T_{me})IU^*], \end{aligned} \quad (150)$$

where '\*' is the complex conjugation operator. In lossless network, the real part of the power,  $P_{avg}$  is zero. Therefore Eq. 150 vanishes for all  $I$  and  $U$ , then we have the following conditions on the Hunt parameters,

$$Z_e = -Z_e^*, \quad (151)$$

$$Z_m = -Z_m^*, \quad (152)$$

$$T_{em} = -T_{me}^*. \quad (153)$$

Eq. 151 and Eq. 152 show  $Z_e$  and  $Z_m$  are purely imaginary in lossless system. If any loss is added to the system,  $Z_e$  and  $Z_m$  cannot have negative real part (resistance) to obey the conservation of energy law. Only positive resistance is allowed.

Eq. 150 tells us a general idea about reciprocity. If  $F$  is 90 degree out of the phase with 'I', then  $T_{em}$  and  $T_{me}$  should be imaginary, therefore we have  $T_{em} = T_{me}$  (Eq. 7, 8). A condenser transducer is a real world example of this 'reciprocal' case.

In an electromagnetic transducer, on the other hand,  $F$  is in phase with  $I$ , therefore the  $F$  is proportional to the  $I$ . In this case,  $T_{em}$  is real, therefore to satisfy Eq. 153,  $T_{me} = -T_{em}$ . This is the definition of the 'anti-reciprocity', the two transfer impedances are real and have different signs. This specific conditions are also discussed in Tellegen (1948). It is a lossless LC network with anti-reciprocity characteristic considering only Brune's impedances (except resistors).

1765 **Two-port network without a Semi-inductor**

1766 Similar to Eq. 129, Eq. 154 is a corresponding ABCD matrix representation of a simple two-port network depicted in Fig. 51. In this figure, the semi-inductor is excluded from the electrical side.

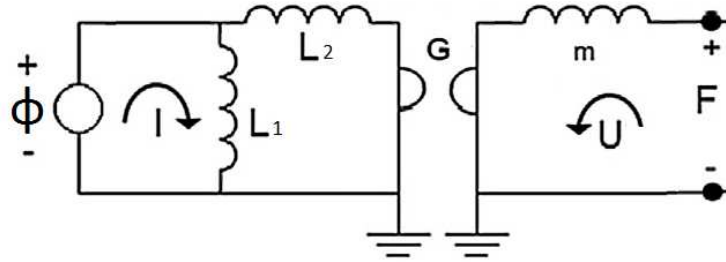


Figure 51: A simple anti-reciprocal network without a semi-inductor

1767

$$\begin{bmatrix} \Phi(\omega) \\ I(\omega) \end{bmatrix} = \begin{bmatrix} 1 & 0 \\ \frac{1}{sL_2} & 1 \end{bmatrix} \begin{bmatrix} 1 & sL_1 \\ 0 & 1 \end{bmatrix} \begin{bmatrix} 0 & G \\ \frac{1}{G} & 0 \end{bmatrix} \begin{bmatrix} 1 & 0 \\ \frac{1}{sm} & 1 \end{bmatrix} \begin{bmatrix} F(\omega) \\ -U(\omega) \end{bmatrix}, \quad (154)$$

1768 where  $s$  is the Laplace frequency ( $\sigma + j\omega$ ) and  $L_1$ ,  $L_2$ ,  $G$ , and  $m$  are the inductance 1 and 2, the  
1769 gyration coefficient, and the mass of the system respectively.

1770 For a simple analysis, the ABCD matrix part in Eq. 154 is separated, and  $L_1$ ,  $L_2$ ,  $G$ , and  $m$   
1771 are set to be '1'. The whole equation is rewritten as

$$\begin{bmatrix} 1 & 0 \\ \frac{1}{s} & 1 \end{bmatrix} \begin{bmatrix} 1 & s \\ 0 & 1 \end{bmatrix} \begin{bmatrix} 0 & 1 \\ 1 & 0 \end{bmatrix} \begin{bmatrix} 1 & 0 \\ \frac{1}{s} & 1 \end{bmatrix} = \begin{bmatrix} 1 & s \\ s & s^2 + 1 \end{bmatrix} \begin{bmatrix} \frac{1}{s} & 1 \\ 1 & 0 \end{bmatrix} \quad (155)$$

1772 Finally we have the second giant ABCD matrix to represent the system in Fig. 51.

$$\begin{bmatrix} \Phi(\omega) \\ I(\omega) \end{bmatrix} = [T_2] \begin{bmatrix} F(\omega) \\ -U(\omega) \end{bmatrix} = \begin{bmatrix} A(s)' & B(s)' \\ C(s)' & D(s)' \end{bmatrix} \begin{bmatrix} F(\omega) \\ -U(\omega) \end{bmatrix} = \begin{bmatrix} \frac{1}{s} + s & 1 \\ 2 + s^2 & s \end{bmatrix} \begin{bmatrix} F(\omega) \\ -U(\omega) \end{bmatrix}, \quad (156)$$

1773 where  $\Delta_{T_2} = -1$ . Converting Eq. 156 into an impedance matrix, Eq. 11 is used to give us

$$Z_2 = \begin{bmatrix} z'_{11} & z'_{12} \\ z'_{21} & z'_{22} \end{bmatrix}, \quad (157)$$

1774 where

$$z'_{11} = \frac{\frac{1}{s} + s}{2 + s^2} = \frac{1 + s^2}{2s + s^3}, \quad (158)$$

1775

$$z'_{12} = -\frac{1}{2 + s^2}, \quad (159)$$

1776

$$z'_{21} = \frac{1}{2 + s^2}, \quad (160)$$

1777

$$z'_{22} = \frac{s}{2 + s^2}. \quad (161)$$

1778 Note that this network is a typical lossless LC network which contains only Brune's impedances.  
1779 Therefore  $z'_{11}$  and  $z'_{22}$  are purely imaginary while  $z'_{12}$  and  $z'_{21}$  are purely real.

1780 Based on Eq. 50,  $Z_{mot}$  of this system can be computed as follows,

$$Z_{mot2} = \frac{1}{s(2 + s^2)} = \frac{1}{2s + s^3}. \quad (162)$$

1781 Substituting the Laplace frequency ‘ $s$ ’ to be  $j\omega$  in Eq. 162,

$$Z_{mot2}|_{s=j\omega} = \frac{1}{2j\omega + (j\omega)^3} = j \frac{1}{\omega^3 - 2\omega}. \quad (163)$$

1782 There is no real part in Eq. 163. In this specific case, any angular frequencies ( $\omega$ ) cannot have real  
 1783 part.  $Z_{mot}$  is always purely imaginary.

1784 Figure 52 represents the simulated Hunt parameters (Eq. 158-161). The two transfer impedances  
 1785 are real, and they are equal in magnitude but different in signs. The input impedance is purely  
 1786 inductive, and the output impedance behaves like a resonator. Figure 53 shows the motional  
 1787 impedance and input impedances with both open and short circuit conditions. Compared to Fig. 44,  
 1788 all are purely imaginary, with no loss in this system (real part is zero).

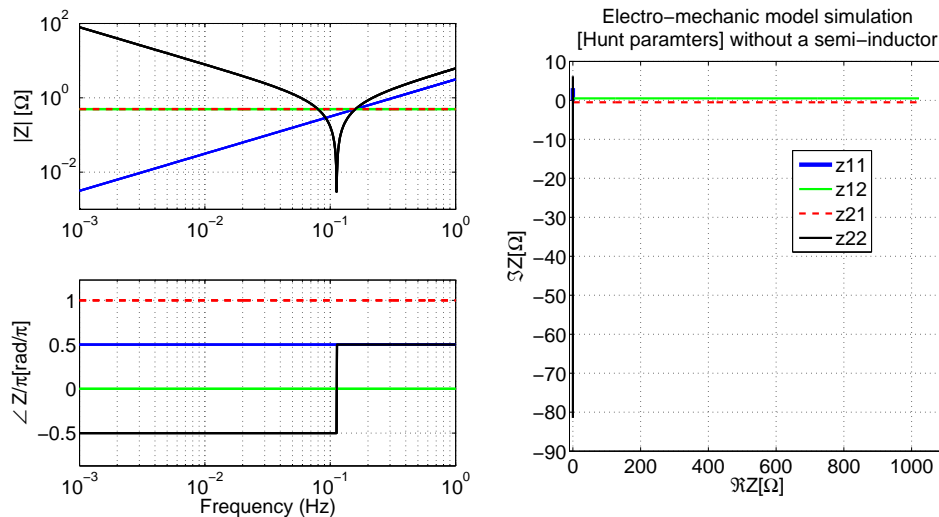


Figure 52: Computed Hunt parameters based on a simple electro-mechanic network shown in Fig. 51 (Eq. 158-161). All parameters  $L_1$ ,  $L_2$ ,  $G$ , and  $m$  are set to be 1 for a simple computation.

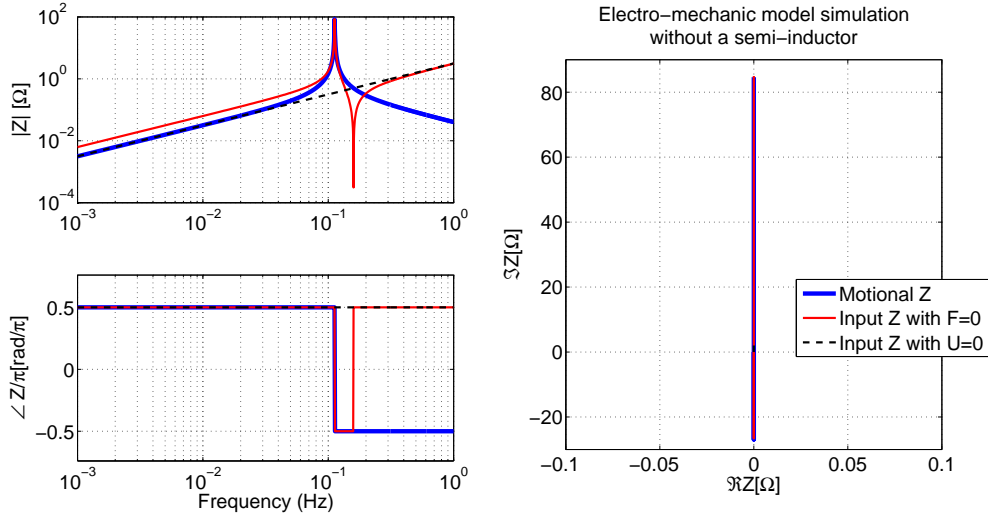


Figure 53: Computed motional impedance(Eq. 163), input impedances with both open( Eq. 158) and short circuit conditions(Eq. 163+Eq. 158) based on a simple electro-mechanic network shown in Fig. 51.

## C Sensitivity Analysis of ED Series SPICE Model

Figure 54 shows the Knowles Electronics commercial SPICE circuit model (Killion, 1992). This SPICE model contains a gyrator and is meant to be equivalent to the physical system, but does not accordingly represent the system in an one-to-one physical manner.

In order to fully understand each component, we implemented the Knowles PSpice model in Matlab using transmission matrices. Unlike PSpice, Matlab provides a more flexible platform for a matrix model manipulation. Matlab does not critically depend on the user's operating system (Knowles' PSpice model is inflexibly tied to both the Cadence Orcad Schematics and Capture, and Windows XP). PSpice requires a DC path to ground from all nodes, thus R1, RK512, RK513, and RK514 components have been added for this purpose.

We then performed a *sensitivity analysis* on the Matlab model by changing each component value by +/- 20% to determine those components for which the output changed by less than -50[dB], within the frequency range of 0.1 - 10[kHz]. Once the small effect components were determined, we removed the components from the original PSpice design for a further Matlab analysis. To compare the difference between the original and the reduced components condition, we calculate each error computed across frequencies,

$$e(f) = \frac{|'Original' - 'Small effect'|}{|'Original'|}, \quad (164)$$

where  $f$  is frequency. Our Matlab simulation result is shown in Fig. 55(a) with the CMAG value defined in the PSpice circuit (in Fig. 54, CMAG=0.92e-7). The 'Original' simulation contains all circuit elements without any modification, whereas the 'Small effect' simulation excludes the small effect components in Fig. 54. The PSpice sensitivity analysis for the semi-capacitor is performed using Knowles PSpice library for the CMAG component<sup>24</sup> shown in Fig. 55(b). The most important result of this sensitivity analysis was that the semi-capacitor in the PSpice model is one of these 'small effect' components.

<sup>24</sup>This simulation result was provided by Knowles Electronics.

1812 Using a series semi-capacitor on the right side of the gyrator is mathematically equivalent to  
 1813 using a shunt semi-inductor on the left side of the gyrator, because of mobility and impedance  
 1814 analogies. However, ideally, circuit elements should be properly associated with their physical  
 1815 properties. It is important to take advantage of using a gyrator to describe the anti-reciprocity for  
 1816 a physically intuitive model of the system. The gyrator is the bridge between the electrical and  
 1817 mechanical systems. For this reason the coil of the receiver should be represented on the electrical  
 1818 side. This realization further motivated our objective to design a simplified and rigorous BAR  
 1819 model.

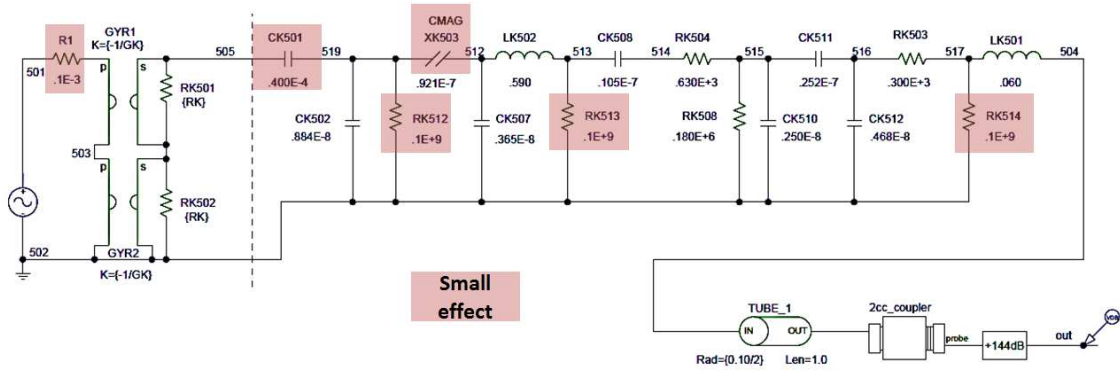


Figure 54: Knowles PSpice model of the ED receiver: The refined PSpice circuit model of ED receiver by reducing ‘small effect’ components which are marked in red. R1, RK512, RK513, and RK514 resistors were added to maintain DC stability of PSpice. Note that the Spice model represents all ED series receivers, including ED7045, ED1744, ED1913, and etc., such that specific parameter value of components vary for each specific receiver.

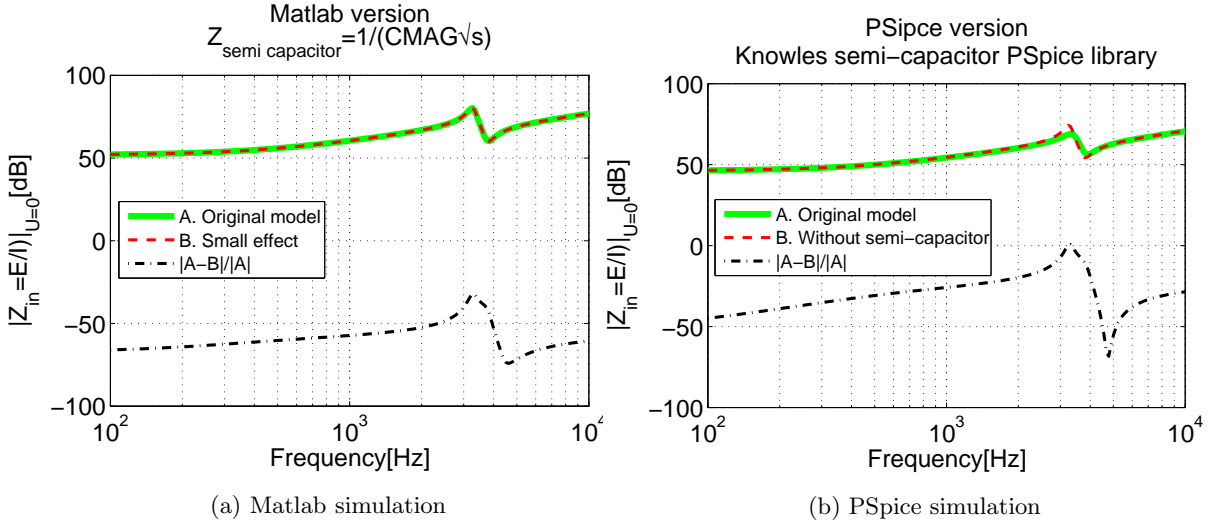


Figure 55: The simulated electrical input impedance' magnitude,  $|Z_{in}|$ , in dB scale. (a) shows the sensitivity analysis using Matlab based on Fig. 54 where  $s = j\omega$ . The 'A. original model' and the 'B. Small effect' conditions are marked with a thick green line and a dashed red line, respectively. The 'B. Small effect' is the simulated result when all 'small effect' components in Fig. 54 are removed in the original PSpice circuit. It represents summed-up sensitivities of 'small effect' components in Fig. 54. (b) represents the sensitivity of the CMAG component only. This analysis is provided by Knowles Electronics using their PSpice library for the CMAG component (This result is plotted in Matlab but the data is acquired via PSpice simulation). Similar to the (a), 'A. Original model' shows the PSpice simulation including all components in Fig. 54, whereas 'B. Without semi-capacitor' simulates the original PSpice circuit only without the semi-capacitor. For both simulations (a) and (b), the difference between the original response and the reduced response is calculated based on Eq. 164 shown as black dashed line.

## 1820 D $Z_{mot}$ : Spatial Relationships Between $\Phi$ , I, B, F, and I

1821 In this section, we will research the fundamental spatial relationship of signals based on Maxwell's  
 1822 equation. There are four well-known Maxwell's equations both in integral and differential forms.  
 1823 Maxwell's equations can be reduced into two main equations, Faraday's law and Ampere's law.  
 1824 When Maxwell developed electro magnetic relationship into mathematical equations, he ended  
 1825 up with 37 quaternion equations to describe all relationships in electro magnetic world. Later  
 1826 on Olive Heaviside reorganized Maxwell's quaternion equations into four reduced complex vector  
 1827 relationships using the  $\nabla$  operator.

1828 Therefore it is a reasonable idea to revisit electro-mechanic parameter's relationship in spatial  
 1829 domain. In quaternion, 3 spatial rotation parameters (i,j, and k) are defined which have the  
 1830 following properties

$$i^2 = j^2 = k^2 = ijk = (k)k = -1. \quad (165)$$

1831 Note Eq. 165 is noncommutative, also i or j are different from the imaginary parameter of Laplace  
 1832 complex time-frequency domain.

1833 Faraday-lenz's law explains generator (a relationship between  $\Phi$  and U through B)

$$\Phi = l(U \times B), \quad (166)$$

1834 while Ampere's law is applying for explaining motor action (a relationship between F and I through  
 1835 B),

$$F = l(I \times B). \quad (167)$$

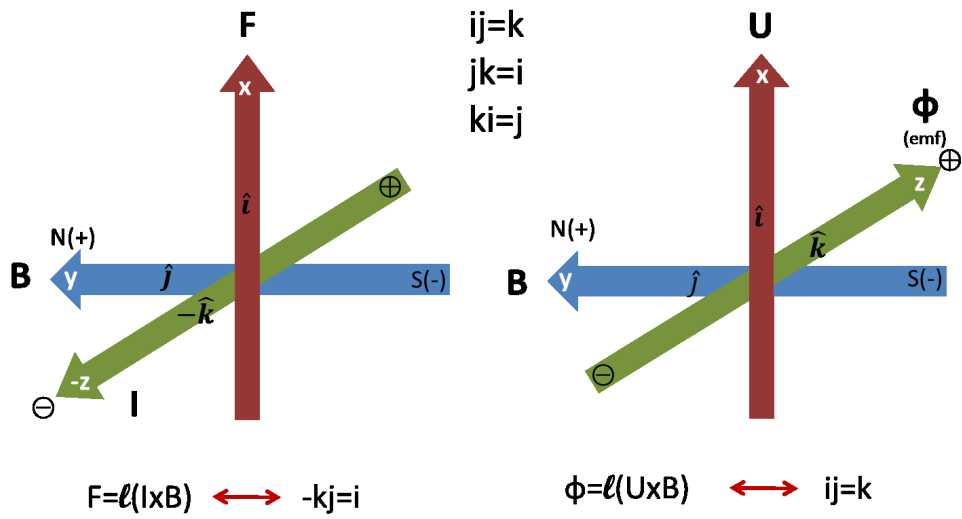


Figure 56: Electro-mechanic system's variables in spatial domain by BeranekBeranek (1954)

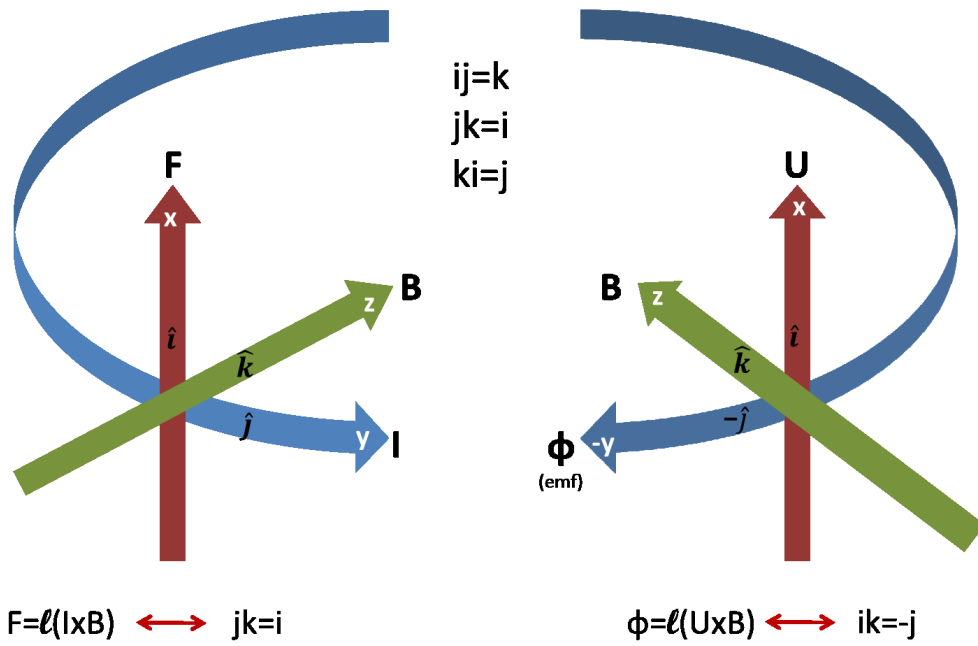


Figure 57: Equivalent with Fig. 56. The choice of each geometry is adapted from Hunt's book Hunt (1954)

1836 Let's consider Fig. 57 picturing variables in 3D spatial domain. Considering the spatial rela-  
 1837 tionship of each variable shown in Fig. 57, Eq. 5 is rewritten as

$$\begin{bmatrix} \Phi_x \hat{i} + \Phi_y \hat{j} + \Phi_z \hat{k} \\ F_x \hat{i} + F_y \hat{j} + F_z \hat{k} \end{bmatrix} = \begin{bmatrix} Z_e & T_{em} \\ T_{me} & Z_m \end{bmatrix} \begin{bmatrix} I_x \hat{i} + I_y \hat{j} + I_z \hat{k} \\ U_x \hat{i} + U_y \hat{j} + U_z \hat{k} \end{bmatrix} \quad (168)$$

1838 We can rewrite Eq. 168 consider the spatial relationship of each parameter depicted in Fig. 57,

$$\begin{bmatrix} 0 \hat{i} + \Phi_y \hat{j} + 0 \hat{k} \\ F_x \hat{i} + 0 \hat{j} + 0 \hat{k} \end{bmatrix} = \begin{bmatrix} Z_e & T_{em} \\ T_{me} & Z_m \end{bmatrix} \begin{bmatrix} 0 \hat{i} + I_y \hat{j} + 0 \hat{k} \\ U_x \hat{i} + 0 \hat{j} + 0 \hat{k} \end{bmatrix} \quad (169)$$

1839 To finalize each relationship in Eq. 169 we have,

$$\begin{bmatrix} \Phi_y \hat{j} \\ F_x \hat{i} \end{bmatrix} = \begin{bmatrix} Z_e & T_{em} \hat{k} \\ T_{me}(-\hat{k}) & Z_m \end{bmatrix} \begin{bmatrix} I_y \hat{j} \\ U_x \hat{i} \end{bmatrix}. \quad (170)$$

1840 Considering spatial rotations in each parameter in Eq. 170, we can repeat  $Z_{mot}$  derivation shown  
 1841 in Eq. 44 and Eq. 45.

$$\Phi_y \hat{j} = Z_e I_y \hat{j} + T_{em} \hat{k} U_x \hat{i} = Z_e I_y \hat{j} + T_{em} U_x \hat{j} \quad (171a)$$

1842

$$F_x \hat{i} = T_{me}(-\hat{k}) I_y \hat{j} + Z_m U_x \hat{i} = -T_{me} I_y \hat{i} + Z_m U_x \hat{i} \quad (171b)$$

1843 Set  $F_x \hat{i}$  to be zero, we have

$$\frac{\Phi_y}{I_y} = Z_e + T_{em} \frac{U_x}{I_y} \quad (172a)$$

1844

$$\frac{U_x}{I_y} = -\frac{T_{me}}{Z_m} \quad (172b)$$

1845 Plugging Eq. 172b into Eq. 172a, finally we have the same Eq. 46

$$Z_{in}|_{F_x=0} = \frac{\Phi_y}{I_y} = Z_e - \frac{T_{em} T_{me}}{Z_m}. \quad (173)$$

1846 The result shown in Eq. 173 is as same as Eq. 46, no spatial dependency is observed. Therefore  
 1847 the spatial relation is already considered in motional impedance formula shown in Eq. 50.

## 1848 E Calculation of Hunt Parameters

1849 Equation 16 includes three unknown Hunt parameters ( $Z_e$ ,  $Z_a$  and  $T_a$ ) that we wish to find. In order  
 1850 to solve for three unknown parameters, 3 different electrical input impedances ( $Z_{in|A}$ ,  $Z_{in|B}$ , and  
 1851  $Z_{in|C}$ ) are measured corresponding to three known acoustic loads, A, B, and C. The load conditions  
 1852 differ in a length of the tubing, attached to the receiver's port. Each tube has different impedance  
 1853 denoted as  $Z_{L|A}$ ,  $Z_{L|B}$ , and  $Z_{L|C}$ , where  $Z_{L|A} = Z_0 \coth(a \cdot tube\_length)$  (for the blocked-end tube,  
 1854  $V = 0$ ),  $Z_0$  is the characteristic impedance of a tube, and  $a$  is the complex propagation function.  
 1855 Parameters  $a$  and  $Z_0$  parameters assume viscous and thermal loss (Keefe, 1984). In  $20^\circ[C]$  room  
 1856 temperature,  $c = 334.8[m/s]$ . Define diameter of  $Z_{L|A,B,C} \approx 1.4[mm]$

1857 Substituting these for  $Z_L$  in Eq. 16:

$$1858 \quad Z_{in|A} = \frac{\Phi}{I} = Z_e + \frac{T_a^2}{Z_{L|A} + Z_a} \quad (174)$$

$$1859 \quad Z_{in|B} = \frac{\Phi}{I} = Z_e + \frac{T_a^2}{Z_{L|B} + Z_a}$$

$$1860 \quad Z_{in|C} = \frac{\Phi}{I} = Z_e + \frac{T_a^2}{Z_{L|C} + Z_a}$$

1860 Given these three measured impedances, we can solve for  $Z_a$ ,  $T_a$ , and  $Z_e$  via the following procedure:

- 1861 1. Subtract two electrical impedance measurements to eliminate  $Z_e$ , such as

$$1862 \quad Z_{in|C} - Z_{in|A} = \frac{T_a^2}{Z_a + Z_{L|C}} - \frac{T_a^2}{Z_a + Z_{L|A}}. \quad (175)$$

2. Take the ratio of various terms as defined by Eq. 175,

$$\left( \frac{Z_a - Z_{L|B}}{Z_{in|C} - Z_{in|A}} \right) = \left( \frac{Z_{in|A} - Z_{in|C}}{Z_{in|B} - Z_{in|C}} \right) \left( \frac{Z_{L|C} - Z_{L|B}}{Z_{L|C} - Z_{L|A}} \right).$$

1862 From this we may solve for the first unknown  $Z_a$ ,

$$1863 \quad Z_a = \frac{(Z_{in|A} - Z_{in|C})(Z_{L|C} - Z_{L|B})(Z_{in|C} - Z_{in|A})}{(Z_{in|B} - Z_{in|C})(Z_{L|C} - Z_{L|A})} + Z_{L|B}. \quad (176)$$

3. Next we find  $T_a$  by substituting  $Z_a$  into Eq. 175

$$1864 \quad T_a = \sqrt{\frac{(Z_{in|C} - Z_{in|A})(Z_a + Z_{L|C})(Z_a + Z_{L|A})}{Z_{L|A} - Z_{L|C}}}. \quad (177)$$

4. Finally  $Z_e$  is given by Eq. 174

$$1864 \quad Z_e = \left( \frac{T_a^2}{Z_{L|A} + Z_a} \right) - Z_{in|A}. \quad (178)$$

## F Hysteresis Loop for a Ferromagnetic Material: $\mathbf{B}$ vs. $\mathbf{H}$

The word ‘*Hysteresis*’ is originated from the Greek, *hystérēsis*, meaning that a state of lagging behind or late, the outcome depends on history of past inputs, as well as current inputs. In the field of magnetism,  $\mathbf{B}$  and  $\mathbf{H}$  relationship in ferromagnetic materials shows this hysteresis characteristic, plotting of this relationship, we call it as ‘Hysteresis loop.’ The key formula for studying this effect is well known as  $\mathbf{B} = \mu\mathbf{H}$ , however the most important thing to discern is ‘Whose’  $\mathbf{B}$ ,  $\mathbf{H}$ , and  $\mu$ ,

$$\underbrace{\mathbf{B}}_{\text{Material's}} = \underbrace{\mu}_{\text{Material's}} \underbrace{\mathbf{H}}_{\text{Applied}} \quad (179)$$

where  $\mathbf{B}$  [ $\text{Wb}/\text{m}^2$ ] is the total magnetic density in (ferromagnetic) material,  $\mathbf{H}$  [ $\text{A}/\text{m}$ ] is the external applied magnetic field to the material, and  $\mu$  [ $\text{H}/\text{m}$ ] is the permeability (one of properties, showing how easily the material can be magnetized) of the material.

Figure 58 visualizes magnetization process in a ferromagnetic material with a greatly simplified way. Without applied  $\mathbf{H}$ , the ferromagnetic material (i.e., iron, nickel., etc...) does not show any magnetic properties (left figure in Fig. 58) having net  $\mathbf{B}=0$ . Once it is exposure to external magnetic field  $\mathbf{H}$ , this material exhibits characteristics as shown in the right drawing of Fig. 58. Now the net  $\mathbf{B} \neq 0$ , it has the same magnetic direction with the applied magnetic field. This is the simplified description of the magnetization, details of this process needs heavy duty knowledge in quantum mechanics which is not relevant in our study Ulaby (2007).

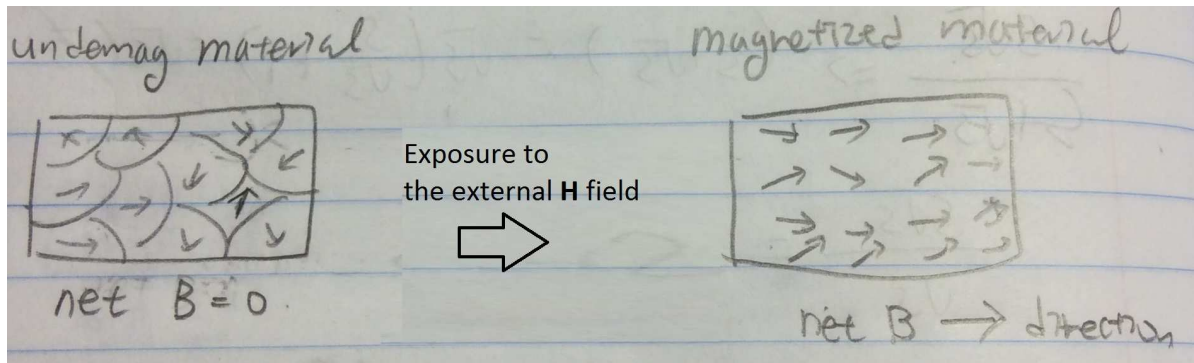


Figure 58: Simplified magnetization process. Undemagnetized ferromagnetic material’s net  $\mathbf{B}=0$ . When ferromagnetic material is exposure to the magnetic field  $\mathbf{H}$ , the net magnetic intensity ( $\mathbf{B}$ ) of the material is no longer 0. It becomes magnetized with the same direction of the applied  $\mathbf{H}$ . Note that details of this process (i.e., breaking the domain walls) needs heavy duty knowledge in quantum mechanics which is not relevant to discuss in our study Ulaby (2007).

Based on the magnetization process, we can discuss magnetic hysteresis. Figure 59 depicts a typical hysteresis loop shown in the ferromagnetic materials. In general (not in a ferromagnetic material),  $\mathbf{H}$  and  $\mathbf{B}$  hold linear relationship, meaning that  $\mu$  of the material is constant. However it is not true for the ferromagnetic materials, as we can see in Fig. 59. The shape of the curve has a specific pattern; each step of the curve needs to be explained. In Fig. 59, the x-axis represents magnetic field  $\mathbf{H}$  that is applied to the material, and the y-axis shows the magnetic intensity ( $\mathbf{B}$ ) of the material.

1. ( $O \rightarrow A$ ): The material’s initial position starts from  $O$ , as strength of the  $\mathbf{H}$  is increased to its positive maximum saturation point (1), the material’s  $\mathbf{B}$  is also increased to reach the point  $A$

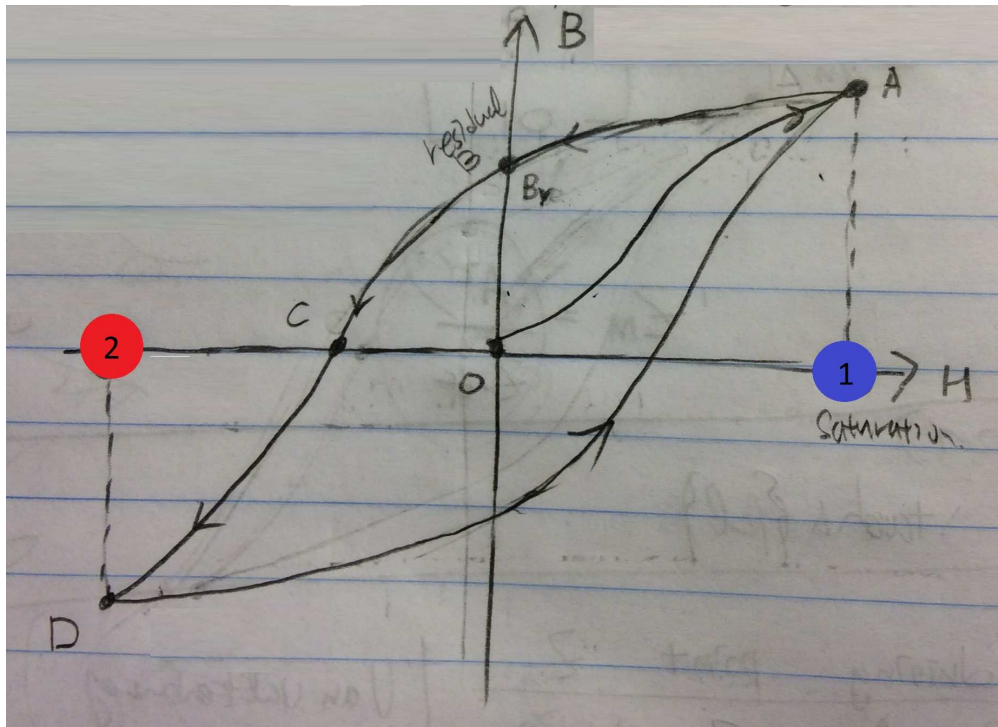


Figure 59: A typical hysteresis curve in ferromagnetic materials. The x-axis represents magnetic field  $\mathbf{H}$  that is applied to the material, and the y-axis shows the magnetic intensity ( $\mathbf{B}$ ) of the material. On the loop, there are five marked points,  $O$ ,  $A$ ,  $B_r$ ,  $C$ ,  $D$ , and two colored points on the x-axis blue(1) and red(2). The blue and red points are two saturation limits of  $\mathbf{H}$  in each direction ( $\pm$ ). The material's initial position starts from  $O$ , as strength of the  $\mathbf{H}$  is increased to its positive maximum saturation point (1), the material's  $\mathbf{B}$  is also increased to reach the point  $A$ . Then the  $\mathbf{H}$  starts to decrease to be zero, but the material's magnetic property still remains at  $B_r$ . This point is named as a residual magnetic point. At this point, the ferromagnetic material has magnetic characteristic without applied magnetic field, therefore it becomes permanent magnet. As  $\mathbf{H}$  is increased its amplitude to the opposite direction (the direction of  $\mathbf{H}$  is still backward),  $\mathbf{B}$  becomes zero at  $C$ . The descending from  $B_r$  to  $C$  is called demagnetization, permanent magnet loses its magnetic characteristic within this process. The line goes down to  $D$ , when the  $\mathbf{H}$  reaches its (negative) maximum saturation limits at 2 (red). Finally,  $\mathbf{H}$  is reversing its direction (i.e., current with sine wave, passing through  $f = \pi/2$ ) and goes through the portion of the hysteresis loop from  $D$  to  $A$  and repeating  $A \rightarrow B_r \rightarrow C \rightarrow D \dots$  until  $\mathbf{H}$  becomes zero

- 1891 2. ( $A \rightarrow B_r$ ): Then the  $\mathbf{H}$  starts to decrease to be zero, but the material's magnetic property  
 1892 still remains at  $B_r$ . This point is named as a residual magnetic point. At this point, the  
 1893 ferromagnetic material has magnetic characteristic without applied magnetic field, therefore  
 1894 it becomes permanent magnet.
- 1895 3. ( $B_r \rightarrow C$ ): As  $\mathbf{H}$  is increased its amplitude to the opposite direction (the direction of  $\mathbf{H}$  is still  
 1896 backward),  $\mathbf{B}$  becomes zero at  $C$ . The descending from  $B_r$  to  $C$  is called demagnetization,  
 1897 permanent magnet loses its magnetic characteristic within this process.
- 1898 4. ( $C \rightarrow D$ ): The line goes down to  $D$ , when the  $\mathbf{H}$  reaches its (negative) maximum saturation  
 1899 limits at 2 (red).
- 1900 5. ( $D \rightarrow A$ ): Finally,  $\mathbf{H}$  is reversing its direction (i.e., current with sine wave, passing through  
 1901  $f = \pi/2$ ) and goes through the portion of the hysteresis loop from  $D$  to  $A$ .

## References

- Allen, J., 1986. Measurement of eardrum acoustic impedance, in: Allen, J., Hall, J., Hubbard, A., Neely, S., Tubis, A. (Eds.), *Peripheral Auditory Mechanisms*. Springer Berlin Heidelberg. volume 64 of *Lecture Notes in Biomathematics*, pp. 44–51.
- Bauer, B.B., 1953. A miniature microphone for transistor amplifiers. *The Journal of the Acoustical Society of America* 25, 867–869.
- Beranek, L.L., 1954. *Acoustics*. McGraw-Hill.
- Beranek, L.L., Mellow, T.J., 2014. *Acoustics sound fields and transducers*. Waltham, MA.
- Boas, R.P., 1987. *Invitation to complex analysis*. New York, NY.
- Brune, O., 1931. Synthesis of a finite two-terminal network whose driving-point impedance is a prescribed function of frequency. Ph.D. thesis. Massachusetts Institute of Technology, Massachusetts.
- Carlin, H.J., Giordano, A.B., 1964. *Network theory, an introduction to reciprocal and nonreciprocal circuits*. Englewood Cliffs NJ.
- Cheng, S., Arnold, D.P., 2013. Defining the coupling coefficient for electrodynamic transducers. *JASA* 134(5), 3561–3672.
- Fay, R.D., Hall, W.M., 1933. The determination of the acoustical output of a telephone receiver from input measurements. *Journal of Acoustic Science of America* V, 46–56.
- Firestone, F.A., 1938. The mobility method of computing the vibration of linear mechanical and acoustical systems. *The Journal of the Acoustical Society of America* 10.
- Hanna, C.R., 1925. Design of telephone receivers for loud speaking purposes. *Radio Engineers, Proceedings of the Institute of* 13(4), 437–460.
- Hunt, F.V., 1954. *Electroacoustics: The analysis of transduction and its historical background*. Harvard University Press. Harvard University, Massachusetts.
- Jensen, J., Agerkvist, F.T., Harte, J.M., 2011. Nonlinear time-domain modeling of balanced-armature receivers. *J. Audio Eng. Soc* 59, 91–101.
- Keefe, D.H., 1984. Acoustical wave propagation in cylindrical ducts: Transmission line parameter approximations for isothermal and nonisothermal boundary conditions. *Journal of the Acoustical Society of America* 75, 58–62.
- Kennelly, A., 1925. The measurement of acoustic impedance with the aid of the telephone receiver. *Journal of the Franklin Institute (JFI)* 200, 467–487.
- Kennelly, A., Affel, H., 1915. The mechanics of telephone-receiver diaphragms, as derived from their motional impedance circles. *Proc. Am. Ac. Arts and Sci.* 51(8), 421–482.
- Kennelly, A., Kurokawa, K., 1921. Acoustic impedance and its measurement. *Proc. Am. Ac. Arts and Sci.* 56(1), 3–42.

- 1937 Kennelly, A., Nukiyama, H., 1919. Electromagnetic theory of the telephone receiver with special  
1938 reference to motional impedance. The 348th meeting of the American Institute of Electrical  
1939 Engineers (A.I.E.E.) .
- 1940 Kennelly, A., Pierce, G., 1912. The impedance of telephone receivers as affected by the motion of  
1941 their diaphragms. Proc. Am. Ac. Arts and Sci. 48, 113–151.
- 1942 Killion, M.C., 1992. Elmer Victor Carlson: A lifetime of achievement. The Bulletin of the American  
1943 Auditory Society 17, 10–21.
- 1944 Kim, N., Allen, J.B., 2013. Two-port network analysis and modeling of a balanced armature  
1945 receiver. Hearing Research 301, 156–167.
- 1946 Lewin, W., 2002a. Lecture 16: Non-conservative fields - do not trust your intuition. University  
1947 Lecture, Electricity and Magnetism (Physics 8.02).
- 1948 Lewin, W., 2002b. Lecture 20: Faraday’s law - most physics college books have it wrong! University  
1949 Lecture, Electricity and Magnetism (Physics 8.02).
- 1950 Lin, F., Niparko, J.K., Ferrucci, L., 2011. Hearing loss prevalence in the United States. Archives  
1951 of Internal Medicine 171(20), 1851–1853.
- 1952 Lynch, T.J., Nedzelnitsky, V., Peake, W.T., 1982. Input impedance of the cochlea in cat. The  
1953 Journal of the Acoustical Society of America 72, 108–130.
- 1954 McMillan, E., 1946. Violation of the reciprocity theorem in linear passive electromechanical system.  
1955 J. Acoust. Soc. Am. 18, 344–347.
- 1956 Mott, E.E., Miner, R.C., 1951. The ring armature telephone receiver. The Bell System Technical  
1957 Journal , 110–140.
- 1958 Parent, P., Allen, J.B., 2010. Wave model of the human tympanic membrane. Hearing Research  
1959 263, 152–167.
- 1960 Puria, S., Allen, J.B., 1998. Measurements and model of the cat middle ear: evidence of tympanic  
1961 membrane acoustic delay. J Acoust Society of America 104, 3463–81.
- 1962 Robinson, S.R., Allen, J.B., 2013. Characterizing the ear canal acoustic impedance and reflectance  
1963 by pole-zero fitting. Hearing Research 301, 168–182.
- 1964 S. Ramo, J.R.W., Duzer, T.V., 1965. Fields and waves in communication electronics. New York,  
1965 NY.
- 1966 Serwy, R., 2012. The limits of Brunes impedance. Master’s thesis. University of Illinois at Urbana-  
1967 Champaign, Illinois.
- 1968 Sommerfeld, A., 1964. Electrodynamics. Academic Press INC.. London, United Kingdom.
- 1969 Tellegen, B., 1948. The gyrator, a new electric network element. Philips Res. Rep t. 3, 81–101.
- 1970 Thorborg, K., Unruh, A.D., Struck, C.J., 2007. A model of loudspeaker driver impedance incorpo-  
1971 rating eddy currents in the pole structure. J. Audio Eng. Soc. .
- 1972 T.S.Littler, 1934. Motional impedance diagram. Journal of Acoustic Science of America V, 235–241.

- 1973 Ulaby, F.T., 2007. Fundamentals of Applied Electromagnetics, 5th ed. Prentice-Hall, Upper Saddle  
1974 River, NJ.
- 1975 Van Valkenburg, M.E., 1960. Introduction to Modern Network Synthesis. Wiley, NY.
- 1976 Van Valkenburg, M.E., 1964. Network Analysis. Prentice-Hall, Englewood Cliffs, NJ. 2nd edition.
- 1977 Vanderkooy, J., 1989. A model of loudspeaker driver impedance incorporating eddy currents in the  
1978 pole structure. J. Audio Eng. Soc. 37(3), 119–128.
- 1979 Warren, D.M., LoPresti, J.L., 2006. A ladder network impedance model for lossy wave phenomena.  
1980 The Journal of the Acoustical Society of America (abst) 119(5), 3377.
- 1981 Weece, R., Allen, J., 2010. A clinical method for calibration of bone conduction transducers to  
1982 measure the mastoid impedance. Hearing Research 263, 216–223.
- 1983 Wegel, R.L., 1921. Theory of magneto-mechanical systems as applied to telephone receivers and  
1984 similar structures. Journal of the American Institute of Electrical Engineers 40, 791–802.
- 1985 Woodson, H.H., Melcher, J.R., 1968. Electromechanical dynamics. John Wiley and Sons. New  
1986 york, London, Sydney.